Landscape Phage-Targeted Drug Delivery to Breast Cancer Cells

by

Olusegun A. Fagbohun

A dissertation submitted to the Graduate Faculty of
Auburn University
in partial fulfillment of the
requirements for the Degree of
Doctor of Philosophy

Auburn, Alabama
December 13, 2010

Key words: Landscape phage, Major coat protein, Targeted liposomes, Breast cancer, Doxil™, Biomarker

Approved by

Valery A. Petrenko, Chair, Professor of Pathobiology
R. Curtis Bird, Professor of Pathobiology
Calvin M. Johnson, Professor of Pathobiology
Stuart B. Price, Professor of Pathobiology
Jacek Wower, Professor of Biochemistry

Abstract

The prevalence of breast cancer is still a public health burden worldwide. Recently, there has been significant progress in the management of breast cancer with the two FDA-approved cancer nanomedicines employing the concept of passive targeting. However, their delivery to the tumor cells can be hindered by insufficient permeation of nanomedicines into solid tumors, such as breast cancer, thereby, inhibiting bystander effects. Therapeutic efficacy of nanomedicines can be increased by active targeting of drug loaded nanocarriers. To this end, there is intense research effort in the quest for physiologically stable and cancer-specific ligands for targeting of nanocarriers to the cancer-specific cellular receptors. Although, a pleothora of ligands have been developed for targeting of drugs to the site of disease, only a few have been successfully used because of the need of their conjugation to drug carriers.

Accordingly, we proposed that using landscape phage coat proteins for targeting of drug-loaded nanocarriers can enhance drug delivery to breast cancer cells. Screening of multibillion landscape phage library can generate peptide ligands targeting cancer-specific receptors. We hypothesize that spontaneous insertion of isolated phage proteins into drug loaded nanocarriers such as liposomes can enhance their cancer-specific cytotoxicity and exclude the need for complex bioconjugations and derivitization procedures required for targeting. We attempted to this hypothesis by screening two landscape phage libraries. Consequently, 132 phage probes specific for the breast cancer cell line, MCF-7 were generated. Coat proteins of selected phages were isolated and inserted into drug loaded liposome (Doxil™). Two phage coat proteins (with

fusion peptides, DWRGDSMDS and GSDWMLGQD) were isolated and inserted into Doxil™. The cytotoxicity of the targeted Doxil™ was compared with non-targeted Doxil™. Our hypothesis was proven further by spontaneous insertion of phage protein (with the fusion peptide DMPGTVLP) into siRNA encapsulated liposomes and applied them to MCF-7 cells. The phage-targeted siRNA-liposome demonstrated significant down-regulation of *PRDM14* gene expression and protein synthesis in the target MCF-7 cells in comparison with non-targeted siRNA.

To determine the molecular mechanism of phage selectivity for breast cancer cells, selected phages were used as affinity matrixes in affinity chromatography to identify their counterpart receptors. Three phages DWRGDSMDS, GSDWMLGQD and DMPGTVLP were identified as ligands for nucleolin. We believe that the novel drug-targeting technique developed in the scope of this dissertation will allow significantly enhanced therapeutic efficacy of modern anti-cancer nanomedicines.

Acknowledgments

The author would like to express the deepest appreciation to his committee members for their guidance and persistent help throughout this project. He is grateful to Dr. Valery Petrenko for his excellent mentoring and direction. The author would also like to appreciate the intellectual contributions of his co-authors in publications emanating from this study: Dr. R. C. Bird, Ms Patricia Deinnocentes, Dr. D. Bedi, Dr. N. Grabchencho, Mr. James Gillespie, Dr. V.P. Torchillin and Ms. Tao Wang.

Table of Contents

List of Tables

List of Figures

CHAPTER 1

INTRODUCTION AND REVIEW OF LITERATURE

1. Introduction

Cancer is the principal cause of death and a public health burden worldwide. Mortality from cancer is projected to increase to an estimated 12 million deaths in 2030 worldwide. In the US, 1,529,560 new cases and 569,490 deaths from cancer are expected in 2010. Likewise, malignancy is culpable for approximately 1 in 4 deaths in the US (Jemal et al., 2010). Accordingly, the development of an adequate treatment modality to constrain cancer mortality rate to its nadir remains a formidable challenge and a major goal of research in biomedical sciences and clinical oncology.

Traditional treatments of cancer inaccessible to surgery or as adjuvant to surgery are multi-modal comprising chemotherapy, immunotherapy, hormonal therapy and radiotherapy. Although, there have been improvements in cancer patient survival by employing cytotoxic chemotherapeutic regimens, this approach is encumbered by poor accessibility of medications to tumor site and non-specific cytotoxicity to normal cells. Selectivity of common cancer chemotherapeutics are often based on their increased uptake by rapidly dividing cells, leading to associated toxicities towards rapidly dividing normal tissues such as bone, gastrointestinal tract and hair follicles (Allen, 2002). Novel nanomedicine pharmaceutical systems emerged recently to achieve site-specific delivery thereby minimizing non-specific toxicity (Lammers et al., 2008). There is an array of nanomedicine carriers comprising liposomes, micelles, dendrimers,

nanotubes and nanoparticles which have been used to delivery cytotoxic cargos to cancer cells. Two of such drug loaded pharmaceutical nanocarriers, Doxil™ (Ortho Biotech Inc, Bedford, OH) encapsulating doxorubicin hydrochloride and Abraxane™ (Abraxis BioScience Inc., Los Angeles, CA) which is an albumin matrix embedded paclitaxel, have been approved by the FDA. The use of nanocarriers for drug delivery is based on their accumulation in solid tumors because of the "enhanced permeability and retention" (EPR) effect that promotes drug loaded nanocarriers to localize in the areas of increased vascular permeability in angiogenic tumors and is referred to as passive targeting (Seymour, 1992; Allen, 2002). Some of these clinically approved drug loaded systems have been made stealth for the reticuloendothelial system and physiologically stable by their coating with polyethylene glycol to evade immune surveillance (Gullotti and Yeo, 2009). However, passive targeting can enhance accumulation pharmaceutical nanocarriers in the tumor interstitium for a prolonged time but cannot control their translocation into the cell. Consequently, the carrier allows only release of the drug into the vicinity of the tumor resulting in a bystander effect (Prokop and Davidson, 2008). Furthermore, drugs ultimately delivered into the cytoplasm are prone to being trapped and eliminated through the endo-lysosomal route. Besides, in multidrug resistant cells, for example with phenotype MCF-7/Adr, overexpression of P-glycoprtein on plasma membranes, Golgi apparatus and nuclear membrane results in extrusion of drugs out of the intracellular compartment thereby leading to reduced drug efficacy (Vasir and Labhasetwar, 2005; Calcabrini et al., 2000).

As a means to improve selective interaction of the drug loaded nanocarriers with the target cell, active targeting has been explored. Active targeting is based on the principle of molecular recognition whereby a ligand-targeted nanocarrier, encapsulating a lethal cargo, is delivered to tumor cell's membrane, microenviroment, cytoplasm or nuclear membrane

displaying the counterpart receptor (Haley and Frenkel, 2008). A plethora of ligands comprising small molecules, peptides, aptamers, proteins and antibodies are currently in use for targeting nanoparticles (Veiseh et al., 2010; Balestrieri and Napoli, 2007). In this set, the application of peptides offers an almost universal approach to targeting nanoparticles because of their intrinsic diversity of binding potentials. Two main types of combinatorial libraries have been a source of binding ligands: one-bead-one-compound (OBOC) combinatorial libraries and phage display libraries, the diversity of OBOC being much lower than the phage display libraries (Aina et al., 2007). Using phage display libraries, with a clone complexicity greater than 1 x 10^9, phage clones can be selected and propagated in *E. coli*. The screening procedure can be iterated to select the highest affinity binding phage clones. Peptides specific for various tumor cells, tissues and organs in model animals have been identified using phage display random libraries with fusion peptides displayed on pIII protein *in vitro*, *ex vivo* and *in vivo*, respectively (Pasqualini et al., 1997; Rajotte et al., 1998; Rasmussen et al., 2002).

In another group, random peptide phage display libraries were used for selection of tumor cell binding ligands in cancer patients (Krag et al., 2006). Phage display libraries were used to generate peptides specific for 59 NCI-60 cell (National Cancer Institute panel of cell lines from different histologic origins and grades, (Kolonin et al., 2006). The panel includes carcinomas of several origins (kidney, breast, colon, lung, prostate, and ovarian), tumors of the central nervous system, malignant melanomas, leukemias, and lymphomas. In addition, phages specific for the target tumor cell lines, tissues or mouse xenografts can be selected from the multi-billion landscape phage libraries, as described previously (Mount et al., 2004; Romanov et al., 2001; Samoylova et al., 2003) and converted to targeted gene- and drug-delivery vehicles

(Mount et al., 2004). In the light of this, we proposed using landscape phage libraries as sources of probes for identifying cancer-cell specific ligands and their use in targeting nano-medicines.

The filamentous bacteriophages Ff (fd, f1 and M13) are part of a large family of bacterial viruses that infect Gram-negative bacteria. They are long, flexible and thin phage with a diameter of 7 nm and length of 800-900 nm (determined by the size of the genome). Their single stranded DNA genome is enclosed in a cylindrical capsid composed of the major coat protein pVIII, and a few copies of the minor coat proteins capping the tips of the phage (Figure. 1).

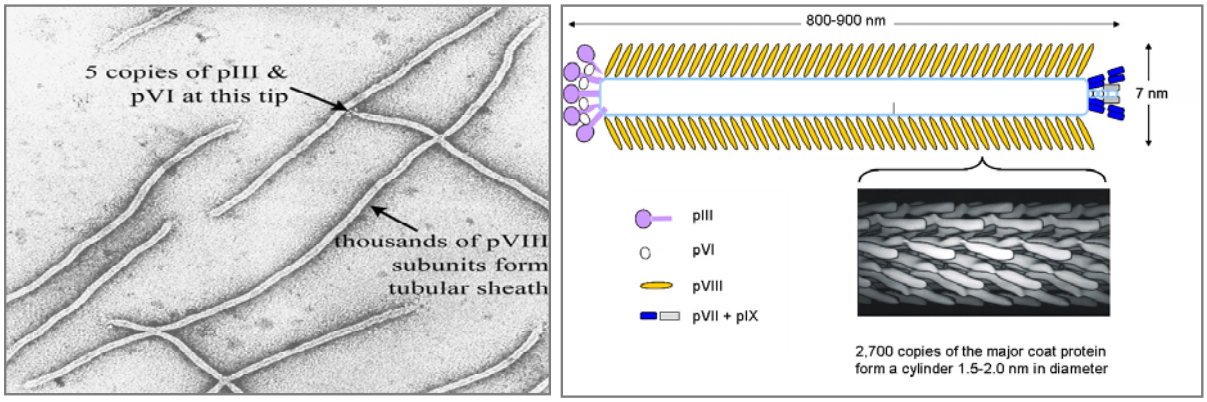

Figure. 1. Filamentous phage. Left: Electron micrograph. The minor pIII proteins are noted (arrow). Right: Schematic and model of segment of ~1% of phage virion with array of pVIII. (Micrograph and model courtesy of Irina Davidovich, Gregory Kishchenko and Lee Makowski).

The phage display library is an ensemble of up to 10 billion different phage clones, each harboring a unique foreign DNA, and therefore displaying a specified guest peptide on the virion surface. Foreign peptides were first displayed on the pVIII protein and soon after display on the minor coat protein pIII was pioneered (IIyichev et al., 1992; Petrenko and Smith, 2005). The foreign peptides replacing the three or four mobile amino acids close to the N-terminus of the wild-type protein pVIII do not affect considerably the general architecture of virions and do not change the conformation of the fusion proteins in membranes (Jelinek et al., 1997; Monette et al., 2001). Consequently, such fusion phages retain their ability to infect the host bacteria *E. coli*

and form up to 1000 identical phage particles per bacterial cell during the doubling period. Such particles were eventually termed “landscape phage” to emphasize the dramatic change in surface architecture caused by arraying thousands of copies of the inserted peptides in a dense, repeating pattern around the tubular capsid (Petrenko et al., 1996). The foreign peptides decorating the phage body create defined organic surface structures (landscapes) varying from one phage clone to the next (Figure 3).

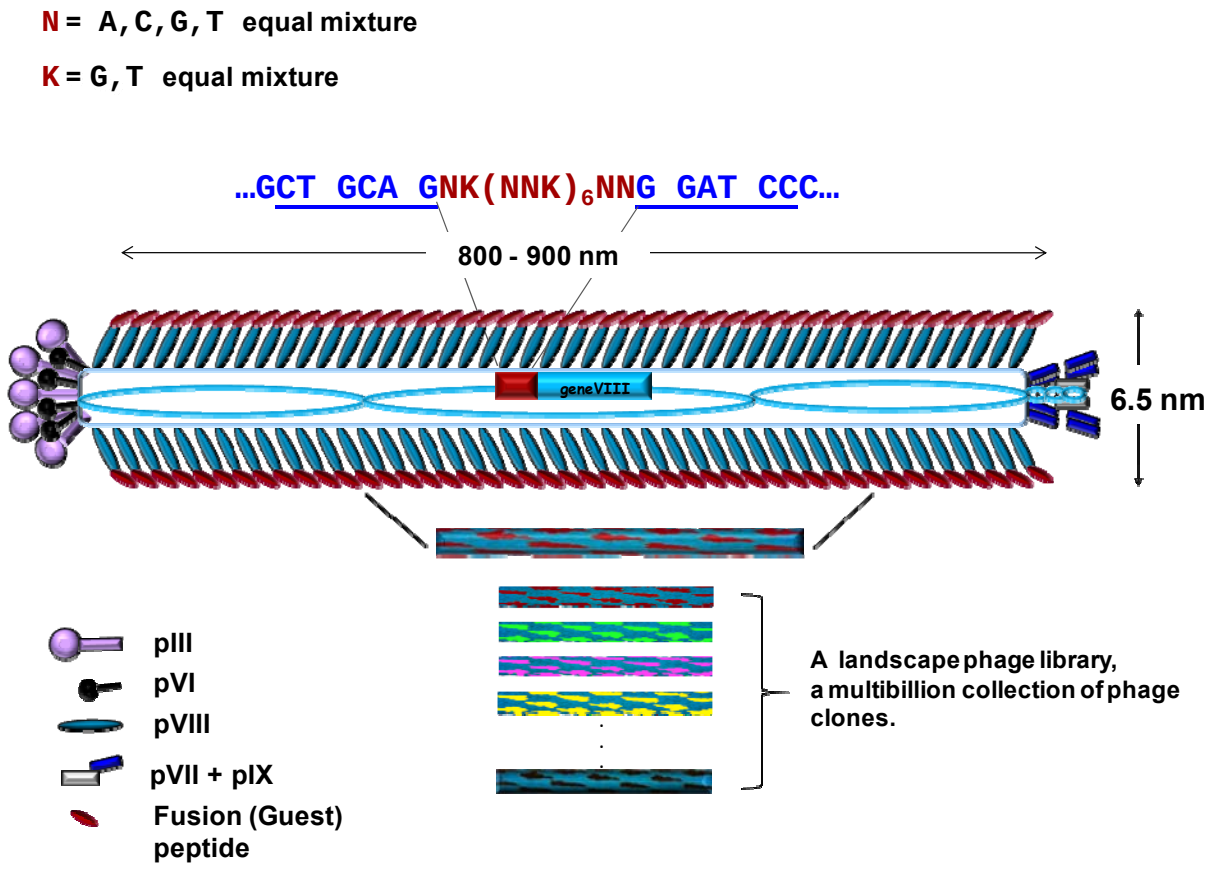

Figure 2. A schematic depiction of the landscape phage library. A phage library involves multi-billion phage clones.

A library is a huge population of such phages, encompassing billions of clones each with different surface structures and biophysical properties (Petrenko et al., 1996). Therefore, the landscape phage is a unique micro-fibrous material that can be selected in an affinity binding protocol. The binding peptide comprising up to 20% of the phage mass and up to 50% of the phage surface may be easily prepared by cultivation of the infected bacteria and isolation of phage particles by precipitation. The application of landscape phage for generating breast cancer specific ligands is described in chapter 2.

In this dissertation work we justified and proved a new strategy for targeting of nanocarriers specifically binding cancer cells based on:

1. Screening of two landscape libraries in a high throughput format for candidates with desired affinities, selectivities and internalization capacities towards the target cells.
2. Isolation of pure phage fusion protein preparations using one-step exclusion chromatography.
3. Self assembly of fusion phage proteins into drug-loaded PEGylated liposomes.

We hypothesized that targeting drug-loaded liposomes with breast cancer selective phage probes can improve drug delivery to tumor sites with a resultant increase in drug efficacy. We also attempted to elucidate the molecular mechanism by which phage probe specificity and selectivity is achieved by isolation and identification of phage-binding receptors on the surface of cancer cells

The first chapter of this dissertation entails a review of breast cancer, targeted drug delivery and phage coat protein biochemistry. Chapter two of this dissertation describes the screening of landscape phage libraries to identify breast cancer specific peptides. The third chapter of this dissertation describes isolation the coat proteins of breast-cancer specific phages, insertion of phage coat proteins into liposomes and determination of their cytotoxicity to breast

cancer cells. Chapter five describes application of phage fusion protein to targeted delivery of siRNAs designed as nanomedicine effectors. Chapter six describes identification of unique phage coat proteins cognate receptors on breast cancer cells.

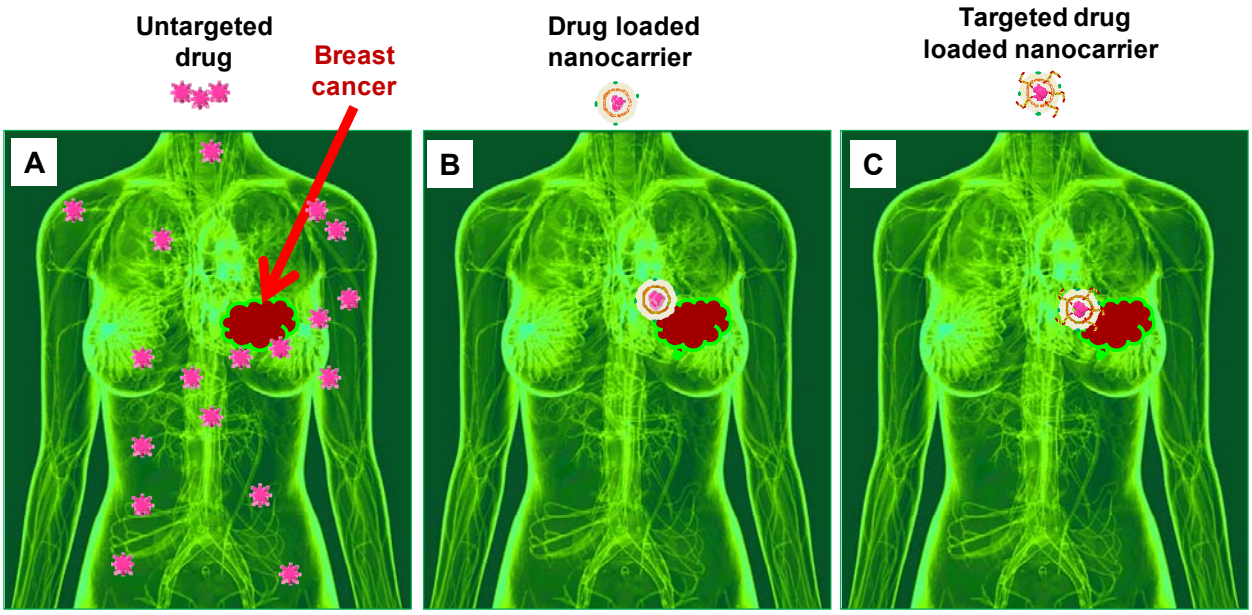

Figure 3. A schematic representation of drug delivery approaches. A: Untargeted drug delivery. The arrow points to breast cancer lesion. The untargeted drugs are depicted as asterisks. B: Passive targeted delivery. A drug loaded liposome at the site of the lesion site. C: Active targeted delivery. Drug encapsulated liposome targeted to tumor by the phage major coat with the propensity for tumor penetration.

We describe stripping breast cancer specific coat proteins from phage particles with chloroform, solubilization with sodium cholate and then grafting them onto Doxil® liposomes (Figure 4).

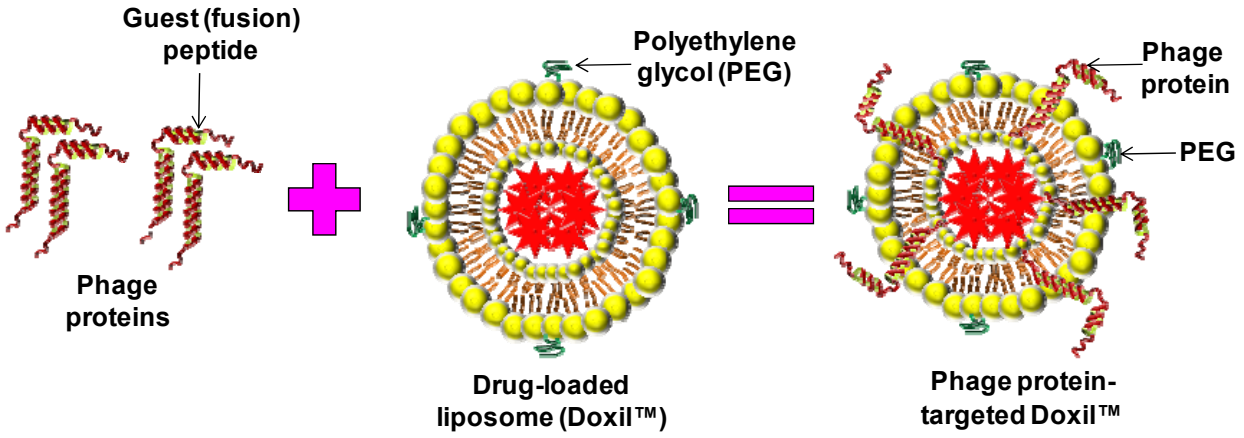

Figure 4. Drug-loaded liposome targeted with phage coat protein. The coat protein spans the lipid bilayer and displays the binding peptide on the surface of the carrier particle. The drug molecules are shown in asterisks.

2. Breast cancer

Breast adenocarcinoma is a cancer or tumor of glandular tissues in the breast, whereas, carcinoma is a neoplasm/tumor originating from epithelial cells of the breast glandular ducts or lobules. Lobular carcinomas can be invasive or non-invasive or less common ductal carcinomas (Merck Medical Manual, www.merckmanuals.com). Ductal carcinomas can be ductal carcinoma *in situ* (DCIS) or invasive ductal carcinoma. Invasive ductal carcinoma is responsible for 80% of cancer cases. Unlike DCIS, invasive ductal carcinoma invades the neighboring adipose tissues of the breast and can metastasize to other parts of the body through the bloodstream or lymphatic vessels.

3. Targeted drug delivery and phage coat protein biochemistry

Solid tumors are made up of two main cellular components, namely the tumor parenchyma and the stroma, with the stroma providing vasculature and other supporting cells (Munn, 2003). As tumor growth progresses, there is greater demand for more nutrients and structures. This results in the formation of new vasculature structures from endothelial cells from neighboring vessels vasculature and from bone marrow (Lyden et al., 2001). However, these

vessels are deficient in their architectural integrity compared to newly form blood vessels in normal tissues such as those found at healing sites (Jain, 2001). This defect has been exploited in passive drug delivery of nanocarriers (nanomedicines) to various tumors.

There are a plethora of drug delivery nanocarriers including liposomes, polymeric micelles, polymeric nanoparticles, dendrimers, viral-based nanoparticles and carbon nanotubes (Cho et al., 2008; Peer et al., 2007). Of all these nanocarriers, liposomes have been the most extensively studied. Liposomes are self assembling phospholipids with a bilayer and a spherical shape. Doxil™, a liposomal formulation encapsulating the anthracycline doxorubicin hydrochloride, is currently used for systemic management of breast and ovarian carcinomas (Markman, 2006). As has been previously indicated, these systems exploit the defective tumor vasculature and lymphatics for the delivery of their toxic cargos. However, passive targeted delivery has intrinsic limitations such as inadequate permeation of tumor tissues and some therapeutics may require intracellular delivery into organs such as the nucleus or mitochondria for their action (Moghimi and Szebeni, 2003). Therefore, active targeting or targeting of nanomedicines with tumor specific ligands, is currently being employed as an improvement to the passive delivery strategy. There are arrays of ligands available for targeting, including growth factors, antibodies and their fragments, carbohydrates, glycoproteins and receptors ligands. Most actively targeted nanomedicines require conjugation of ligands to the nanomedicines which often involves chemistry which may alter the structure and function of the ligands. Targeting of cancer nanomedicines with cancer selective-phage coat proteins provide a simple and economic approach for development of cancer targeted nanomedicines (Wang et al., 2010a; Jayanna et al., 2010). Previously, we developed a new approach to preparation of targeted liposomes that relies on the use of the phage fusion coat proteins as targeting ligands. In

our approach, a cancer cell-specific phage protein was inserted into the liposome exploring its intrinsic "membranophilic" properties (Jayanna et al., 2009). Fusion proteins carrying tumor-cell binding peptides inherit the major structural features of the "wild-type" major coat protein VIII (Figure 4). They have a positively charged C-terminus (amino acids 45-55), which navigates the protein through the liposome membrane, probably using the mechanisms intrinsic for cationic cell-penetrating peptides (Tseng et al., 2002). The highly hydrophobic "membranophilic" segment (amino acids 27-40) allows the protein to accommodate readily in the membrane (Tseng et al., 2002) while the amphiphilic N-terminus (amino acids 1-26), which are soluble in water, can interact with PEG residues on the surface of the "stealth" liposomes and display the N-terminal cancer cell-binding octamer or nonamer on the liposome shell.

CHAPTER 2

LANDSCAPE PHAGE PROBES FOR BREAST CANCER CELLS

1. Abstract

It has been shown in prove-of-concept experiments that efficacy of existing anticancer therapeutics can be improved through specific targeting to breast cancer cells by conjugation with peptides interacting with cancer-specific cellular receptors. To obtain a panel of anti-breast cancer cell ligands, two landscape phage display libraries were screened to isolate 132 unique phages that bind, internalize or interact with breast carcinoma cell lines MCF-7 and ZR-75-1. When tested for their selective interaction with these cells, in comparison with control HepG2 cells, MCF-10A cells and serum, 16 of the phage probes selectively interacted with the breast cancer cell lines. The selected phage probes have been used as promising ligands for development of nanomedicines more precisely targeted to breast cancer cells, as described in chapter three.

2. Introduction

Phage libraries of random peptides fused to the major coat protein pVIII of the filamentous phage are referred to as landscape phage libraries. Screening such libraries offers a new and powerful strategy for discovering peptide-fusion phage proteins that bind cell-surface receptors and internalize into target cells (Petrenko and Smith, 2005; Samoylova et al., 2003; Romanov et al., 2001; Jayanna et al., 2009; Petrenko, 2008).

Herein, we report the isolation of selective phage probes for MCF-7 and ZR-75-1 cells. Three selection strategies were used to screen multibillion-clone landscape phage libraries f8/8 and f8/9. The selective interactions of phage guest peptides with these cells were tested in comparison with other cells, MCF-10A (non-neoplastic human mammary epithelial cells), HepG2 (human hepatocellular carcinoma) and serum.

3. Materials and Methods

3.1 Cell lines

All cell lines were cultivated at 37°C in 5% CO_2. The human breast adenocarcinoma cell line MCF-7, (American Type Culture Collection (ATCC) ,HTB 22™) was used for selection and was cultivated in 25 cm^2 cell culture flasks (Corning Inc., Corning, NY) containing L-15 Leibovitz medium with L-glutamine (Sigma-Aldrich, St. Louis, MO) supplemented with 10% fetal calf serum (FCS). For the selectivity procedure, MCF-7 and human hepatocellular carcinoma HepG2 (ATCC, CRL-2235™) cell lines were grown in 96-well culture plates containing L-15 Leibovitz medium with L-glutamine (Sigma-Aldrich, St. Louis, MO) supplemented with 10% FCS. Human non-tumorigenic mammary epithelial cell line MCF-10A (ATCC, CRL-10317™) was maintained in mammary epithelial cell basal medium supplemented with 0.4% bovine pituitary extract, 0.1% human epidermal growth factor, 0.1% hydrocortisone, 0.1% GA-1000 and 0.1% insulin. (Invitrogen, Gibco Cell Culture, Portland, OR).

3.2 Phage display libraries

Landscape phage libraries, f8/8 and f8/9 containing 2 x 10^9 different clones each (Petrenko et al., 1996; Kuzmicheva et al., 2009) were screened to isolate clones binding MCF-7 cells. All procedures for handling phages, including propagation, purification, titering, isolation of phage clones, and isolation of phage DNA have been described (Brigati et al., 2008).

Escherichia coli (*E. coli*) strain K91BlueKan (Kan^r) {Hfr C thi lacZΔ M15 lac Y::mkh lacI^Q} used for propagating phages was kindly provided by George Smith (Yu and Smith, 1996).

3.3 Selection of breast cancer cell-binding phages

Three selection strategies were employed to isolate breast cancer specific phage probes from libraries f8/8 and f8/9.

A. Non-biased selection

The screening of the phage libraries were run in parallel. An aliquot of each phage library containing 100 billion phage particles in blocking buffer (0.5% BSA in serum free medium) was incubated in empty cell culture flasks at room temperature to deplete phage particles binding cell culture flasks. Unbound phages recovered from the depletion were incubated with confluent MCF-7 cells at room temperature for 1 h. Unbound phages were removed and cells were washed ten times with washing buffer (0.1% BSA, 0.1% Tween 20 in serum free medium) to remove any remaining unbound phage particles. Unbound phages and washings were stored for titering in host *E. coli* (K91 BlueKan). MCF-7 cell-bound phages were eluted with elution buffer (0.1 M glycine-HCl, pH 2.2) for 10 min on ice and neutralized with 1 M Tris-HCl (pH 9.1) as illustrated (Figure 5). Phages in eluate were concentrated in centrifugal concentrators as recommended by the manufacturer (Centricone 100 kDa, Fisher Scientific, Pittsburgh, PA). Concentrated eluted phages were titered and amplified in host *E. coli* and used as input in further rounds of selection which were similar to the procedure described above with the exception of depletion with cell culture flask. Four rounds of selection were performed altogether and phage clones selected in different selection rounds were randomly picked, isolated as individual clones, sequenced and propagated for further characterization. In each round, the enrichment of phages binding to the cells was determined by titering of input and

output phages. The ratio of output to input phage increased from one round to another indicating successful selection for phage clones that bind to the target MCF-7 cells.

B. Biased selection: acid and detergent extraction of cell bound phages and internalizing phages

The phage library (f8/8 or f8/9) was depleted against cell culture flask, serum and human fibroblasts (W1-38). Retrieval of cell-bound phages was as described for the non-biased strategy. To recover cell-internalizing phages, cells were washed twice in washing buffer to remove remaining bound phages. The washings were designated as post-elution washings 1 (PEW1) and post-elution washings 2 (PEW2) and were stored for titering in host *E. coli.* MCF-7 cells with associated phages were scraped from the flask with 5 ml of serum-free medium and collected by centrifugation at 130 x g for 10 min. The supernatant was removed and the cell pellet was lysed with lysis buffer [2% deoxycholate (sodium salt), 10 mM Tris-HCl, and 2 mM EDTA (pH 8.0)]. The eluate fraction (cell-surface bound phages) and the lysate (cell-internalized phages) were amplified separately in *E. coli* and used in subsequent rounds of selection but with no depletion steps. After four rounds of selection, phage clones were titered and amplified in bacteria and then individual phage clones were randomly picked from the plates. DNAs of randomly picked phage clones encoding to the oligonucleotide insert were amplified by PCR, sequenced and translated to reveal peptide sequences responsible for binding or internalizing of phage to/into cancer cells.

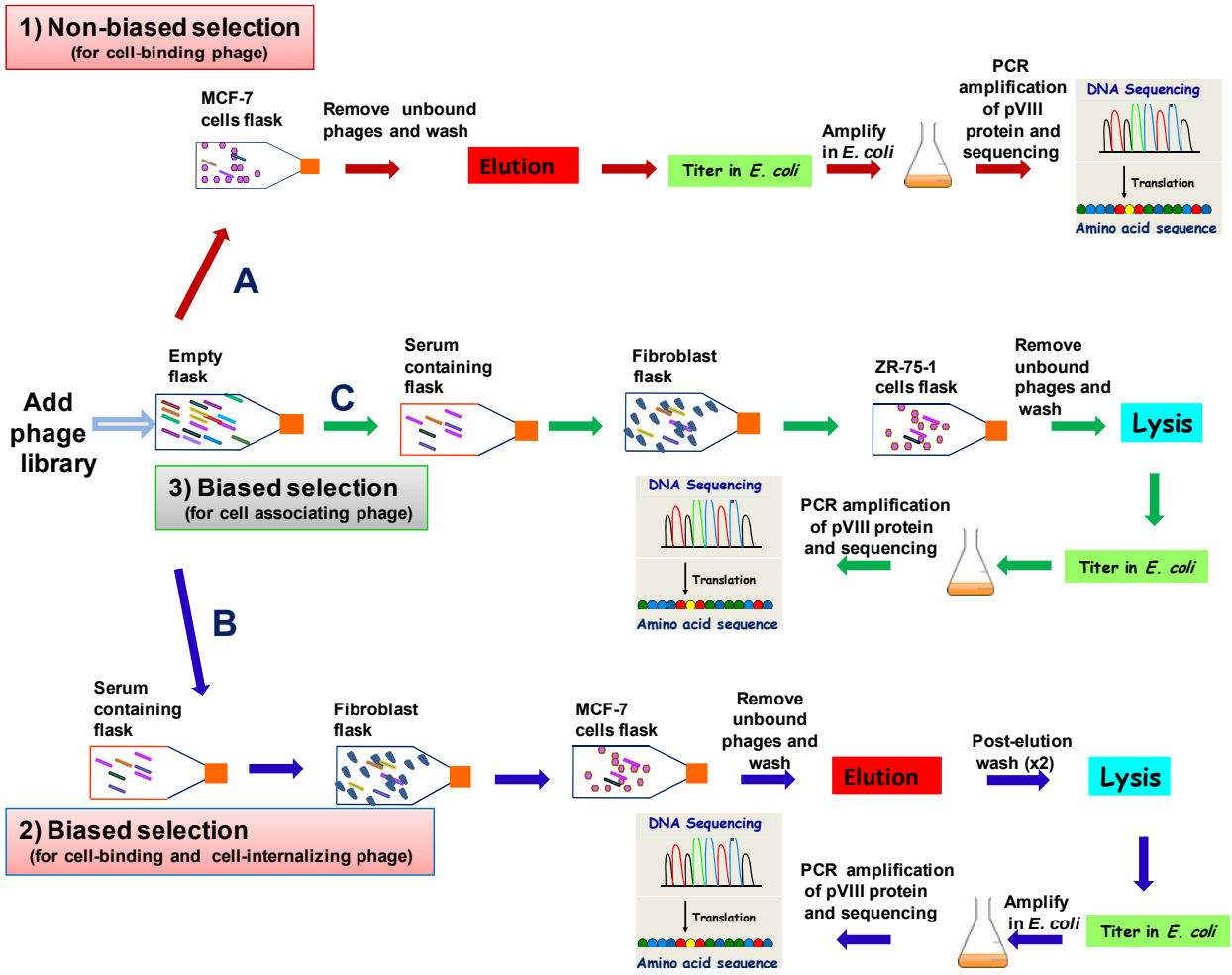

Figure 5. A schematic illustration of selection of landscape phage probes binding and or internalizing into breast cancer cell lines, MCF-7 and ZR-75-1. Pathways A, B or C depict non-biased, biased (acid and detergent extraction) or biased (detergent extraction) procedures, respectively.

C. Biased selection: detergent extraction of cell-interacting phage

The strategy of biased selection of phage probes for breast cancer cells was used to obtain a population of phage that interact with breast cancer cells. In this procedure, the phage library was depleted of phage clones binding cell culture flasks, serum or fibroblasts as described previously. Subsequently, the depleted sub-library was incubated with confluent mammary ductal adenocarcinoma cells (ZR-75-1) for 1 h at room temperature in serum-free

medium. Cell-interacting phages were recovered by lysing the cells with deoxycholate buffer, without preliminary treatment of cells with acid. The lysed fraction was amplified for further rounds of selection with no depletion steps. The ratio of output to input phage increased from one round to another indicating successful selection for phage clones that interact with ZR-75-1 cells. After four rounds of selection, phage clones were randomly picked from the plates. DNAs of randomly picked phage clones encoding to the oligonucleotide insert were amplified by PCR, sequenced and translated to reveal peptide sequences responsible for binding cancer cells. All peptides from three selection strategies were assigned into families based on their consensus peptide motifs.

3.4 Selectivity of phage clones for breast cancer cells**.**

Individual phage clones obtained using the three selection strategies were characterized further for their selectivity toward target cells MCF-7 and ZR-75-1 in comparison with control cells MCF-10A (non-neoplastic breast epithelia), HepG2 (hepatocellular carcinoma) and serum in a phage capture assay. Briefly, target cells (MCF-7, ZR-75-1), MCF-10A cells and HepG2 cells were cultivated in triplicate to confluence in separate wells of 96-well cell culture plates. Serum was incubated in separate wells in triplicate as a control. Cells incubated with serum-free medium at room temperature for 1 h were treated with phage probes (1×10^6 cfu) and incubated at room temperature for 1 h. Unbound phages were carefully removed and cells were washed with 100 µl washing buffer for 5 min eight times to remove non-interacting phages. Cells were lysed with 25 µl lysis buffer (2.5% CHAPS) for 10 min on a shaker. The lysate containing cell-interacting phages were titered in *E. coli.* Phage recovery was calculated as the ratio of output phage to input phage. An unrelated phage with non-relevant guest peptide VPEGAFSS was used as the control (Figure 6)

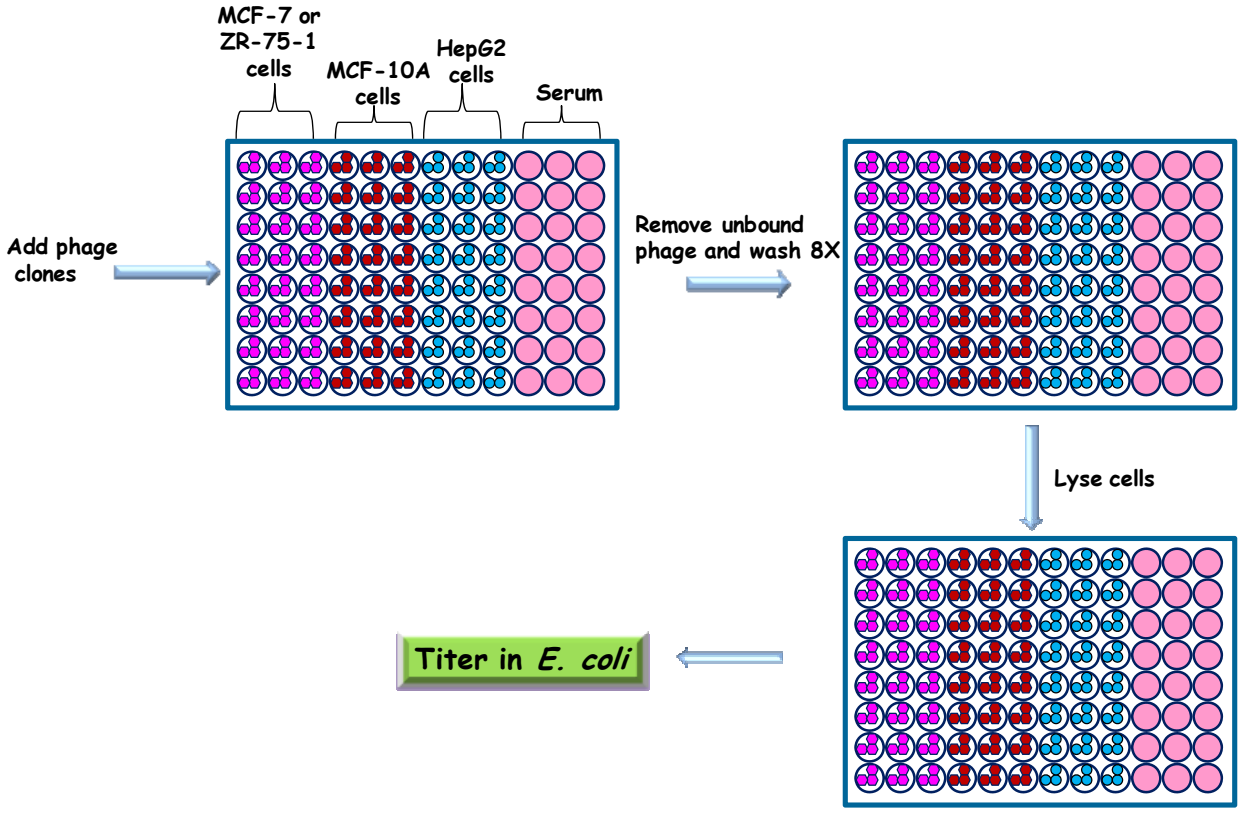

Figure 6. Phage selectivity towards targets cells in comparison with other cells. Selectivity is based on binding of phage guest peptides to receptors overexpressed on target cells in comparison with other cells (non-neoplastic breast epithelial cells, MCF-10A and hepatocellular carcinoma cells, HepG2) and serum. This was estimated as phage recovery (%) = output (cell-associated) phage/input phage. The unrelated phage bearing the peptide VPEGAFSS was used as the control.

3.5 Mode of phages interaction with breast cancer cells

To reveal how breast cancer selective phages interact with MCF-7 cells at different metabolic conditions, we used a phage capture assay in 96-well plates. An unrelated phage was used as the control. In this assay, eluate, PEW1, PEW2 and lysate were titered to determine the amount of phages in these fractions. The experiment was carried out at room temperature, at 37ºC without serum and at 37ºC with serum. Target cells (MCF-7) were cultivated in triplicate for each phage clone and grown to confluence in wells of 96-well cell culture plates. Cell culture

growth medium was aspirated from the wells containing the confluent cells and washed with serum-free growth media. Then, cells were incubated with 100 µl serum-free medium at room temperature for 1 h. Each phage clone (~10^6 cfu) was added in 100 µl blocking buffer to the corresponding well and incubated for 1 h at room temperature. Unbound phages were removed and the cells were washed with 100 µl washing buffer for 5 min, eight times, to remove any remaining unbound phage. Surface bound phages were recovered by treating wells with elution buffer (0.1 M glycine-HCl, pH 2.2). The eluate was neutralized with 4.7 µl neutralizing buffer (1 M Tris-HCl, pH 9.1). Wells were washed twice with 25 µl washing buffer for 5 min per wash. To retrieve internalizing phages, wells were treated with 25 µl lysis buffer (2.5% CHAPS (3-[(3-Cholamidopropyl)dimethylammonio]-1-propanesulfonate), 0.5% BSA) for 10 min on a shaker. The eluate, PEW1, PEW2 and lysate were titered in *E. coli* (K91 BlueKan) and phage recovery (%) = output (cell-associated) phage/input phage was calculated. The procedure was repeated a second and third time by changing the incubation conditions from serum-free room temperature to 37ºC serum free and at 37ºC in the presence of serum, respectively (Figure 7).

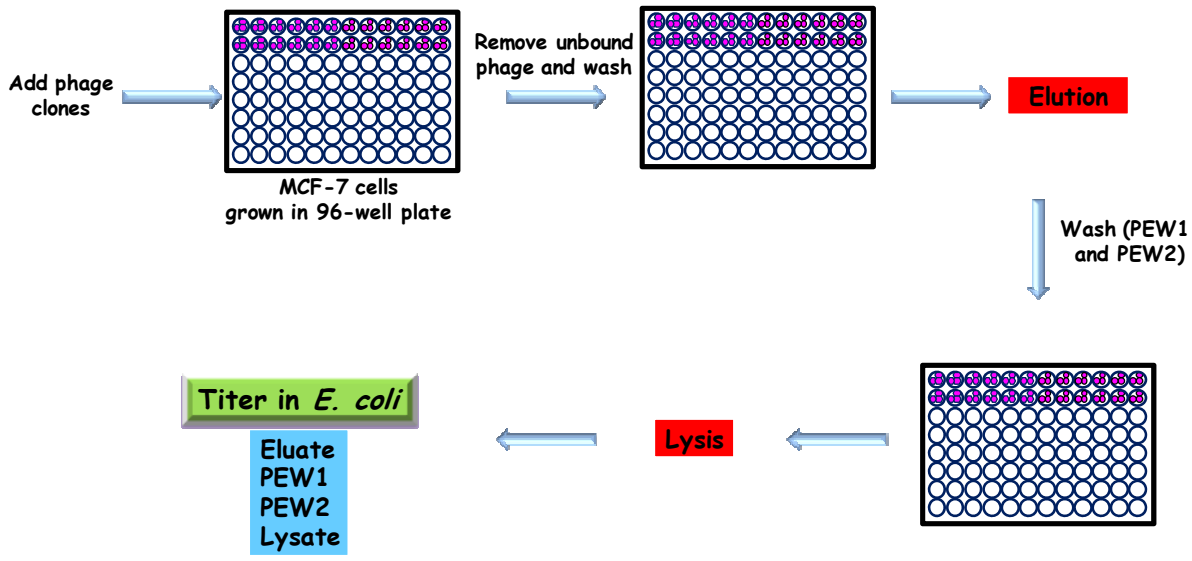

Figure 7. Mode of interaction of phages with intact MCF-7 cells in different metabolic conditions. The mode of interaction is based on binding of phages to unique macromolecules on the cell surface and/ or internalization of phages by mechanisms yet to be determined. Mode of interaction was estimated as phage recovery (%) = output (cell-associated) phage/input phage. *rtp-sf* represents room temperature-serum free, whereas *sf* and *s* depict serum-free and serum, respectively. The unrelated phage bearing the peptide VPEGAFSS was used as the control.

3.6 Analysis of breast cancer selective phage probes

Sequences of guest peptides from the breast cancer selective phages were statistically analyzed using RELIC (receptor ligand contacts) database, a suite of programs for the analysis of peptide populations. RELIC/POPDIV software was used to calculate the diversity of selected peptides.

4. Results

The eukaryotic cell surface is a landscape of macromolecules encompassing mainly receptors. Some receptors, underpresented in normal cells, have been observed to be overexpressed in neoplastic cells. To identify phage displayed peptides binding or mimicking cognate ligands to unique or overexpressed receptors in breast cancer cells, we used three

selection strategies based on screening two phage display libraries: f8/8 with an octapeptide insert and f8/9 with a nonapeptide insert, fused to the phage pVIII protein. The selected phages from the screens were characterized for selectivity toward breast cancer cells and the structures of their fusion peptides were analyzed using the RELIC suite of programs.

4.1 Selection of phages

The f8/8 library was employed to isolate phage clones binding MCF-7 breast cancer cells using non-biased selection and phage clones interacting with ZR-75-1 breast cancer cells using biased selection including acid and detergent extraction. Phage clones binding and internalizing into MCF-7 cells were also retrieved from f8/8 and f8/9 libraries using the biased (acid and detergent) selection strategies respectively (Table 1). Selections for the two libraries were run in parallel. For all three selection strategies, phage clones binding the cell culture flask were first depleted as a first step. However, in biased selection procedures, phage clones were further depleted against serum and then fibroblasts. For all selection strategies, cells were incubated with the target breast cancer cells, washed 10 times and cell binding phages were eluted. For the biased selection (acid) and biased selection (detergent), cells were washed twice and internalizing phages were retrieved with deoxycholate and CHAPS extraction, respectively. For every selection round, eluted phages, post-elution washing phages and internalized phages, each were titered in host *E. coli* (Figure 8).

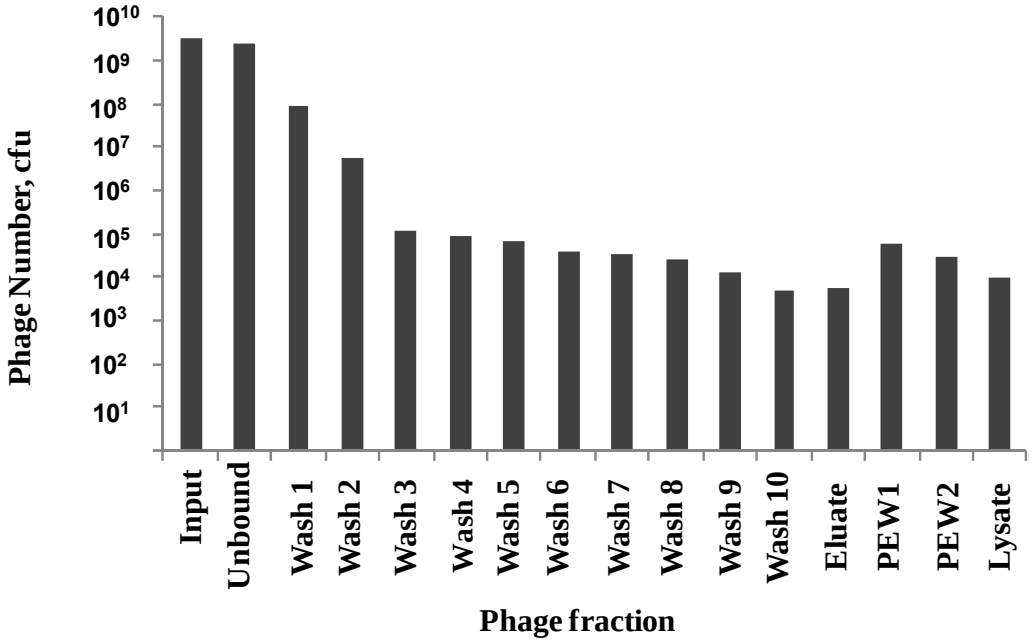

Figure 8. Representative data for titering of phage fractions at sequential steps of the biased screening procedure. Phages from each fraction were titered in host *E. coli* to confirm the specificity of the screening procedure. Specificity of screening is indicated by a gradual decrease in phage numbers from input through the washings followed by an increase in output (eluate).

The specificity of the selection or screening procedure is indicated by a gradual decrease in phage numbers from input through the washings followed by an increase in output (eluate). This increase may be due to specifically binding phage clones being eluted. For the two libraries, the PEW1 and PEW2 phage contents were observed to be higher than the eluate. This suggests that some of the internalized phage escaped from the cytoplasm into the post-elution washings due to a change in pH from acid elution (pH 2.2) compared to the washings (pH 7.0). After the fourth selection round, 100 phage clones obtained by titering of final eluates in *E. coli* from each library and each selection procedure, were randomly picked and their DNA corresponding to the region of the oligonucleotide insert were amplified by PCR, sequenced and translated to reveal the structures of amino acids responsible for their cell binding ability. In

total, 132 phage clones were isolated and classified into 40 families based on their consensus peptide motifs.

Table 1. Phage selection strategy. Three selection strategies were used to screen two phage libraries f8/8 and f8/9 against breast cancer cells MCF-7 and ZR-75-1.

Selection strategy	Phage library	Breast cancer cell	Depletion cell	Type of phage isolated
A. Non-biased selection (acid extraction)	f8/8 and f8/9	MCF-7	None	Cell-binding phages
B. Biased selection (acid and detergent extraction)	f8/8 and f8/9	MCF-7	Fibroblast	Cell-binding and internalizing phages
C. Biased selection (detergent extraction)	f8/8	ZR-75-1	Fibroblast	Cell-interacting phages

4.2 Selectivity of phage probes for breast cancer cells.

Phage clones obtained using three selection strategies were tested for their selectivity towards target cells MCF-7 and ZR-75-1 in a phage capture assay. Phage probes that preferentially bind MCF-7 cells and where recovery was at least 5 fold greater than those of MCF-10A and serum were considered selective for both breast cancer cells and hepatocellular carcinoma cells. Phage probes with recovery in MCF-7 cells of 3 times greater or more than that of HepG2 were considered selective for breast cancer cells. Using these criteria, 16 phage probes were found to be selective for breast cancer cells whereas 32 were found to be selective for both breast and liver cancer cells (Table 2 and Figure 9).

Table 2. Phage selectivity. Phage selectivity was based on the selective interaction of phages toward MCF-7 cells in comparison with controls, HepG2 (liver cancer), and MCF-10A (non-neoplastic epithelial) cells. Some consensus peptide motifs are indicated as colored letters.

Breast cancer selective	**Breast and liver cancer selective**	
AGTDAWSGD	DSSGSWSGD	DNLWLQGAD
EPQGNWSGD	DSSMSWSGD	DSSWMSTQD
VDWSSVSGD	GSSEVWSGD	GSDWMLGQD
DGNWLVGSD	GNSDAWSGD	VDYDMIGDQ
APTWSETSD	GSEQSWTGD	DNSMWAAQD
ESWSSSTSD	VEQASWTG	DMSYIASED
DMPGTVLP	EGSWTGSM	EGQSGIAYD
DNPNMYLD	DTGALWSS	DWRGDSMDS
GTGPLDSYD	DTNLWSSSD	DWQSGNVAD
ESAQLEGYD	DSYWAGNSD	DVYSLAYPD
VPTDTDYS	DSDFFTSQ	GTYQDPLPD
ETNLPWNDD	DTDFFTSQ	VVGDSDYNS
GHSLPPDM	ELVSMEGLD	VPSYDADPS
DGRENPLT	EYDGLDPNA	GWENNAATD
DSGFLLQSQ	EFGGAWSTD	DHSIPPSM
VEEGGYIAA	ESWQSSNLD	VDVGALEVM

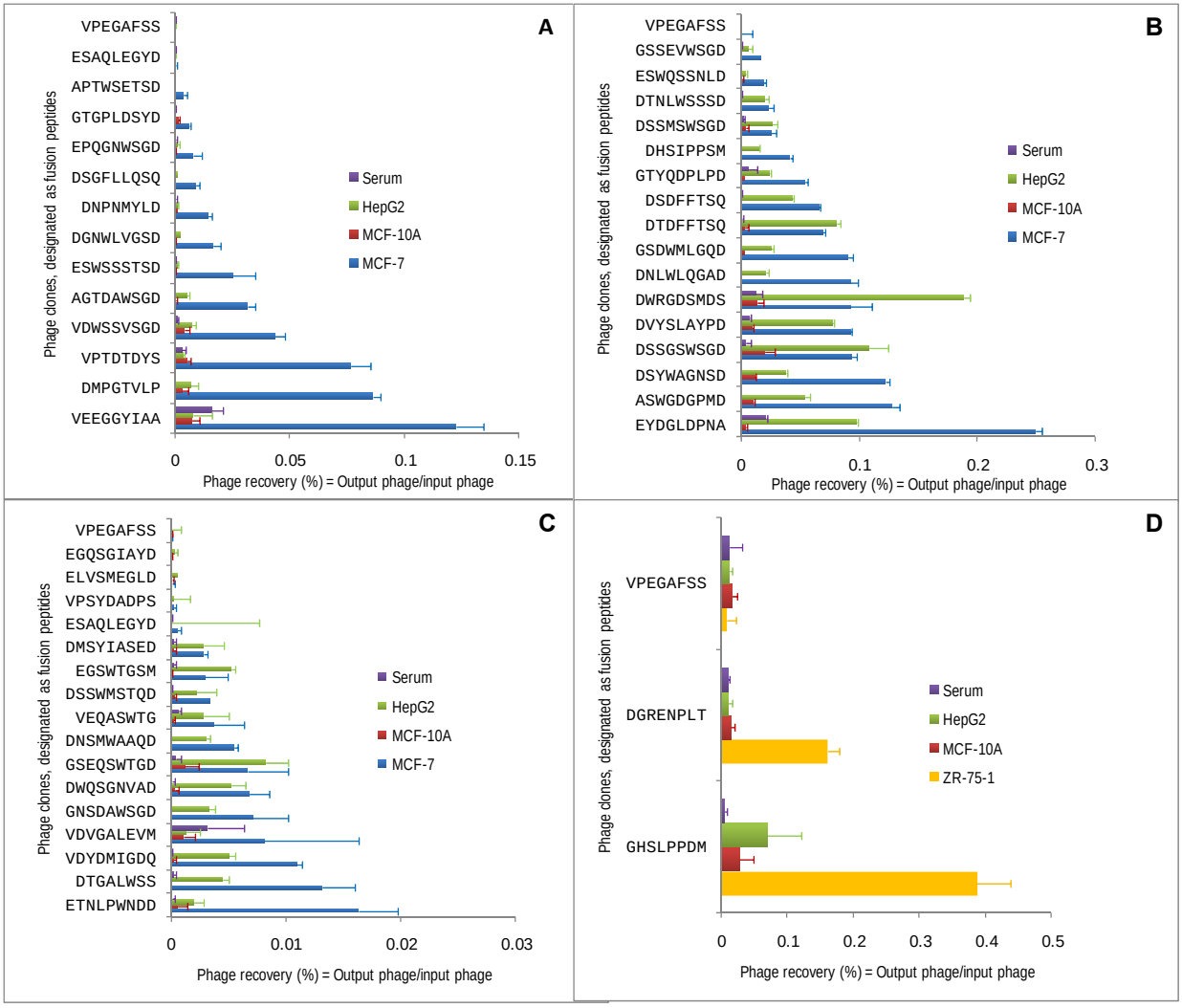

Figure 9. Selectivity of phages toward target cells MCF-7 and ZR-75-1. Selectivity of phage clones was based on ability of phage guest peptides to interact with receptors expressed on target cells in comparison with other cells (non-neoplastic breast epithelial cells, MCF-10A, hepatocellular carcinoma cells, HepG2) and serum. This was estimated as phage recovery (%) = output (cell-associated) phage/input phage. Unrelated phage bearing the peptide VPEGAFSS was used as the control. Panel A shows phages highly specific for breast cancer adenocarcinoma cells MCF-7, panels B and C reveal phages selective for both breast cancer adenocarcinoma cells and hepatocellular carcinoma whereas panel D shows phages highly selective for the breast cancer ductal carcinoma cells ZR-75-1.

4.3 Mode of interaction of phages with breast cancer cells

To study how breast cancer-selective phages interact with MCF-7 cells under different metabolic conditions, the interaction of seven breast cancer-selective phages was tested at room temperature, 37ºC without serum, and at 37ºC with serum as under materials and methods. An unrelated phage displaying the peptide VPEGAFSS was used as the control. The interaction of the seven phage probes with MCF-7 under the three experimental conditions is shown in Figure 10. Phage clone DWRGDSMDS including the RGDS motif was the best binder at room temperature, although at 37°C cell binding and presence in the PEW1, PEW2 and lysate was higher than at room temperature. The phage clone displaying the peptide VEEGGYIAA was the best binder at 37°C in the absence of serum and the most abundant in the PEW1, PEW2 and lysate. Phage clones with guest peptides VPTDTDYS and DMPGTVLP which were selected as binders were consistently found in the eluate, their abundance tended to increase with increase in temperature to 37°C and with treatment with serum. In contrast, for the phage clone displaying the peptide DHSIPPSM isolated from PEW1, the recovery this phage fraction in PEW1 and other fractions were almost the same at room temperature. However, increase in temperature to 37°C tended to increase its binding. The phage clone displaying the peptide DNLWLQGAD, isolated from the lysate (internalizing phage) fraction, was present in the lysate fraction at the same level as in PEW1 and PEW2 fractions at room temperature; however, the amount in the eluate fraction was higher. The phage clone bearing the peptide EFGGAWSTD, retrieved from the PEW2 fraction during selection appeared to be equally distributed between PEW2 and lysate fractions at room temperature. However, the interactions of phage clone GSDWMLGQD, isolated from the lysate fraction appeared to be the same under all three experimental conditions. In contrast to all of these selected clones the control phage VPEGAFSS did not show any significant interaction with MCF-7 cells under any of the three experimental conditions.

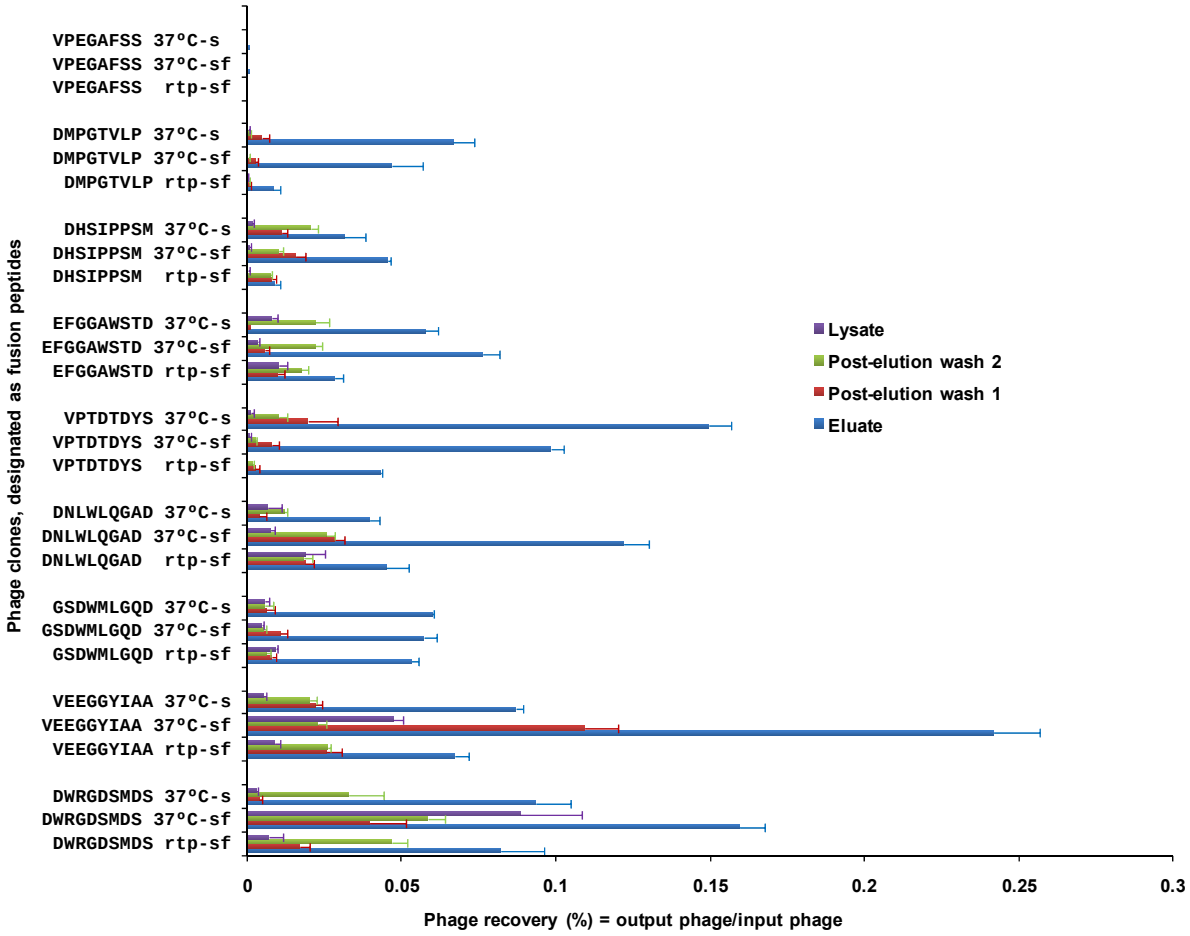

Figure 10. Mode of phage interaction with MCF-7 cells.
Mode of phage interaction with intact MCF-7 cells under three different metabolic conditions was evaluated. The mode of interaction was based on binding of phages to unique macromolecules on the cell surface and/or internalization of phages by mechanisms yet to be determined. Mode of interaction was estimated as phage recovery (%) = output (cell-associated) phage/input phage. *rtp-sf* represents room temperature-serum free, whereas *sf* and *s* depict serum free and serum, respectively. The unrelated phage bearing the peptide VPEGAFSS was used as the control.

4.4 Statistical analysis of breast cancer selected peptides

The RELIC suite of programs provides statistical analysis of small peptide population affinity selected for interaction with a target. RELIC confirmed that breast cancer selected peptides were specific for macromolecules or receptors on the surface of breast cancer cells. An

important indicator of effective selection of phages with displayed peptides is the reduction in diversity of peptide sequences selected compared to an equivalent number of randomly selected phages from the library. The RELIC POPDIV program revealed that the 59 peptides from the f8/8 primary libraries had a diversity of 0.00144±0.00077 while the 75 breast cancer-selected peptides from the f8/9 primary library had a diversity of 0.00071±0.00035. In contrast, the 73 random peptides from the f8/8 library and 62 random peptides from the f8/9 library had diversities of 0.00914±0.00449 and 0.00301±0.00165, respectively. The breast cancer selected peptides from the two libraries contained remarkably lower diversity compared to either unselected peptides.

5. Discussion

Generation of highly selective ligands to cancer cell receptors or macromolecules is important for precise diagnosis and treatment of malignancies. Screening of phage display libraries provides an easy and economic approach to generate highly specific and selective ligands to target cancer cells. Furthermore, screening of landscape phage libraries is advantageous because of their multivalent display of binding peptides that result in strong binding to the cells and high cell transduction efficiency (Ivanenkov et al., 1999). Phages specific for cell lines have been successfully selected from the multibillion landscape phage libraries (Romanov et al., 2001; Samoylova et al., 2003).

By screening the two landscape phage display libraries f8/8 (with octapeptide inserts) and f8/9 (with nonapeptide inserts) and using three selection techniques, we identified 132 phage clones able to bind, penetrate or internalize into breast cancer cells MCF-7 and ZR-75-1. Characterization of phage probes using a phage capture assay revealed phage probes highly selective for breast cancer cells and phage probes selective for both breast cancer cells and

hepatocellular carcinoma cells. The mode of interaction of phages with MCF-7 cells was studied under three different metabolic conditions. Some of the phages were assumed to internalize into MCF-7 cells by receptor mediated endocytosis whereas some may bind macromolecules or receptors without internalization.

The two of the three selection procedures employed in the screening procedure involved depletions of phages binding cell culture flasks, serum and fibroblasts with washing of unbound phages to achieve recovery thereby ensuring the high stringency required for target-specific phage selection. In the process of isolating cell internalizing phages, we also titered post elution washings. This novel approach resulted in the recovery of some phage probes also present in the lysate fraction (cell internalizing phages) and a phage probe with sequence DWRGDSMDS including the motif RGDS, known to bind integrins. We hypothesized that the change in pH in the elution step (pH 2.2) and the washings (pH 7.0) could have resulted in cell shock causing some of the already internalized phages to escape into the post-elution washings. This is corroborated by the fact that cell internalizing phage with the RGDS motif that may bind integrins has been isolated through screening of phage libraries against malignant melanomas and breast carcinoma (Pasqualini et al., 1997). The reduction in the diversity of the libraries through statistical analysis with RELIC POPDIV, confirmed the effectiveness of the three screening procedures in isolating our phage probes.

The selectivity of phage probes for breast cancer cells, in comparison with hepatocellular carcinoma, non-neoplastic breast epithelia and serum, were studied. Phage probes whose recovery from MCF-7 cells was at least 5-fold greater than those of MCF-10A and serum were considered selective for both breast cancer cells and hepatocellular carcinoma cells, whereas, phage probes recovered from MCF-7 cells at 3 times greater level than that of HepG2 were

considered selective for breast cancer cells. 16 phage probes were selective for breast cancer cells, whereas, 32 phage probes were selective for both breast cancer cells and hepatocellular carcinoma cells. Interestingly, some members of these two groups of phage probes encode one of the tripeptides, SGD, GSD, TSD, and TGD, which may be involved in binding a receptor common to both breast cancer cells and hepatocellular carcinoma cells (Table 3). To investigate the mechanism of binding or internalization of phage into MCF-7 cells, seven selective phage probes were studied under three different metabolic conditions. Our results demonstrated that the phage probes DWRGDSMDS encoding the motif RGDS and phage probe VEEGGYIAA could bind and penetrate intact MCF-7 cells. This characteristic was enhanced by a change in temperature from room temperature to 37ºC. However, this effect was reduced in the presence of serum, implying that serum may inhibit or compete with these phage probes. Based on the proposed mechanism of internalization of peptides encoding RGDS motifs by receptor mediated endocytosis (Ruoslahti, 1996), we can speculate that the phage probe VEEGGYIAA may also internalize into MCF-7 cells by receptor mediated endocytosis.

In contrast, phage probe GSDWMLGQD interactions with MCF-7 cells remained constant under all three metabolic conditions. This may be due to low expression levels or oversaturation of a cancer specific receptor or macromolecules that this peptide binds. The recovery of phage probe DNLWLQGAD isolated from the lysate (cell internalizing) fraction level was higher in the lysate fraction at room temperature confirming its propensity for internalizing into intact MCF-7 cells. Interestingly, phage probes VPTDTDYS and DMPGTVLP isolated from the eluate (cell binding) fraction showed higher levels in the eluate fractions when the temperature was increased from room temperature to 37ºC in the presence of serum. This result revealed that the specific avidity of these phage probes for cancer cells increases with

increase in temperature with or without serum. Phage probe DHSIPPSM recovery from the PEW1 also showed a relatively higher level in the PEW1 fraction at 37ºC. We speculate that this phage probe internalized into the cell and escaped from the cytosol into PEW1 fraction because of cell shock due to the change in the pH between the elution step and post elution washing 1. The mode of interaction of phage probe EFGGAWSTD recovered from the PEW2 fraction was similar to the phage probe DWRGDSMDS, also retrieved from the PEW2.This phage probe was probably localized in some cellular compartment such as the endosomes and perhaps escaped into the PEW2 fraction due to the speculated pH change. The phage probe can also be speculated to have interacted with a receptor possessing internalization ability. The control phage VPEGAFSS did not show appreciable interaction with MCF-7 cells.

In conclusion, we identified 16 phage probes selectively interacting with breast cancer cells and 32 interacting with both breast cancer cells and hepatocellular carcinoma cells. Some of the phage probes have both cell binding and penetrating properties. The phage probes were also speculated to bind to receptors expressed on the surface of breast cancer cells. The most prominent phage binders DMPGTVLP, DWRGDSMDS and GSDWMLGQD were chosen for further study as drug-targeting ligands, as described in chapter 3.

CHAPTER 3

NOVEL PHAGE PROTEINS FOR TARGETED DRUG DELIVERY TO BREAST CANCER CELLS

1. Abstract

The application of targeted nanomedicines for intracellular delivery of drugs has been proven to enhance therapeutic indices in both *in vitro* and *in vivo* studies. We have demonstrated the generation of breast cancer-specific phages by screening multibillion landscape phage display libraries and their successfully used to target Doxil™ to enhance drug efficacy. We discovered that two of the new phage coat proteins, once incorporated into Doxil™, increased specific cytotoxicity. Electron microscopy revealed the insertion of the phage proteins into Doxil™ membranes. Epifluorescence microscopy and flow cytometry confirmed the selectivity of the modified Doxil formulations toward MCF-7 cells in comparison with control MCF-10A cells. Cytotoxicity of phage protein DWRGDSMDS modified Doxil in MCF-7 cells was observed to be significantly higher than that of unmodified Doxil™ 24 h post-treatment. This further corroborates the effectiveness of targeting nanomedicines with phage coat proteins in improving drug delivery.

2. Introduction

The efficacy of anti-neoplastic drugs is often hindered by non-specific cytotoxicity to normal cells resulting in sub-optimal administration of drugs. Consequently, passive drug

delivery was developed to increase drug therapeutic window by site-specific delivery of drugs to target tissues. This is based on extravasations and permeation of drugs to the tumor interstitium which is limited to the tumor periphery. The resulting inability of nanomedicines to effectively permeate the interior of the tumor is an apparent drawback to this delivery approach (Vasir and Labhasetwar, 2005). As such, targeting of nanomedicines with various cancer-specific ligands is currently being studied to improve drug permeation into solid tumors. Antibody targeted delivery of nanomedicines to tumors has been demonstrated to improve drug potency but their use can be limited by inadequate tissue penetration, immunogenicity and selectivity in solid tumors (Schrama et al., 2006, Elbayoumi et al., 2007, Sawant et al., 2008). In the same vein, various antibody fragments and peptides have been applied to target nanomedicines to cancer cells (Park et al., 2001; Dharap et al., 2005; Law et al., 2006). For example, the RGD motif containing peptides that bind to integrins has been widely used for targeted delivery of nanomedicines both *in vitro* and *in vivo* (Arap et al., 1998; Zitzmann et al., 2002). Howbeit, targeting with peptides require their chemical conjugation to nanomedicines which may affect the structure and function of the peptide as a functional cell binding moiety.

We proposed the concept of exploring the multivalent display of proteins on landscape phages, which increases their avidity for target cells and, in addition, allows the use of intact fusion phage proteins with an intrinsic membranophilic feature to target nanomedicines. We have recently proved this concept wherein the cancer-selective phage protein DMPGTVLP was grafted into drug encapsulated liposomes (Doxil™) to enhance cytotoxicity to MCF-7 cells (Wang et al. 2010a). And, in a more recent study, this peptide was also demonstrated to translocate into the cell and exhibited endosomal escape (Wang et al. 2010b). Here, we applied

the same concept for targeting Doxil to MCF-7 cells with two new breast cancer-selective proteins DWRGDSMDS and GSDWMLGQD.

3. Materials and Methods

3.1 Cell lines and modified Doxil™ preparation

MCF-7 cell line (ATCC ,HTB 22™) was cultivated in 25 cm^2 cell culture flasks (Corning Inc., Corning, NY) in L-15 Leibovitz medium with L-glutamine (Sigma-Aldrich, St. Louis, MO) supplemented with 10% fetal calf serum in 5% CO_2 at 37°C.

Doxil™ (Ortho Biotech, Bedford, OH), stealth long circulating liposome encapsulated doxorubicin hydrochloride, was tagged with the isolated phage protein. The stealth liposome is composed of 3.19 mg/ml of N-(carbonyl-methoxypolyethelene glycol 2000)-1, 2-distearoyl-sn-glycero-3 phosphoethanolamine sodium salt (MPEG-DSPE), 9.58 mg/ml of fully hydrogenated of soy phosphatidylcholine (HSPC) and 3.19 mg/ml cholesterol. Doxorubicin hydrochloride with the generic name (8S,10S)-10-[(3-amino-2,3,6-trideoxy-α-L-lyxo-hexopyranosyl)oxy]-8-glycolyl-7,8,9,10-tetrahydro-6,8,11-trihydroxy-1-methoxy-5,12-naphthacenedione hydrochloride was encapsulated in the stealth liposome. The mixture also contains ammonium sulfate, histidine as a buffer, hydrochloric acid and/or sodium hydroxide for pH control and sucrose to maintain isotonicity.

3.2 Isolation and Purification of the Major Coat Protein

The major coat proteins of the phage probes: DWRGDSMDS and GSDWMLGQD were isolated and purified. Each phage probe was solubilized as described (Sprujit *et al*, 1989). Briefly, 350 µl containing 2.7 x 10^{13} virions in phosphate buffered saline was mixed with 700 µl cholate stabilizing solution (120 mM sodium cholate, 10 mM Tris-HCl, pH 8.0, and 0.2 mM EDTA) and 2.5% v/v chloroform. The suspension was incubated for 48 h at 37ºC with rotation.

Subsequently, the suspension was applied to a sepharose 6B-CL column (1 cm x 45 cm) (Amersham, Uppsala, Sweden) for gel exclusion chromatographic separation of the phage major coat proteins from phage DNA and cholate micelles. The major coat protein was eluted with the elution buffer (10 mM sodium cholate, 10 mM Tris-HCl and 0.2 mM EDTA, pH 8.0). The chromatographic profile was visualized with an Econo UV monitor (Bio-Rad, Hercules, California) and 5 ml fractions were collected using a Model 2110 Fraction Collector (Bio-Rad, Hercules, California). Concentration of protein in each fraction was determined using an ND-1000 spectrophotometer (Thermo Fisher Scientific, Wilmington, DE) and using DNAStar software (DNAStar Inc., Madison, Wisconsin) to predict protein concentration (mg/ml) at 1 A280 and molar extinction coefficients (liters/molecentimeter).

3.3 Preparation of coat protein modified liposomes

To append the major coat protein to Doxil®, 36 µg of phage coat protein, in 10 mM cholate, 10 mM Tris-HCl and 0.2 mM EDTA, was incubated with 450 µl Doxil® (~ 7.2 mg of phospholipids) in 1X TBS at 37°C for 16 h. Subsequently, cholate and non-inserted coat proteins were removed by dialysis against a gradually decreasing concentration of cholate in this fashion: 10 mM cholate in TBS (pH 7.4) for 1 h, 5 mM cholate in TBS for 1 h and with TBS containing no cholate overnight in a Slide-A-Lyzer Cassette (Thermo Scientific, Rockford, IL) with a cut-off size of 10,000 MWCO. Thereafter, the mixture was applied to a superose™ 6 column (1 cm x 30 cm; GE Healthcare Biosciences AB, Uppsala, Sweden) in 10 mM Tris-HCl, 0.2 mM EDTA (pH 8.0) to purify the modified Doxil. The chromatographic profile was visualized with an Econo UV monitor (Bio-Rad).

3.4 Transmission electron microscopy

To further demonstrate the grafting of phage coat protein into Doxil™, transmission electron microscopy was used. Briefly, 2 µM of DWRGDSMDS-Doxil or Doxil®, in 10 mM Tris-HCl, 0.2 mM EDTA (pH 8.0), was dispensed onto formvar-copper coated grids (Ted Pella Inc, Redding, California) and allowed to stand for 20 min. Excess sample were removed and the grid was allowed to dry and observed using a Zeiss EM10 transmission electron microscope (Carl Zeiss SMT Inc., Peabody, MA).

3.5 Estimation of doxorubicin concentration in unmodified and modified Doxil™

Doxil® (20 mg/10 ml) was treated with an equal volume of 1% Triton-X for 15 min. Two-fold serial dilution of the mixture was made in 1X PBS. Thereafter, absorbance of the dilutions at 490 nm was obtained and used to plot a standard curve. The curve was used to extrapolate the various concentrations doxorubicin in the modified Doxil®

3.6 Specificicty and selectivity of modified Doxil toward MCF-7 cells

To study the specific and selective interaction of phage modified Doxil toward MCF-7 cells in comparison with MCF-10A, cells epiflourescence microscopy, flow cytometry and electron microscopy were used.

3.7 Optimization of Doxil™ concentration for flow cytometry and microscopy

Serial dilutions of a phage modified-Doxil (DWRGDSMDS-Doxil) was made and incubated with 1 x 10^6 MCF-7 cells at 37ºC with rotation for 1 h. Then, the cells were washed with Improved MEM (Zn^{++} Option) and filtered using a 50 µm CellTrics filter (Partec GmbH, Germany) and analyzed on a MoFlo flow cytometer in the green (530/40 nm) and orange (580/30 nm) channels. Summit 5.2 software (Dako, Carpintera, CA) was used for analysis. Mean channel fluorescence values were plotted against the different concentrations of phage modified Doxil™.

3.8 Demonstration of enhanced interaction of modified doxil with MCF-7 cells using flow cytomtery and epifluorescence microscopy.

For flow cytometry, 7.3 x 10^5 MCF-7 cells were incubated with their respective doxil formulations, unmodified doxil, DWRGDSMDS-doxil and GSDWMLGQD-doxil; each encapsulating 50 μM doxorubicin for 90 min at 37ºC, 5% CO_2. Subsequently, cells were washed with Improved MEM (Zn^{++} Option) and filtered using a 50 μm CellTrics filter (Partec GmbH, Germany) and doxorubicin fluorescence was measured on a MoFlo flow cytometer in the orange channel (580/30 nm). Summit 5.2 software (Dako, Carpintera, CA) was employed for analysis.

For microscopy, 2.7 x 10^5 MCF-7 cells were seeded into chamber slides and grown until 90% confluent. Cells were washed with Hanks balanced salt solution (pH 7.4). Phage modified Doxil and Doxil™ encapsulating 50 μM of doxorubicin in serum free Leibovitz' L-15 medium was dispensed into their respective wells and incubated for 4 h at 37ºC, 5% CO_2. Subsequently cells were washed with PBS (pH 7.4) fixed in 4% paraformaldehyde for 15 min and overlayed with DAPI (4', 6-diamidino-2-phenylindole) nuclear stain for 15 min. Thereafter, cover slips were mounted on slides and the preparations were observed using a Cytoviva® microscope system (Cytoviva Inc., Auburn, AL) at X 40 magnification using triple band pass (for DAPI, FITC and PE) filters. Images were captured using the DAGE® software (DAGE exponent, Michigan City, IN).

3.9 Modified doxil selectivity toward MCF-7 cells using flow cytometry and epifluorescence microscopy

Target MCF-7 cells and control MCF-10A cells were cultivated in 75 cm^2 cell culture flasks (Corning Inc., Corning, NY) until confluence. Subsequently, cells were dislodged by trypsinization and suspended in 1 ml of GIBCO™ Improved MEM (Zn^{++} Option) liquid. MCF-

10A cells were stained with 5-chloromethylfluorescein diacetate (CellTracker™, Green CMFDA; Molecular Probes, Carlsbad, CA). Equal numbers of MCF-7 and MCF-10A cells (7.3 x 10^5 cells each) were mixed and incubated with modified Doxil encapsulating 50 μM doxorubicin for 90 min at 37ºC, 5% CO_2. Cell mixtures treated likewise, but incubated only with unmodified Doxil™ served as the control. After incubation, cells were washed with Improved MEM (Zn^{++} Option) and filtered using a 50 μm CellTrics filter (Partec GmbH, Germany) and Green CMFDA and doxorubicin fluorescence measured on a MoFlo flow cytometer in the green (530/40 nm) and orange (580/30 nm) channels, respectively. Summit 5.2 software (Dako, Carpintera, CA) was used for analysis.

For microscopy, equal amounts of MCF-7 cells and Green CMFDA cells (2.7 x 10^5) were prepared as described for flow cytometry. After incubation, cells were seeded into slide chambers and incubated for 15 min. Subsequently, cells were washed with PBS (pH 7.4) fixed in 4% paraformaldehyde for 15 min and stained with DAPI nuclear stain for 15 min. Thereafter, cover slips were mounted on slides and the preparation was observed using a Cytoviva® microscope system (Cytoviva Inc., Auburn, AL) at 40X magnification using triple band pass (for DAPI, FITC and PE) filters. Images were captured using DAGE® software (DAGE exponent, Michigan City, IN).

4.0 Cytotoxicity kinetics assay

MCF-7 cells (ATCC, HTB 22™) were grown in L-15 Leibovitz medium with L-glutamine (Sigma-Aldrich, St. Louis, MO) supplemented with 10% fetal calf serum in 75 cm^2 cell culture flasks (Corning Inc., Corning, NY) at 37°C, 5% CO_2. After 75% confluence, cells were trypsinized with 0.25% trypsin and 0.1% EDTA for 5 min and suspended in L-15 Leibovitz medium. Cells were centrifuged at 1000 rpm (Beckman Coulter Allegra™ 21R Centrifuge; Rotor

S4180) for 5 min and re-suspended in L-15 Leibovitz medium. Cells were seeded into 96-well culture plates at a density of 4 x 10^4 cells/well and cultivated at 37°C, 5% CO_2 until 60% confluence. Afterwards, L-15 Leibovitz medium was removed from the cells and washed with 100 µl of Improved MEM $Zinc^{++}$ (Richter's Modification) liquid (Invitrogen, Carlsbad, CA) with L-Glutamine, L-Proline at 2 mg/ml, gentamicin sulfate at 50 µg/ml, without phenol red and supplemented with 10% fetal calf serum. 100 µl of Improved MEM ($Zinc^{++}$ Option) containing Doxil formulations (modified or unmodified as control) containing 24 µM of doxorubicin was dispensed into the corresponding wells, in triplicate, and incubated at the following time intervals: 4, 12 and 24 h. Cells incubated with Improved MEM ($Zinc^{++}$ Option) alone served as the cell control for cell viability. Subsequently, Doxil formulations were aspirated from the wells at their allocated the time and washed twice with Improved MEM ($Zinc^{++}$ Option). Then, 100 µl of Improved MEM ($Zinc^{++}$ Option) containing 20 µl of CellTiter 96® AQ_{ueous} One Solution Reagent was dispensed to all cells and incubated for 90 min at 37°C, 5% CO_2. Thereafter, absorbance was read at 490 nm using a TECAN SpectraFluor Plus®. The average absorbance value of the culture medium background was subtracted from all absorbance value of experimental wells.

4.1 Statistical analysis

Statistical analyses of results were performed using Statistical Analysis System (SAS) software. Means of data were represented as means ± STD and were compared using the Student's t- test. Results were considered statistically significant if the p-value was less than 0.05.

4. Results

4.1 Isolation and Purification of the Major Coat Protein

Phage coat proteins were solubilized using a detergent solution containing sodium cholate and chloroform. The proteins were purified by elution with sodium cholate using a gel size exclusion chromatography strategy. The DNA fraction profile was observed first followed by the coat protein fraction. The third fraction could be detergent micelles and some bacterial contaminants (Figure 12). The DNA and protein content purity in fraction was determined using UV spectroscopy (A_{260}/A_{280} ratio)

A

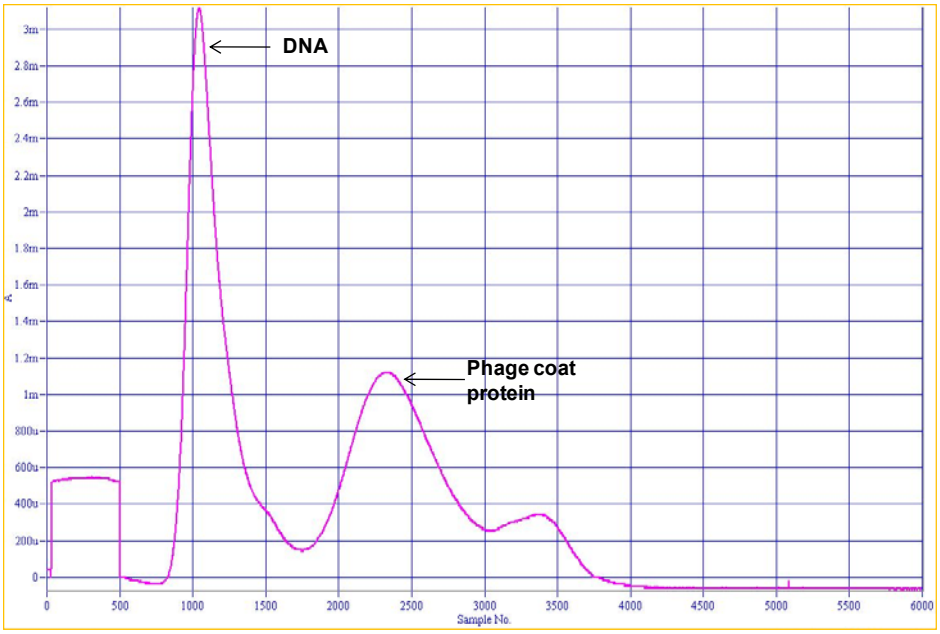

B

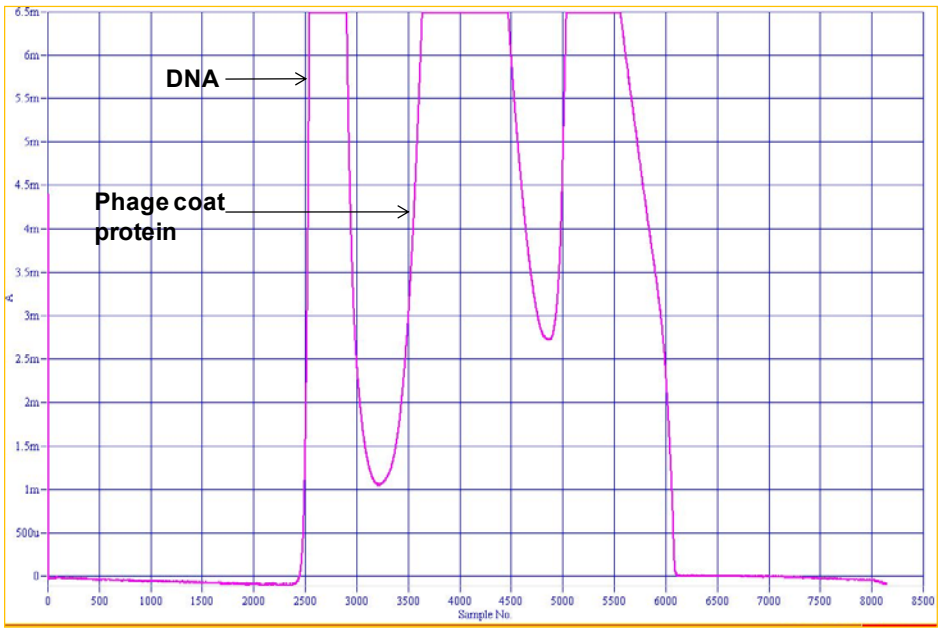

Figure 11. Gel size exclusion chromatogram of solubilized phage coat proteins. Panels A and B depict the chromatograms of phage probes DWRGDSMDS and GSDWMLGQD, respectively. The fractions were eluted with sodium cholate on a sepharose column.

4.2 Preparation of coat protein modified liposomes.

Modified liposomes were prepared by incubating Doxil with phage coat proteins in the presence of 15 mM sodium cholate that does not lead to disruption of Doxil, however, does allow solubilization of proteins and facilitates their spontaneous insertion into liposomes. Subsequently, gradient dialysis with decreasing concentrations of sodium cholate was applied to ensure uniformity in protein integration into Doxil. Finally, gel size exclusion chromatography was used to obtain purified phage coat protein modified Doxil. The presence of a single peak of targeted Doxil in the chromatographic profile demonstrated the effectiveness of the procedure.

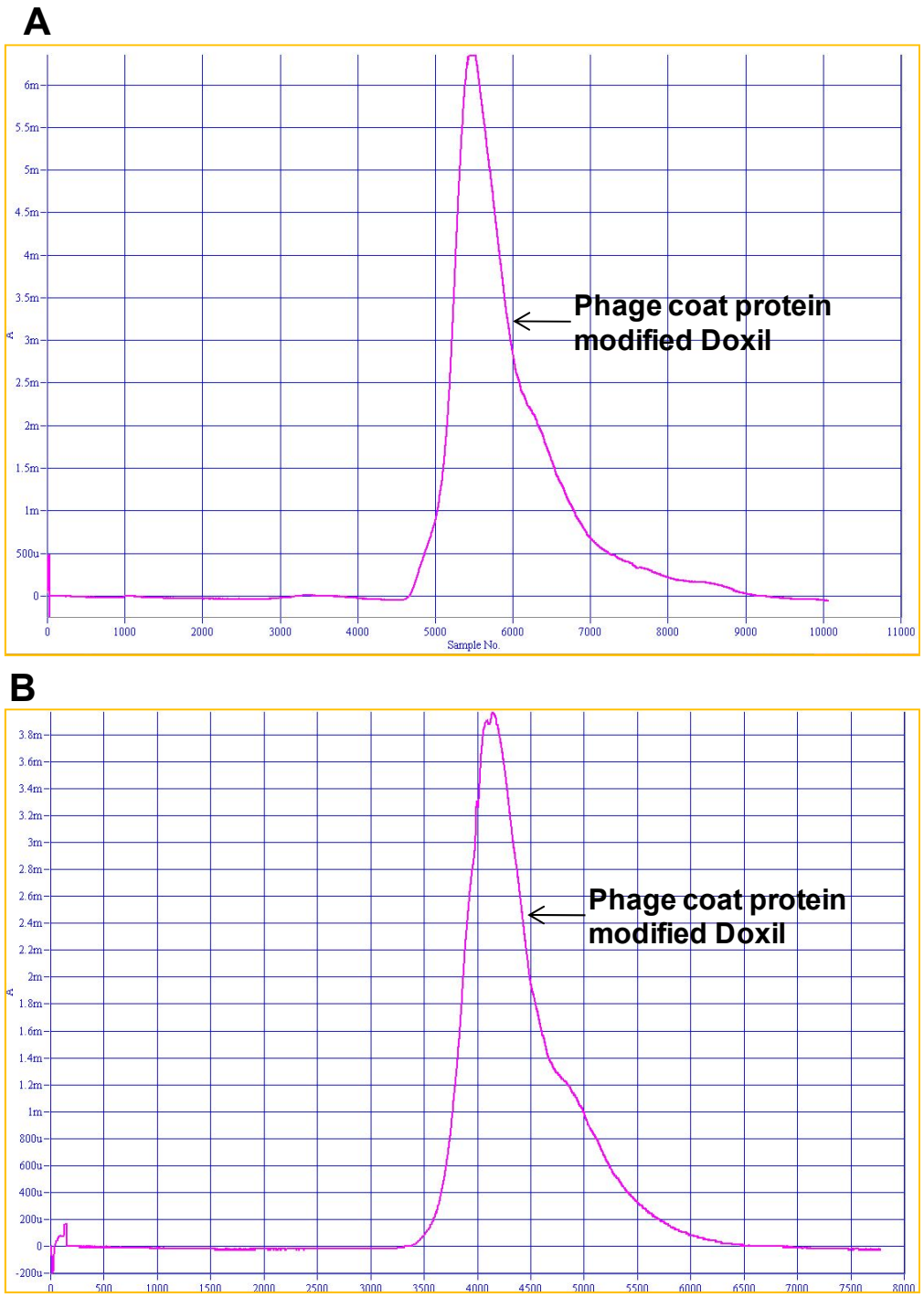

Figure 12. Gel size exclusion chromatogram of phage coat protein modified-Doxil. Panels A and B depict the chromatograms of phage probe DWRGDSMDS-Doxil and GSDWMLGQD-Doxil, respectively. Modified liposomes were eluted as a single peak using Tris-HCl (pH 8.0) on a superose column.

4.3 Transmission electron microscopy

Transmission electron microscopy was used to validate the grafting of the coat protein onto Doxil. The black dots in panel B are phage coat proteins binding or internalizing into Doxil™. The control unmodified Doxil™ showed no black dots on their surfaces.

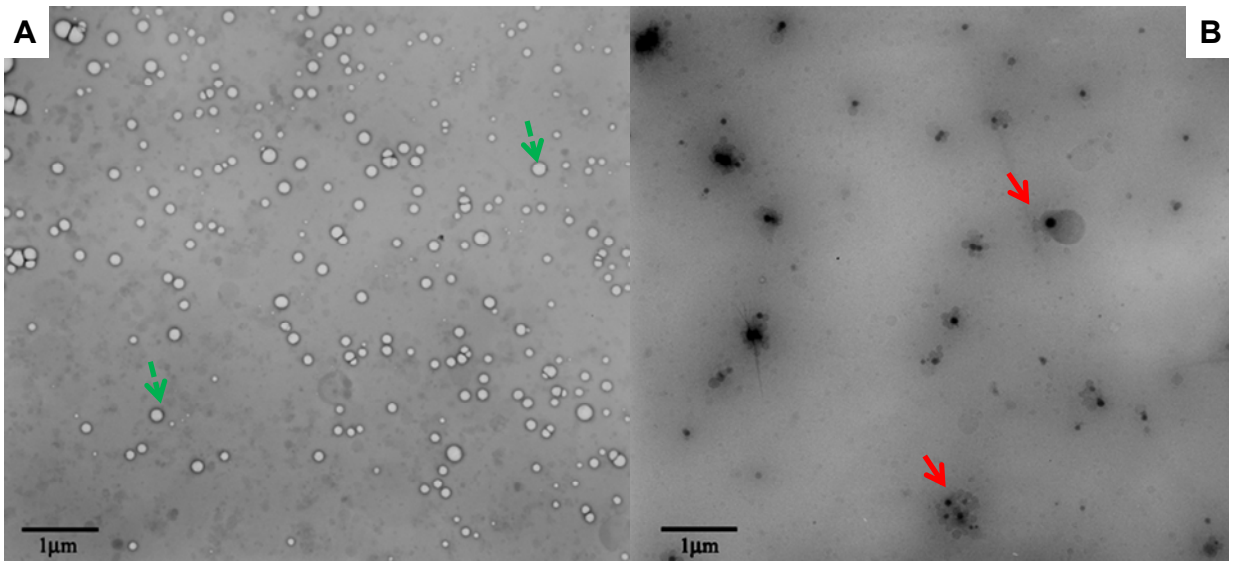

Figure 13 Electronmicrograph of Doxil and DWRGDSMDS-modified Doxil. The dotted green arrows in panel A point to Doxil™ whereas the bold red arrows in panel B indicate phage modified Doxil.

4.4 Doxorubicin concentration estimation

To estimate the concentration of modified Doxil to be used in selectivity and cytotoxicity procedures, the known concentration of doxorubicin in Doxil was used to generate the coefficient of determination (r^2), which was used to extrapolate the concentration of modified Doxil. Serial dilutions of Doxil were made and their absorbance values at 490 nm were plotted against doxorubicin concentrations to determine r^2 as 0.992 (Figure 14).

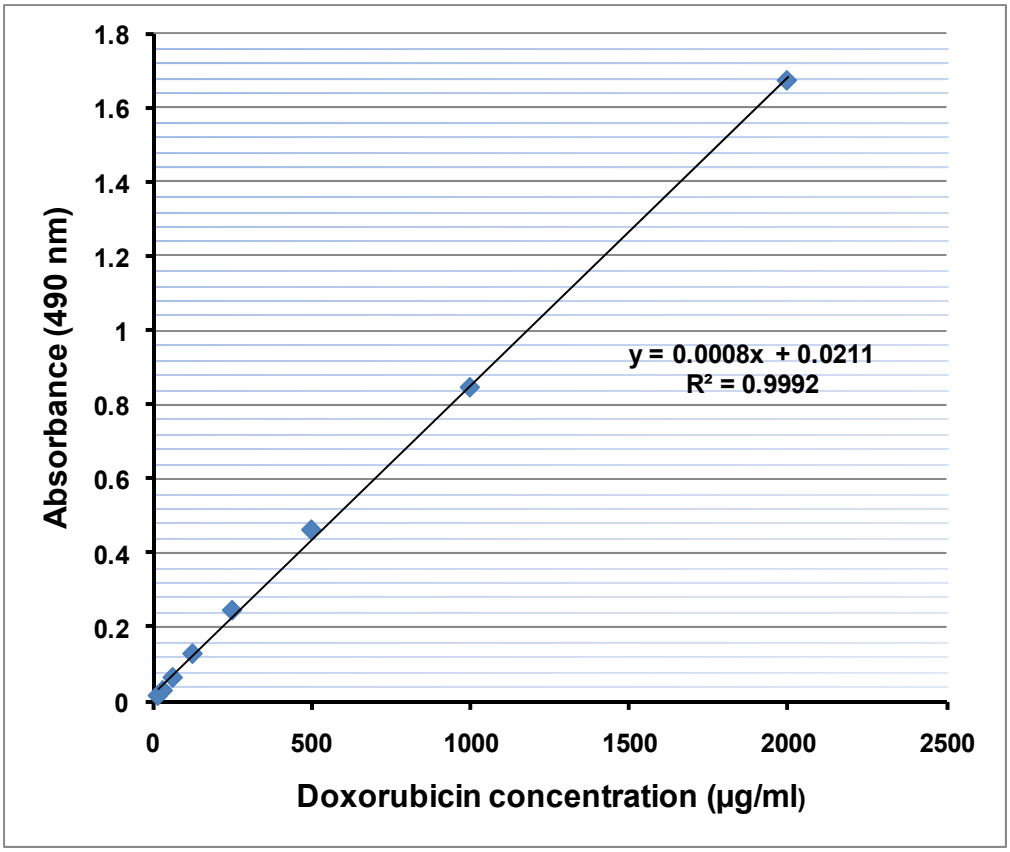

Figure 14. Estimation of the concentration of modified Doxil. Doxil® was treated with an equal volume of 1% Triton-X-100 and 2-fold serial dilutions of the mixture were made in 1X PBS. The absorbance of the dilutions at 490 nm were obtained and used to plot the standard curve.

4.5 Enhanced interaction and selectivity of modified Doxil toward MCF-7 cells

Enhanced and selective interactions of phage modified Doxil with MCF-7 cells in comparison with Doxil were studied using epiflourescence microscopy, flow cytometry and electron microscopy.

4.6 Optimization of Doxil™ concentration for flow cytometry and microscopy

Flow cytometry was used to determine the optimum concentration of modified Doxil to be used in modified Doxil interaction and selectivity towards MCF-7 cells. The procedure was as outlined above.

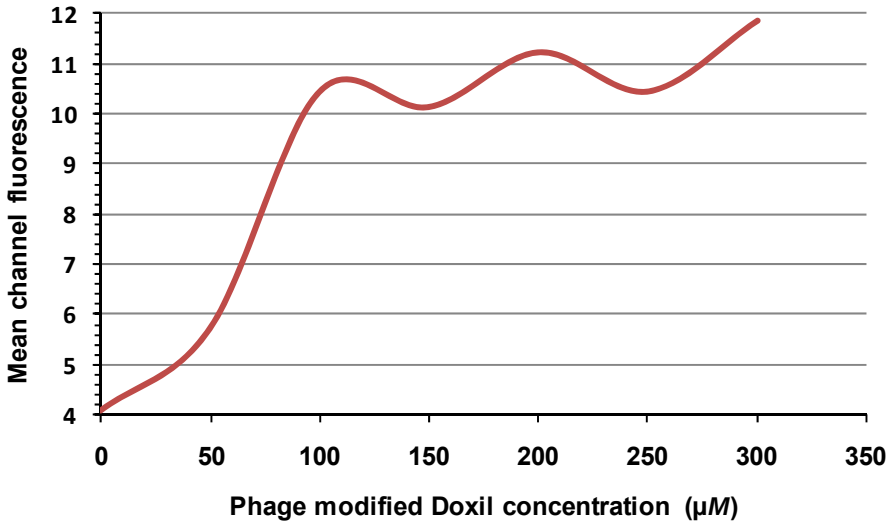

Figure 15. Optimization of Doxil™ concentration. Mean channel fluorescence of DWRGDSMDS-Doxil treated MCF-7 cells was used to obtain the optimum concentration of modified Doxil to be used for flow cytometry and epifluorescence microscopy. MCF-7 cells were treated with phage modified Doxil concentrations ranging from 50 µM to 300 µM and the mean channel fluorescence of treated cells were measured using flow cytometry.

4.7 Demonstration of enhanced interaction of modified Doxil with MCF-7 using flow cytometry and epifluorescence microscopy.

Enhanced interaction of phage modified Doxil with MCF-7 cells in comparison with the unmodified Doxil™ was demonstrated using flow cytometry (Figures 16 and 17) and epifluorescence microscopy (Figure 18). MCF-7 cells were treated with modified Doxil encapsulating 50 µM doxorubicin for 90 min at 37ºC. The enhanced interaction of the modified Doxil was expected to promote increased doxorubicin fluorescence of treated cells in comparison with the control unmodified Doxil™ treated cells.

In flow cytometry, the enhanced interaction of the two phage protein modified Doxil preparations with MCF-7 cells were demonstrated by increased doxorubicin fluorescence in the orange channel (Figures 16 B1-B2; C1-C2 and 17) in comparison with unmodified Doxil treated cells (Figures 16 A1-A2 and 17). The scatter of orange dots in panel A1 was due to doxorubicin

fluorescence whereas the unstained cells showed no fluorescence. In panel A2, the shift of the orange peak to the right indicates doxorubicin fluorescence of Doxil™ treated MCF-7 cells. The orange dots and peak in A1 and A2 depicting doxorubicin fluorescence of unmodified Doxil (Doxil™) treated MCF-7 cells served as the control for the phage modified Doxil treated cells in panels, B1-B2 and C1-C2. Flow cytometric analysis of phage DWRGDSMDS modified Doxil revealed, an increase in forward scatter of orange dots in B1 and also a higher orange peak in B2 compared to the controls A1 and A2. Also, for GSDWMLGQD modified Doxil treated MCF-7 cells, an increase in the forward scatter of orange dots in C1 and a higher orange peak in C2 in comparison with the control (A1 and A2) were observed.

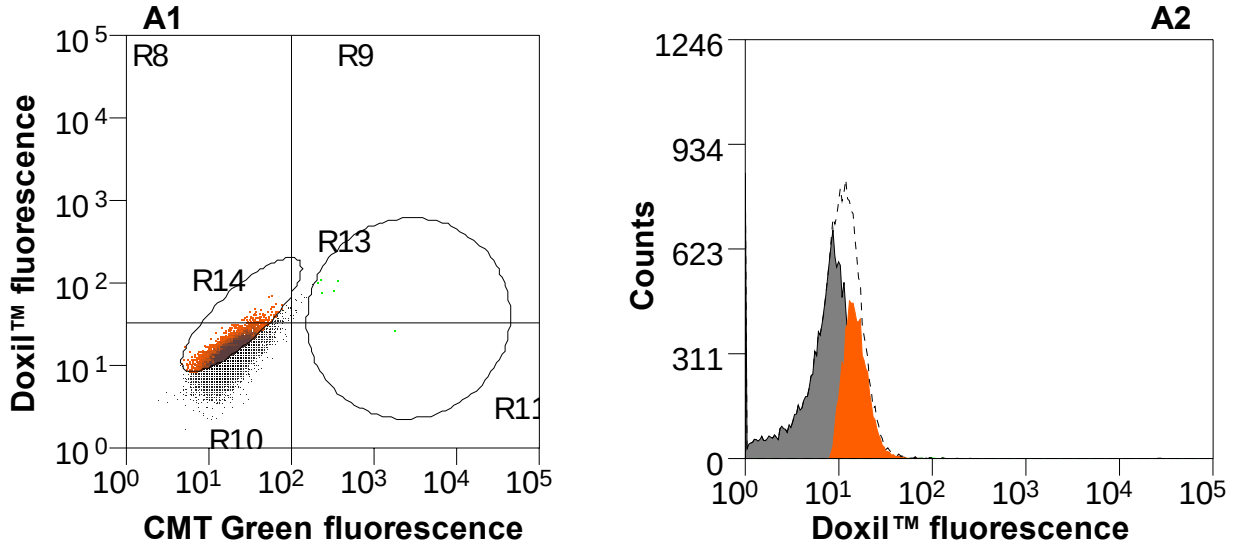

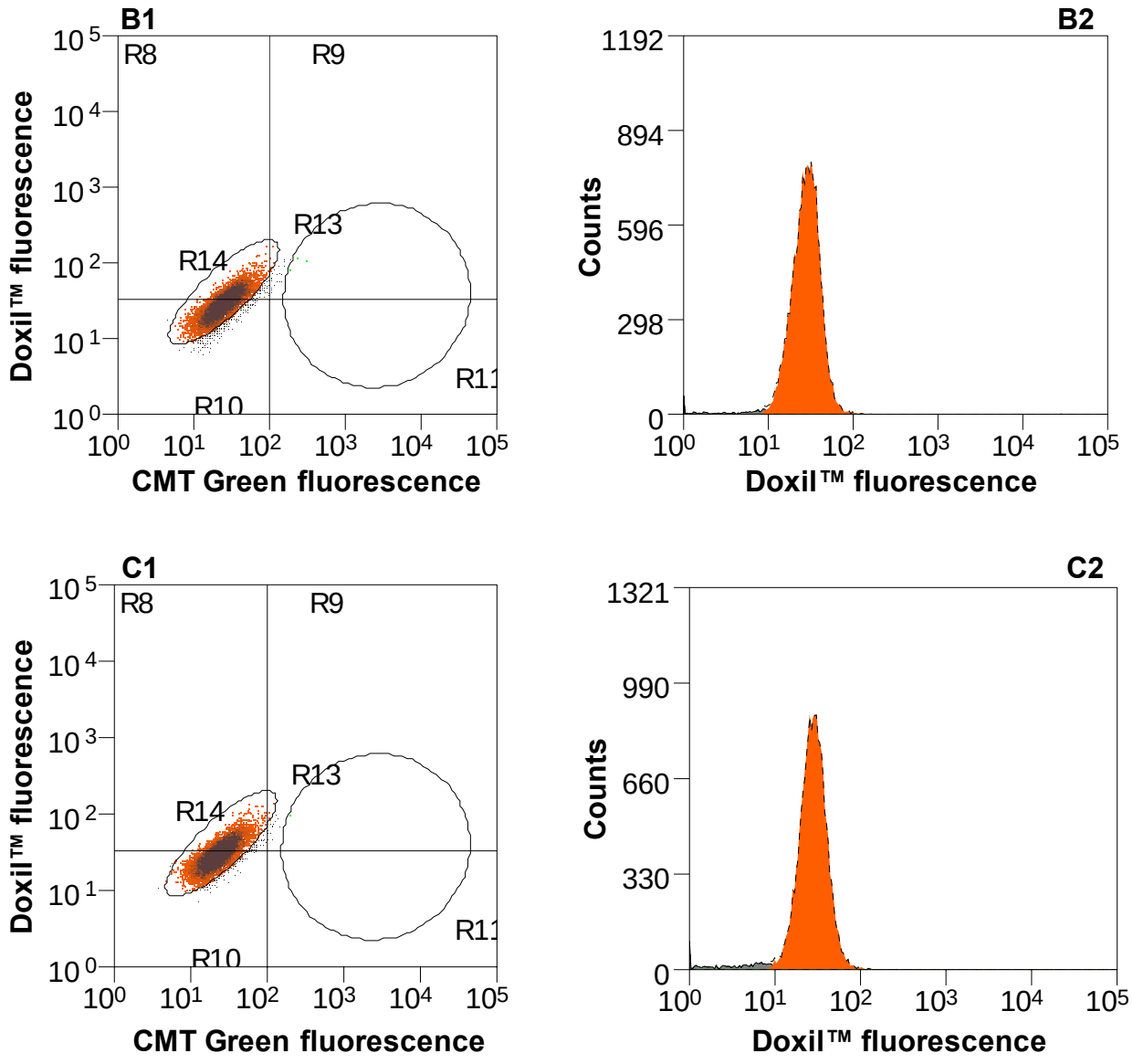

Figure 16. Enhanced interaction of modified Doxil with MCF-7 breast cancer cells. MCF-7 cells were treated with unmodified Doxil™ and phage protein modified Doxil, DWRGDSMDS-Doxil and GSDWMLGQD-Doxil for 90 min at 37ºC. Doxorubicin fluorescence of treated cells were evaluated by flow cytometry in 580/30 nm channel (orange). (**A**) Flow cytometric analysis of Doxil™ treated MCF-7 cells. Doxorubicin fluorescence is shown in panels A1 and A2 as orange dot plots and histogram, respectively; the black dots and gray histogram illustrate the untreated MCF-7 cells serving as the baseline. **(B)** Flow cytometric analysis of DWRGDSMDS-Doxil treated cells. Doxorubicin fluorescence are depicted in panel B1 and B2 as orange dot plots and histogram, respectively. (**C)** Flow cytometric analysis of GSDWMLGQD-Doxil treated MCF-7 cells. Panels C1 and C2, orange dot plots and histogram represent doxorubicin fluorescence of treated cells.

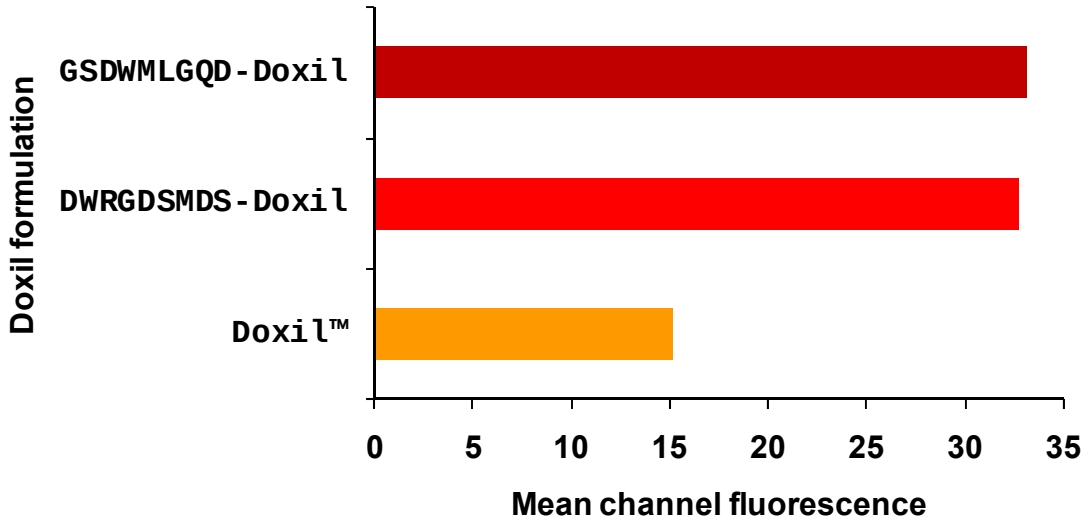

Figure 17. Mean channel fluorescence of MCF-7 cells treated with three different Doxil formulations. MCF-7 cells were treated equal concentrations DWRGDSMDS-doxil or GSDWMLGQD-doxil for 90 min. Cells treated with the unmodified Doxil™ served as the control. Mean channel fluorescence of the cells were determined using flow cytometric analysis.

The enhanced interaction of modified Doxil MCF-7 cells was further demonstrated using epifluorescence microscopy (Figure 18). MCF-7 cells were incubated with two modified Doxil preparations, DWRGDSMDS-Doxil or GSDWMLGQD-Doxil at 37ºC for 4 h. The unmodified Doxil cells and the untreated cells served as controls. The orange fluorescence indicates doxorubicin fluorescence whereas the blue fluorescence indicates DAPI nuclear fluorescence. Enhanced interaction of modified Doxil preparations with MCF-7 cells was demonstrated by increase in fluorescence of intra-cytoplasmic and perinuclear fluorescence of cells in panels C and D in comparison with unmodified Doxil treated cells and untreated cells in panels B and A, respectively (Figure 18)

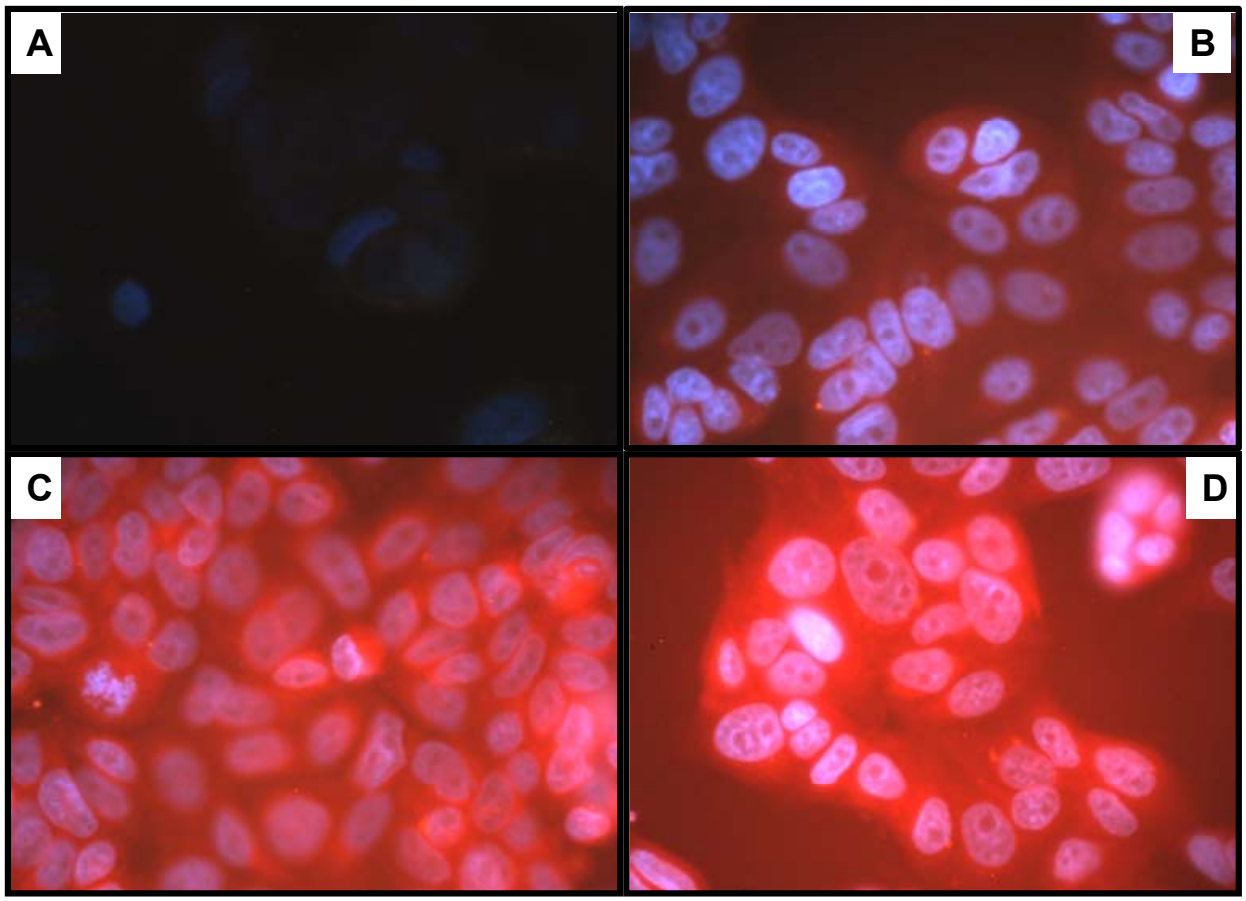

Figure 18. Epifluorescence microscopic demonstration of enhanced interaction of modified Doxil with MCF-7 cells. Panel A shows untreated MCF-7 cells whereas panels B, C and D show Doxil™, GSDWMLGQD-Doxil and DWRGDSMDS-Doxil treated MCF-7 cells, respectively. Cells were fixed, counterstained with DAPI and observed under the triple-band pass filter.

4.8 Analysis of selectivity of modified Doxil toward MCF-7 cells using flow cytometry and epifluorescence microscopy

Flow cytometry and epifluorescence microscopy were employed to demonstrate the selectivity of modified Doxil formulations toward MCF-7 cells in comparison with control MCF-10A cell, (non-neoplastic breast epithelial cells) and unmodified Doxil™. In flow cytometry, the selective interaction of the two phage protein modified Doxil preparations toward MCF-7 cells in comparison with control Green CMFDA-stained MCF-10A cells was revealed by increased doxorubicin fluorescence in the orange channel (Figures 19, B1-B2; C1-C2, and 20) in

comparison with unmodified Doxil treated cells showing increased green fluorescence (Figures 19, A1-A2, and 20). In other words, the modified Doxil interacted with MCF-7 cells more frequently than with the Green CMFDA-stained MCF-10A cells whereas the unmodified Doxil (Doxil™) interacted more frequently than with the Green CMFDA-stained cells than MCF-7 cells.

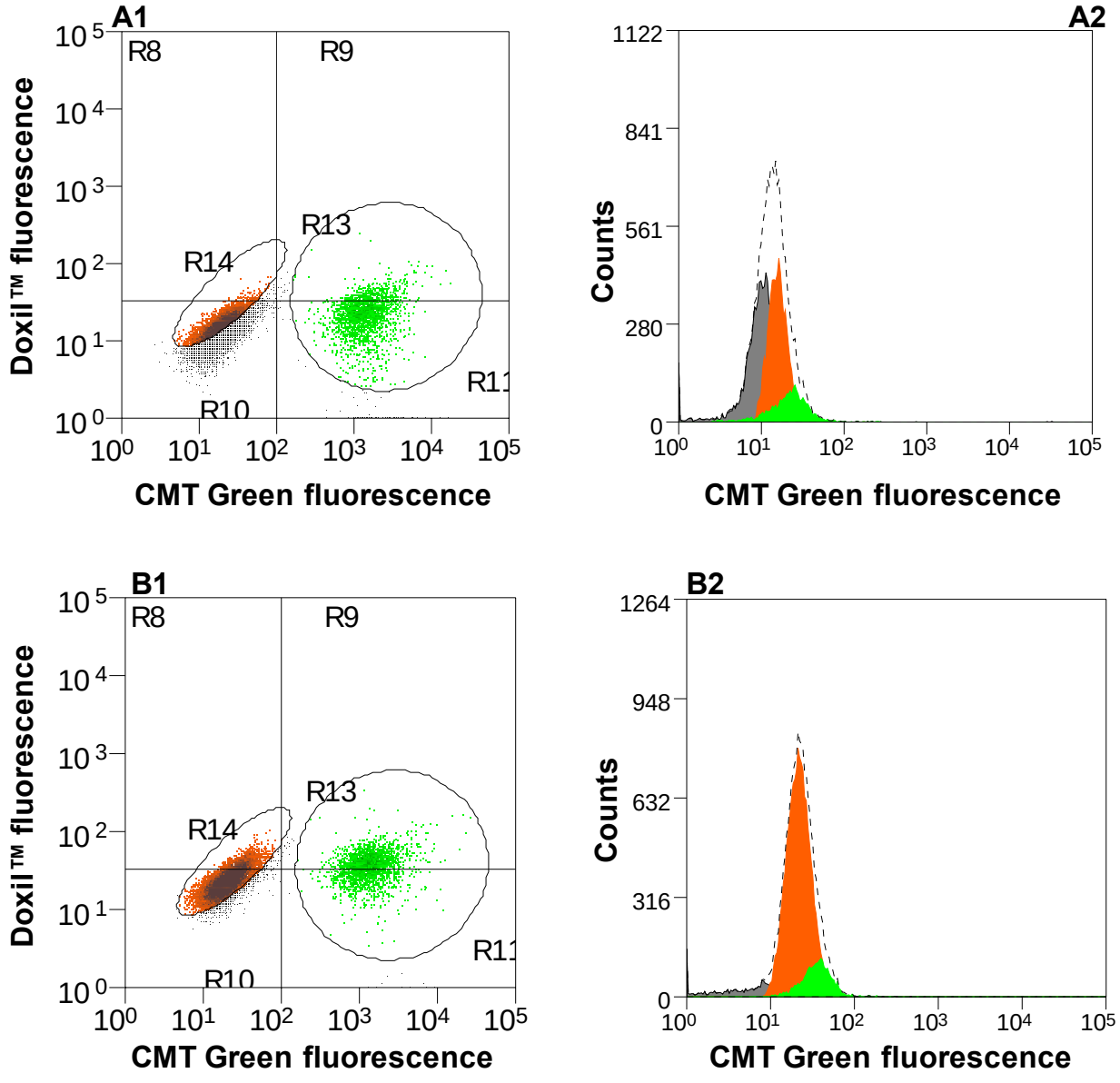

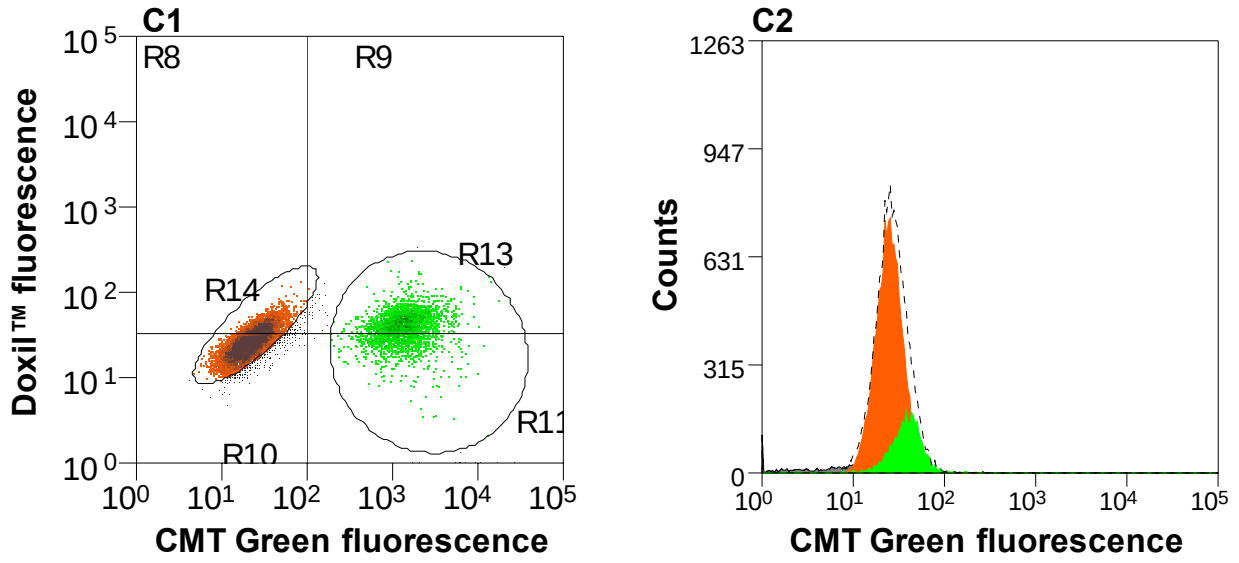

Figure 19. Flow cytometric analysis of the selective interaction of phage modified Doxil toward MCF-7 cells. Equal numbers of MCF-7 and Green CMFDA stained-MCF-10A cells were mixed and incubated with modified Doxil encapsulating 50 µM doxorubicin for 90 min at 37ºC. Cell mixtures, treated likewise with the unmodified doxil (Doxil™), served as the control. Doxorubicin and green fluorescence of treated cells were evaluated using flow cytometry in 580/30 (orange) and 530/40 (green) nm channels, respectively. (**A**) Flow cytometric analysis of Doxil™ treated cell mixture. Doxorubicin fluorescence is shown in panels A1 and A2 as orange dot plots and histograms whereas the green fluorescence from Green CMFDA-stained MCF-10A are depicted as green dots and histograms; the black dots and gray histograms illustrate the untreated MCF-7 cells serving as the control. **(B)** Flow cytometric analysis of DWRGDSMDS-doxil treated cell mixtures. Doxorubicin and green fluorescence are depicted in panel B1 and B2 as orange dot plots, histograms and green dot plots and histograms. (**C)** Flow cytometric analysis of GSDWMLGQD-doxil treated cell mixtures. Panels C1 and C2, orange dot plots, histograms and orange dot plots and histograms represent doxorubicin and green fluorescence of treated cells.

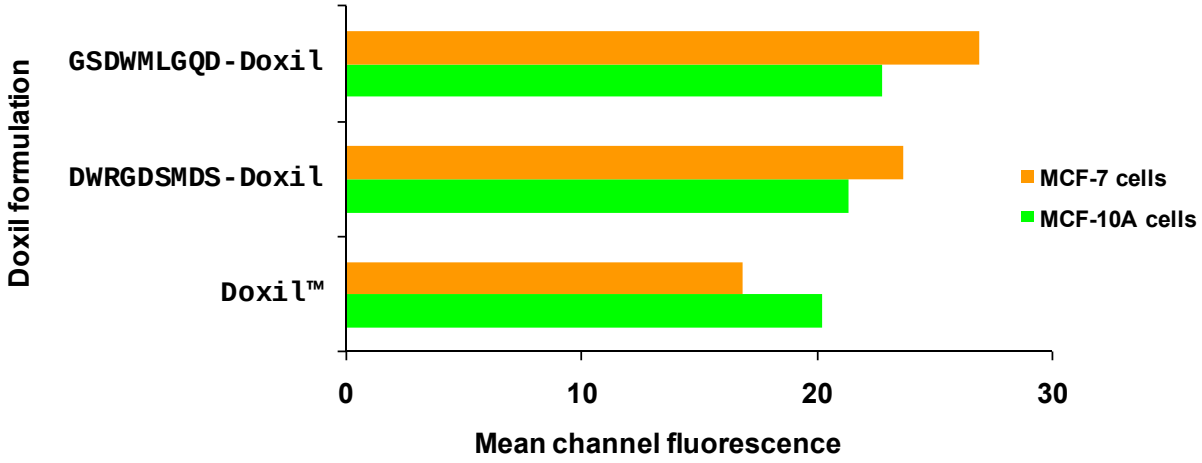

Figure 20. Selectivity of phage modified-Doxil toward MCF-7 cells depicted by mean channel fluorescence. Mean channel fluorescence of doxorubicin (orange) and Green CMFDA (green) from a mixture of MCF-7 and Green CMFDA-stained MCF-10A cells treated with three different Doxil formulations were analyzed by flow cytometry. The cell mixtures were treated with equal concentrations of DWRGDSMDS-Doxil and GSDWMLGQD-Doxil for 90 min at 37ºC. Cell mixtures treated with the unmodified Doxil™ served as the control.

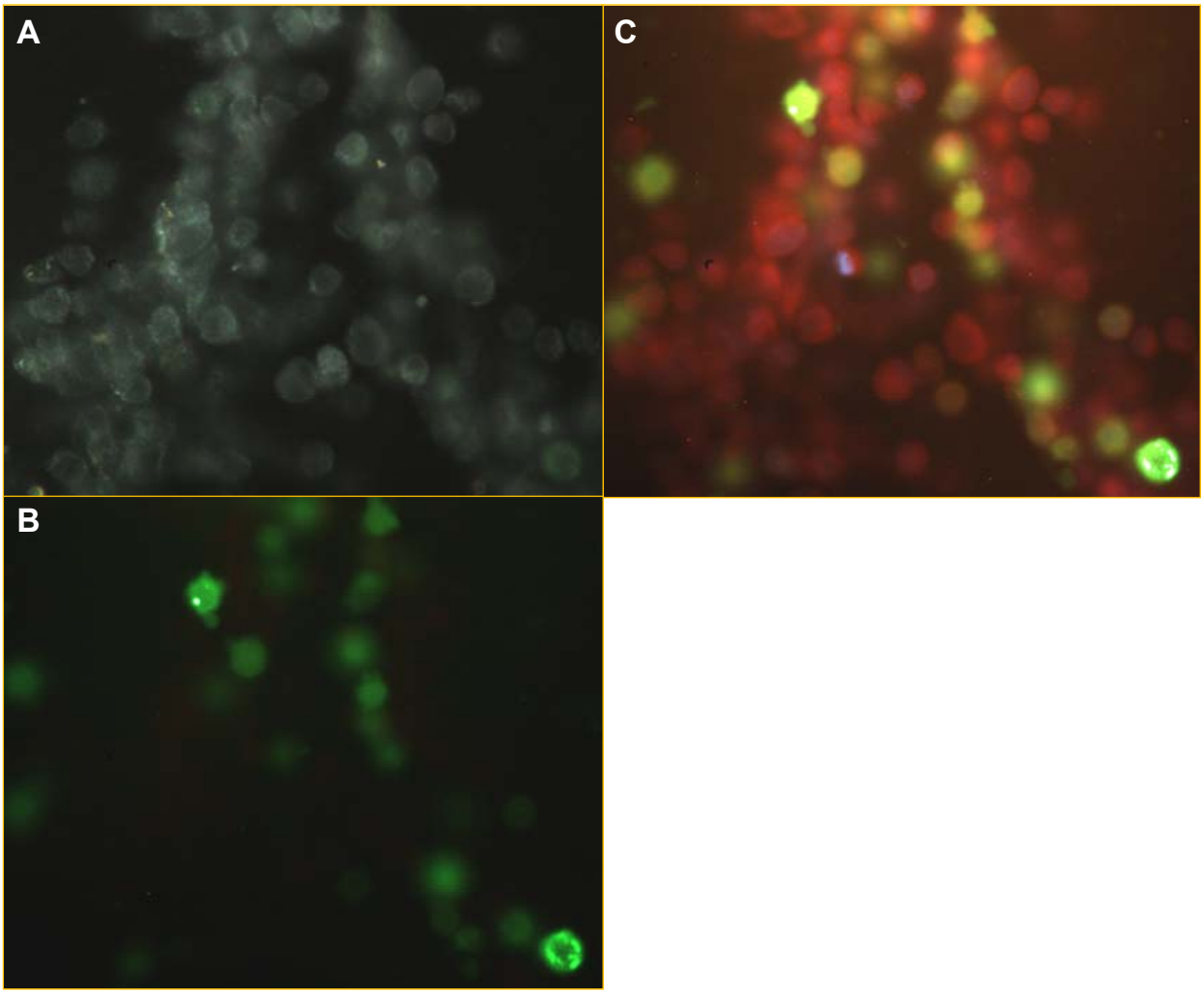

Figure 21. Modified Doxil selectivity towards MCF-7 cells in comparison with MCF-10A cells. Epifluorescence microscopy of the mixture of MCF-7 and Green CMFDA-stained MCF-10A cells treated with phage modified Doxil under three different filters in the same field. Panel A shows a representative field using the dark field, while panels B and C reveal the same field under fluorescein isothiocyanate filters or triple-band pass filter, respectively.

4.9 Cytotoxicity kinetics assay

We hypothesized that these newly isolated breast cancer-selective phages would be comparable to our previous study of targeting Doxil™ to MCF-7 cells using the breast cancer-selective phage DMPGTVLP. As such, equivalent concentrations of breast cancer-selective phages DWRGDSMDS and GSDWMLGQD-modified Doxil and unmodified control Doxil™ cytotoxicity were assessed for specificity using the MTS cytotoxicity assay.

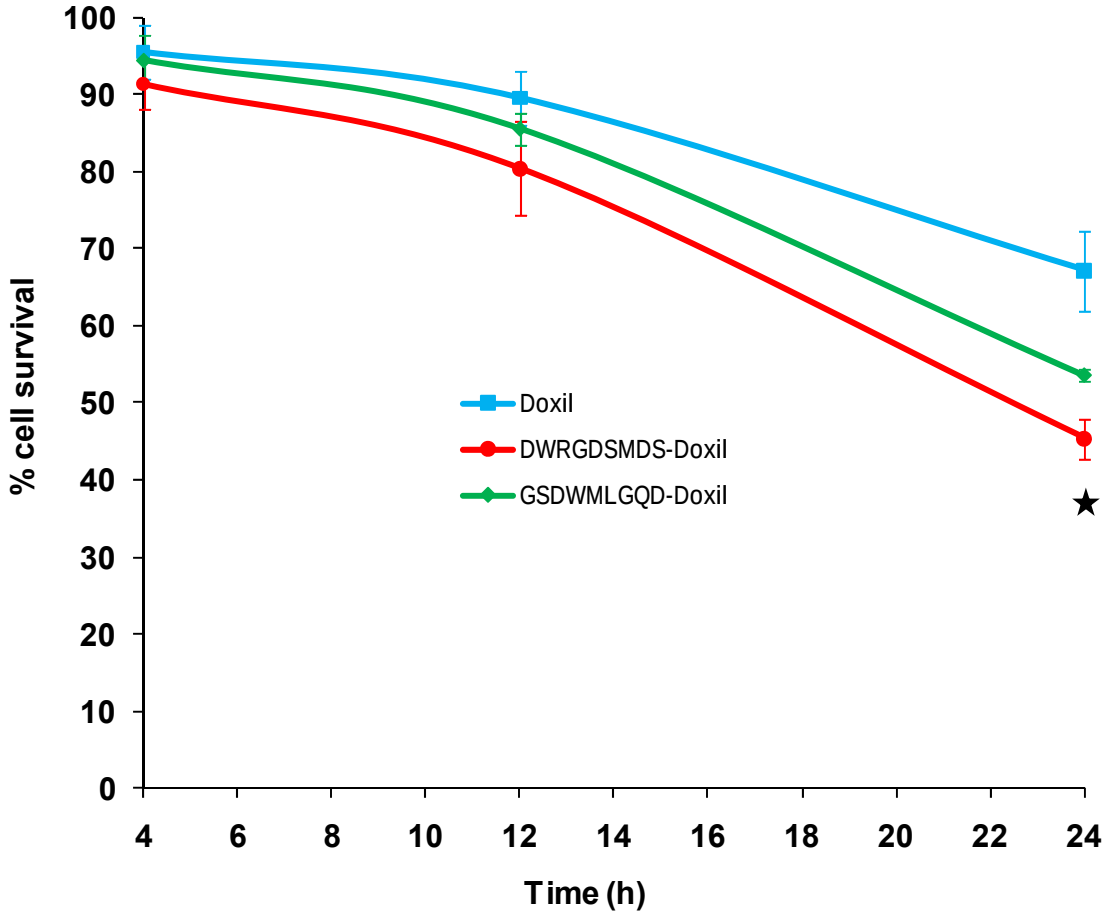

Figure 22. Kinetics of MCF-7 cytotoxicity based on the MTS assay. MCF-7 cells were incubated with 72 µM of modified Doxil formulations for 24 hours. Results were expressed as percent control and indicates mean ± standard deviation, n=6, *p< 0.05. The graph depicts the cytotoxic effects of 72 µ*M* each of three Doxil formulations: Doxil™, phage DWRGDSMDS modified Doxil and phage GSDWMLGQD modified Doxil of MCF-7 cells at three time points, 4,12 and 24 h. Cytotoxicity was studied using the CellTiter 96® AQ_{ueous} One Solution Reagent.

5. Discussion

The ultimate of aim of prescribing nanomedicines in cancer management is to extirpate cancer cells with minimal side effects. A decade ago, intense research effort resulted in some clinically approved nanomedicines employing a passive delivery approach to discharge drugs to tumor tissues. This tumor-selective delivery method exploited the leaky tumor vasculature and impaired lymphatic system. However, passive delivery was limited by insufficient delivery of

drugs to the tumor interior. As a consequence, targeting of nanomedicimes with ligands such as antibodies, vitamins, aptamers and peptides are currently being used to actively target and deliver nanomedicines to cancer intracellularly. Nevertheless, targeting of nanomedicines with the aforementioned ligands requires complex conjugation chemistry which can alter their structures and functions (Frisch et al., 2010; Sharma et al., 2006).

We have previously demonstrated the concept of targeting nanomedines using cancer-selective proteins for intracellular delivery of cancer medications (Jayanna et al., 2010; Wang et al, 2010a). These results were corroborated in our current study employing breast cancer selective phages DWRGDSMDS and GSDWMLGQD to target Doxil to MCF-7 cells. The DWRGDSMDS targeted Doxil demonstrated a significant increase in drug potency in comparison with control untargeted Doxil™. Also, the results from flow cytometry and epifluorescence microscopy revealed the enhanced binding and internalization of DWRGDSMDS-Doxil and GSDWMLGQD-Doxil in comparison with the control unmodified Doxil™. The breast cancer-selective DWRGDSMDS containing the RGD motif has been shown to bind integrin and internalize into cells by receptor mediated endocytosis. The tripeptide GSD in the breast cancer selective phage GSDWMLGQD has been speculated to be involved in binding of the phage to MCF-7 cells in our previous study (Chapter 1). In addition, flow cytometric analysis also revealed the selective binding of DWRGDSMDS-Doxil and GSDWMLGQD-Doxil to MCF-7 cells in comparison with MCF-10A.

In conclusion, we have confirmed the concept of targeting nanomedicines with cancer selective phage coat proteins. This approach should provide a rapid and economic way to generate targeted nanomedicines to a variety of malignancies.

CHAPTER 4

DELIVERY OF siRNA INTO BREAST CANCER CELLS *VIA* PHAGE FUSION PROTEIN-TARGETED LIPOSOMES

1. Abstract

Efficacy of siRNAs as potential anticancer therapeutics can be increased by their targeted delivery into cancer cells via tumor-specific ligands. Phage display offers a unique approach to identify highly specific and selective ligands that can deliver nanocarriers to the site of disease. In this study, we have described a novel approach for intracellular delivery of siRNAs into breast cancer cells through their encapsulation into liposomes targeted to the tumor cells with preselected intact phage proteins. The targeted siRNA liposomes were obtained by a fusion of two parental liposomes containing spontaneously inserted siRNA and fusion phage proteins. The presence of pVIII coat protein fused to a tumor cell-targeting peptide in the liposomes was confirmed by western blotting. The novel phage-targeted siRNA-nanopharmaceuticals demonstrate significant down-regulation of *PRDM14* gene expression and protein synthesis in target MCF-7 cells. This approach offers the potential for development of new anticancer siRNA-based targeted nanomedicines.

2. Introduction

Small (short) interfering fragments of RNA (siRNA) are known to inhibit specific protein synthesis by suppressing target gene expression at the mRNA level by a mechanism called RNA interference (RNAi). They are considered prospective anticancer drugs because of their high

specific gene silencing efficiency and low toxicity (Iorns et al., 2007). However, systemic delivery of siRNAs into tumor cells is a challenging task because siRNAs are themselves unstable in the blood stream and cannot penetrate efficiently through cellular membranes (Whitehead et al., 2009). For these reasons, other means of siRNA delivery to target cells have been devised. They include the encapsulation of siRNA in liposomes or other nanoparticles, viral and bacterial delivery of siRNA precursors, or stabilization of siRNA molecules *via* their chemical modification (Kim et al., 2009).

Among various nano-carrier systems, PEGylated "stealth" liposomes may be considered as ideal vehicles for siRNA delivery, mainly due to their biological inertness, non-toxicity and protection of siRNAs from nucleases (Zheng et al., 2009). Moreover, therapeutic efficacy of liposomes can be further increased by their coupling with tumor-specific ligands that enhance their selective interaction with tumors, or control unloading of their cargo within tumors. For example, siRNA-loaded immunoliposomes targeted with anti-transferrin antibody produced specific inhibition of Her-2 expression in breast cancer animal models and effected tumor growth inhibition in a pancreatic cancer animal model (Pirollo and Chang, 2008). Attachment of cell-penetrating peptides (CPP), a family of peptides able to translocate across the cell membrane, was also used to deliver siRNA into cancer cells. It was shown that liposomes bearing a synthetic arginine-rich CPP are stable and can efficiently transfect lung tumor cells *in vitro* (Wang et al., 2006). A recent study has also shown that systemic delivery of siRNA encapsulated in targeted liposomes can efficiently depress MDM2, c-myc, and vascular endothelial growth factor oncogenes expression in metastatic murine melanoma cells (Li et al., 2008). Taken together, targeted siRNA-containing liposomes represent a promising cancer treatment option. However, despite its promise, targeted liposome technology is not without difficulties. Preparation of the

targeting ligands, such as antibodies, and their conjugation to lipids to make usable quantities of addressed vesicles, has proven challenging with unique differences in each targeted particle. Therefore, a new challenge, within the frame of this concept, is development of highly selective, stable, easy to produce and physiologically acceptable ligands and their integration into targeted nanoparticulate formulations. These considerations and others led us to think of phage proteins as easily available targeting components of drug carriers (Koivunen et al., 1999; Lee et al., 2004; Medina et al., 2001; Pastorino et al., 2006).

The integration of phage display technology with the nanocarrier-based drug delivery platforms is emerging as a new drug targeting approach (Petrenko, 2008). Evolved as a result of advances in combinatorial chemistry and recombinant DNA technology, phage technique provided a new way of identification of tumor-specific peptide ligands in a high throughput fashion (Aina et al., 2007; Krumpe and Mori, 2006; Sergeeva et al., 2006). Initially, foreign proteins were fused to the N-terminus of the minor coat protein pIII of filamentous phage yielding a chimeric "fusion phage" in which up to 5 copies of the foreign antigen were displayed on a tip of a virion (Smith, 1985). The identified peptides were then chemically synthesized and coupled to drug carriers (Chang et al., 2009). A number of phage-borne peptides specific to various tumors were identified (Krumpe and Mori, 2006) and some of these peptides have been successfully used to deliver nanocarriers to diseased organs.

In an alternative phage display format, a sequence encoding a foreign peptide was spliced in-frame into gene *gpVIII*, encoding the major coat protein pVIII, leading to the "landscape" fashion of the phage display allowing thousands copies of guest peptide fused to the phage coat protein to cover whole virion surface (Ilyichev et al., 1992). The tumor-specific landscape phages can be affinity selected from multibillion clone libraries by their ability to interact

specifically with cancer cell surface receptors and/or penetrate into the cells (Petrenko, 2008; Jayanna et al., 2010). Fusion coat protein pVIII, is dominant in the landscape phage and have been proposed as easily available targeting ligands for pharmaceutical liposomes (Jayanna et al., 2010; Jayanna et al., 2009). This new approach is well justified by the ability of the phage coat proteins to spontaneously insert into lipid bilayers (Soekarjo et al., 1996). The "membranophilic" property of the major coat protein was exploited to insert target-specific peptides fused to the N-terminus of the phage coat protein into liposomes. The resulting liposomes demonstrated functional binding specificity toward model streptavidin-conjugated colloidal gold particles and target breast and prostate cancer cells (Petrenko, 2008; Jayanna et al., 2010; Jayanna et al., 2009). The rationale behind this novel targeting concept is that a hybrid phage protein fused to a cancer cell-specific peptide serves a dual function in liposome targeting: it's surface-exposed N-terminus navigates the liposomes to the target cellular receptors while the hydrophobic C-terminus anchors the targeting peptides to the liposomal membrane (Figure 23).

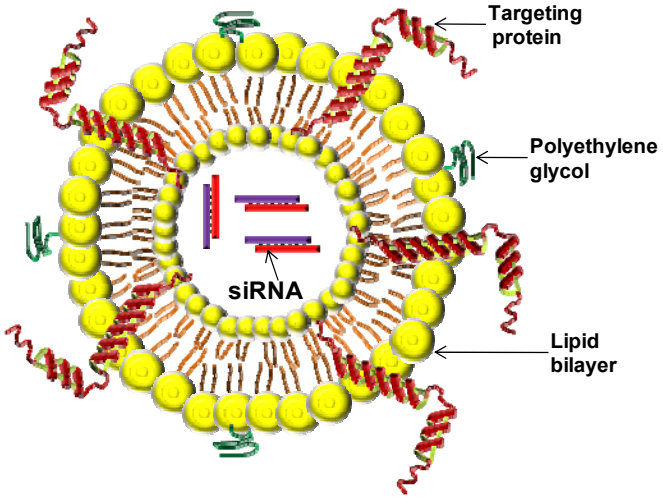

Figure 23. siRNA-loaded liposome targeted by the pVIII protein created by exploiting the amphiphilic nature of the phage coat protein. The hydrophobic helix of the pVIII is anchored in the lipid bilayer, whereas the N-terminal tumor-specific peptide is displayed on the surface of the liposome. The siRNA molecules are pictured as strands inside the liposomes.

We have adapted the phage-based targeting strategy for siRNA delivery to breast cancer cells. We applied, for the first time, the fusion of phage proteins with liposomes for construction of siRNA-loaded nano-vehicles specifically interacting with cancer cells. As a target for siRNA-mediated silencing, we chose the *PRDM14* gene - a member of the family of genes that encode proline rich domain proteins (PRDM) and may play an important role in breast cancer carcinogenesis (Nishikawa et al., 2007). Our studies showed that gene-specific siRNA duplexes, encapsulated in phage protein-targeted PEGylated liposomes, specifically inhibit the expression of the target *PRDM14* gene in breast cancer cells.

3. Materials and Methods

3.1 Reagents

L-α-phosphatidylcholine (ePC); 1,2-dipalmitoyl-*sn*-glycero-3-[phospho-*rac*-(1-glycerol)] (sodium salt; DPPG); 1,2-dioleoyl-3-trimethylammonium-propane (chloride salt; DOTAP); 1,2-distearoyl-*sn*-glycero-3-phosphoethanolamine-N-[amino(polyethyleneglycol)$_{2000}$] (ammonium salt; PEG$_{2000}$-PE); and cholesterol (CHOL) were purchased from Avanti Polar Lipids Inc. (Alabaster, AL). Sodium cholate, 2.5% CHAPS: 3-[(3-cholamidopropyl)dimethylammonio]-1-proanesulfonate, bovine serum albumin (66 kDA), phenylmethanesulfonyl fluoride (PMSF), and proteinase K were purchased from Sigma (St. Louis, MO); 16% non-gradient tris-tricine polyacrylamide gel (Jule Inc.Milford, CT); Immobilon-P PVDF membrane was purchased from Millipore (Billerica, MA); NeutrAvidin™-HRP and BCA protein assay kits, and chemiluminescent substrate solution was purchased from from Pierce (Rockford, IL); biotinylated-SP-conjugated Affinitipure goat antirabbit IgG was purchased from Jackson Immunoresearch (West Grove, PA).

3.2 Cells

Cell lines were obtained from the American Type Culture Collection (ATCC, Manassas, VA). The human breast adenocarcinoma cell line MCF-7 (ATCC, HTB 22™), which was used for selection of binding phage, was cultivated in 25 cm^2 cell culture flasks (Corning Inc., Corning, NY) containing L-15 Leibovitz medium with L-glutamine (Sigma-Aldrich, St. Louis, MO) supplemented with 10% fetal calf serum (Hyclone, Fisher) at 37°C in 5% CO_2. For phage testing, MCF-7 and human hepatocellular carcinoma HepG2 (ATCC, CRL-2235™) cells were grown in 96 well culture plates containing L-15 Leibovitz medium with L-glutamine supplemented with 10% FCS. Immortal human non-tumorigenic mammary epithelial MCF-10A cells (ATCC, CRL-10317™) were maintained in mammary epithelial cell basal medium supplemented with 0.4% bovine pituitary extract, 0.1% human epidermal growth factor, 0.1% hydrocortisone, 0.1% GA-1000 and 0.1% insulin. (Invitrogen, Gibco Cell Culture, Portland, OR).

3.3 Oligonucleotides and siRNAs

For silencing of the PRDM14 gene, were used siRNAs as described previously (Nishikawa et al, 2007) and purchased from Integrated DNA Technologies (Coralville, Iowa, USA) Scrambled siRNAs were purchased from Applied Biosystems (Foster City, CA).

5' CCAG UGAAGUGAAGACCUATT 3'-s(iPRDM14-F)

5' UAGGUCUUCACUUCACUGG TT 3'-(siPRDM14-R)

5’-GGACAAGGGCGAUAGGAAATT-3’ (siPRDM14-2F)

5’-UUUCCUAUCGCCCUUGUCCTT-3’ (siPRDM14-2R)

5’-GGGAAAAUCUUCUCAGAUCTT-3’ (siPRDM14-3F)

5’-GAUCUGAGAAGAUUUUCCCTT-3’ (siPRDM14-3R)

For RT-PCR analysis of *PRDM14* and *GAPDH* gene expression, primers: PRDM14 sense: 5'GTGCGGTCCCGGGATGGCTCTAC,

PRDM14 antisense: 5'-GGGGCGGTGGAATTAAAGTGTCAG,

GAPDH sense: 5'-GGGGAGCCAAAAGGGTCATCATCT, and

GAPDH antisense: 5'-GACGCCTGCTTCACCACCTTCTTG were used

Primers were designed using Primer Select expert sequence analysis software (DNASTAR inc., Madison, Wisconsin).

Phage display library and bacterial strain

Landscape phage display library f8/8 (Petrenko, 1996), constructed based on the type 8 phage display system, was used in selection procedures. In this system, foreign peptides are displayed as an extension of each major coat protein unit due to an in frame random oligonucleotide insertion in the gene *gpVIII* resulting in the display of ~4000 guest peptide units on the surface of the population of phage particles. The f8/8 library has random octapeptide inserts and a complexity of 1.4 x 10^9 particles. All general methods of handling phage, including propagation, purification, titering, production of pure phage clones, and isolation of phage DNA have been previously described (Brigati et al., 2008). *Escherichia coli* (*E. coli*) strain K91BlueKan (Kan^r) {Hfr C thi lacZΔ M15 lac Y::mkh $lacI^Q$} used for phage tittering and propagation was kindly provided by George Smith (University of Columbia-Missouri).

3.4 Selection of breast cancer cell-specific phage

The selection protocol previously described was used to identify phage clones selectively binding to MCF-7 cells (Brigati et al., 2008). An aliquot of the phage library containing 100 billion phage particles in 2 ml of blocking buffer (0.5% BSA in serum free medium) was incubated in an empty 25 cm^2 cell culture flask at room temperature for 1 h to deplete phage

particles binding cell culture flasks. At the same time, the MCF-7 cells were washed twice with serum-free Lebovitz (L-15) media and incubated for 1 h at 37°C, 5% CO_2 in serum-free L-15 media that was removed immediately before application of the phage. Phages that did not bind to the empty flask were transferred to 90% confluent MCF-7 cells in a culture flask and incubated for 1 h at room temperature. Unbound phages were aspirated and cells were washed ten times with washing buffer (0.1% BSA, 0.1% Tween 20 in serum free medium) to remove any remaining unbound phage virions. Cell-bound phages were eluted with 2 ml of elution buffer (0.1 M glycine-HCl, pH 2.2, 1 mg/ml BSA and 0.1 mg/ml phenol red) for 10 min on ice and neutralized with 2 ml of neutralizing buffer (1 M Tris-HCl, pH 9.1). Eluted phages were titered and amplified in host bacterial *E. coli* K91 Bluekan cells, purified by precipitation with polyethylene glycol and used as input in further rounds of selection. Four rounds of selection were performed altogether. In each selection round, the phage input and output were titered in bacteria as described previously (Brigati et al., 2008) and the results of the selection were expressed as the percentage of the ratio of output to input phage. The ratio of output to input phage, increased from one round to another, indicating successful selection of phage clones that bind to target MCF-7 cells. Phages obtained in the final selection round were isolated as individual clones, sequenced and propagated for further characterization.

3.5 Selectivity of phage

Binding specificity and selectivity of the phage DMPGTVLP (designated by the sequence of the inserted foreign peptide) was determined in a phage capture assay adapted for 96-well culture plate format. Selectivity of the phage clones towards breast cancer MCF-7 cells was tested in comparison with MCF-10A and HepG2 cells and serum. The non-relevant phage clone with guest peptide VPEGAFSS (streptavidin binder, Petrenko and Smith, 2000) was used

for comparison as a negative control. Briefly, target MCF-7 cells and control MCF-10A and HepG2 cells were cultivated in triplicate to 80-90% confluence in 96-well cell culture plates. As a control, selected wells were treated with media alone. Before application of phage, media in the wells was replaced with serum-free media for 1 h. Each phage (~10^6 cfu/well) was added to the designated wells in 100 µl of blocking buffer (0.5% BSA in serum free medium) and incubated for 1 h at room temperature. The buffer containing unbound phage was carefully removed and the cells were washed eight times with 100 µl of cold washing buffer. To collect cell-associated phage, 25 µl of lysis buffer (2.5% CHAPS, 3-[(3-cholamidopropyl)dimethylammonio]-1-proanesulfonate, Sigma-Aldrich, St. Louis, MO, in serum-free medium) was then added to each of the wells and incubated for 10 min on a shaker (20 cycles/min) at room temperature. Starved host bacterial cells (125 µl) were added to each well and incubated for 15 min at room temperature. Following this, 180 µl NZY containing 0.4 µg/ml tetracycline was added to the mixture and further incubated for 45 min at 37ºC. The entire mixture was finally spread on NZY microbiological plates containing 20 µg/ml tetracycline and incubated overnight. Phage titers were presented as a ratio of output to input phage to determine recovery percentage. All assays were performed in triplicate.

3.6 Mode of phage interaction with breast cancer cells

To estimate the role of cellular metabolism in phage binding, association of phage with cells was studied under different temperature conditions, with or without addition of serum. MCF-7 cells (2.0 x 10^5 cells/well) were cultivated in Leibovitz medium in triplicate to confluence in three 96-well cell culture plates; serum-treated wells served as a negative control. Cell culture medium was aspirated and wells containing the confluent cells were washed with serum-free medium. To assess the role of cell metabolism in association of the phage with live

cells, the incubation of phage with cells was carried out at room temperature without serum, at 37 ºC without serum, and at 37 ºC with serum. In the room temperature experiment, the cells were incubated with 100 µl serum-free medium at room temperature for 1 h and phage clone (~10^6 cfu in blocking buffer) was added to the corresponding well and incubated for 1 h at room temperature. Unbound phages were removed and the cells were carefully washed with 100 µl washing buffer eight times for 5 min to remove any remaining unbound phage. Surface-bound phages were recovered by treating wells with acid elution buffer (0.1 M glycine-HCl, pH 2.2), and the eluates were neutralized with 4.7 µl neutralizing buffer (1 M Tris, pH 9.1). Wells were additionally washed twice with 25 µl washing buffer for 5 min per wash and post-elution washings were collected (fractions PEW-1 and PEW-2). To retrieve internalizing phages, wells were treated with 25 µl lysis buffer for 10 min on a rocker. The eluate, PEW-1, PEW-2 and lysate fractions were titered in *E. coli* K91 BlueKan cells and phage recovery was calculated as the ratio of input phage to output phage. The procedure was modified by the incubation of cells with phage at 37 ºC instead of room temperature to study the effect of temperature on the binding and internalization of phages. In another experiment, the incubation was carried out at 37ºC in the medium supplemented with serum. The blocking buffer was also prepared from serum-containing medium.

3.7 Preparation and purification of the phage fusion coat protein

Phage fusion 55-mer coat protein

A**DMPGTVLP**DPAKAAFDSLQASATEYIGYAWAMVVVIVGATIGIKLFKKFTSKAS

(foreign 8-mer peptide shown with bold font) was prepared by stripping the DMPGTVLP phage in cholate buffer (Jayanna et al., 2009). Briefly, the mixture of 350 µl phage in TBS buffer (~1 mg/ml) and 700 µl of 120 mM cholate in 10 mM Tris-HCl, 0.2 mM EDTA, pH 8.0, was

incubated at 37^{o}C for 1 h. Fusion proteins were purified from viral DNA and bacterial proteins by size-exclusion chromatography using a Sepharose 6B-CL (Amersham Biosciences) column (1 cm × 45 cm), which was eluted with 10 mM cholate in 10 mM Tris-HCl, 0.2 mM EDTA pH 8.0. The chromatographic profile was monitored with an Econo UV monitor (Bio-Rad, CA); 5 ml per fraction were collected and stored at 4^{o}C. The protein was isolated as an aggregate with molecular weight ~46 KDa (8-mer) determined by chromatography on the column calibrated with standard molecular weight markers: Aprotinin (6.5 kDa), cytochrome C (12.4 kDa), Carbonic Anhydrase (29 kDa) and Albumin, bovine serum (66 kDA) (Sigma, St. Loius, MO), as described (Soekarjo et al., 1996). Concentration of the protein was measured spectrophotometrically using the formula: Absorbance unit AU_{280} = 0.7 mg/ml, determined using PROTEAN program (DNA STAR Inc., Madison, Wisconsin).

Protein-liposome formulation

A lipid film composed of ePC, CHOL, DPPG, DOTAP and PEG_{2000}-PE) (molar ratio 45:30:20:2:3) was prepared in a round bottom flask by removing chloroform. The film was further dried for 4 h under high vacuum (Pappalardo et al., 2009; Sawant et al., 2006) and then rehydrated in sterile PBS buffer pH 7.4 (made in nuclease-free water to avoid contamination in the subsequent steps) up to a final liposome concentration of 40 mg/ml. To obtain the "plain" undecorated liposomes (liposome formulation with no embedded protein), the hydrated lipids were bath sonicated for 10-15 min and finally extruded through a 200 nm polycarbonate membrane. Each phage peptide was incorporated into the lipid formulation by an overnight incubation at 37 °C (1:200 wt phage-protein: liposomes) in a final sodium cholate concentration of 15 mM and up to a final lipid concentration of 10.3 mg/ml. The formulation was dialyzed

overnight (dialysis membrane cutoff size 2000 Da) against PBS buffer pH 7.4 to remove the excess of sodium cholate.

siRNA-liposome formulation

A lipid film composed of ePC:CHOL:DOTAP:PEG2k-PE (60:30:10:2 molar ratio) was made in a round bottom flask removing the chloroform. The film was further dried for 4 h under high vacuum, and then rehydrated in sterile PBS buffer pH 7.4 (in nuclease-free water) up to a final liposome concentration of 10.3 mg/ml. The hydrated lipids were bath sonicated for 10-15 min and finally extruded through 200 nm polycarbonate membrane. Then, the "plain" liposomes (liposome formulation with no siRNA) were incubated at room temperature for 3.5 h with a mixture of three siRNA fragments at a molar ratio DOTAP:siRNA/10:1.

siRNA-protein-liposome formulation

To make siRNA-protein-liposomes, the siRNA-liposomes and protein-liposomes were incubated in a 1:2 volume ratio (50 µl siRNA-liposomes and 100 µl protein-liposomes) overnight at 4 °C.

Size distribution and zeta potential (ζ) analysis

All formulations were characterized by size, size distribution and zeta potential (ζ) using the dynamic light scattering (DLS) on a Zeta Plus instrument (Brookhaven Instrument Corporation) and Zeta Phase Analysis Light Scattering (PALS) with an ultrasensitive zeta potential analyzer instrument (Brookhaven Instruments, Holtsville, NY). A portion (5 µL) of each liposome suspension was diluted up to 1 ml in deionized water and then analyzed for the size distribution; for the zeta potential each sample was diluted in 1 mM KCl (5 µl/1.5 mL).

PicoGreen fluorescent assay

To check the amount of free siRNA in solution, we used a fluorescent assay based on the interaction of the PicoGreen (Invitrogen, Carlsbad, CA) reagent and free (nonencapsulated in liposomes) siRNA. Fluorescence intensity in this assay is proportional to the amount of the siRNA. Only free siRNA is able to react with the probe and to emit fluorescence. The siRNA associated to the liposomes is shielded and not accessible to the probe. For analysis, siRNA-protein-liposomes (1 µl of preparation diluted in 10 µl nuclease-free water) was incubated with 990 µl of PicoGreen solution (1/200 dilution of the probe in TBE buffer) at 37 °C for 10 min. The same amount of free siRNA in PicoGreen solution was used as a reference to determine the amount of siRNA not associated with lipids. As blanks, the same dilution of phage-liposomes and plain PicoGreen solution were used and subtracted from the final sample fluorescence. PicoGreen-siRNA fluorescence intensity was detected at excitation wavelength of 480 nm and emission wavelength of 520 nm in a Hitachi F-2000 fluorescence spectrometer (Hitachi, Japan). The portion of the free siRNA was calculated according to the following formula: % siRNA in solution= (PicoGreen fluorescence liposomes/PicoGreen fluorescence free).

Knockdown of *PRDM14* gene

To study *PRDM14* gene knockdown, 1 x 10^5 MCF-7 cells in 6-well culture plates were transfected with *PRDM14*-specific siRNA (40 nM) or scrambled siRNA (40 nM) mixed with Lipofectamine RNAiMAX (Invitrogen, Carlsbad, CA). siRNAs that target *PRDM14* gene were composed of three duplexes: siPRDM14-1F/siPRDM14-1R, siPRDM14-2F/siPRDM14-2R, or siPRDM14-3F/siPRDM14-3R (see Materials and Methods). Portions (4.8 µl) of each siRNA (106 nM) were mixed with 250 µl of Opti-MEM I medium (Invitrogen, Carlsbad, CA) in 1.5 ml Eppendorf tube. Lipofectamine RNAiMAX was mixed gently before use by inverting, 6 µl of the homogenized preparation was added to 250 µl of Opti-MEM I medium and the composition

was mixed gently by inverting. Lipofectamine preparation (250 µl) was added to the siRNA diluted in Opti-MEM I medium (250 µl), mixed gently and incubated for 10-20 min at room temperature. The siRNA-lipofectamine preparation was mixed with 1 x 10^5 MCF-7 cells in the well of a 6-well culture plate and adjusted to 2 ml with L-15 media (10% FBS without antibiotics) resulting in 40 nM total concentration of siRNA. The plate was rocked gently at room temperature and incubated at 37ºC for 72 h. The medium was changed every 24 hrs. After 72 h incubation,

For knockdown of *PRDM14* gene by siRNA-phage fusion protein-liposomes, 1.6 µl of siRNA-DMPGTVLP-liposomes (50 µM) or 1.6 µl of scrambled siRNA-DMPGTVLP-liposomes (50 µM), or 0.56 µl of siRNA-liposomes (150 µM) were mixed with 100,000 MCF-7 cells in the well of a 6-well culture plate and adjusted to 2 ml with L-15 media (10% FBS without antibiotics) resulting in 40 nM total concentration of siRNA. The plates were proceeded and RNA isolated as described above.

Analysis of *PRDM14* gene expression by RT-PCR

Total RNA was extracted using an RNeasy Micro-kit (QIAGEN GmbH, Hilden, Germany) according to the manufacturer's protocol. Reverse transcription of total RNA and cDNA amplification by PCR was carried out using 25 ng of total RNA in 25 µL of reaction mixture using a one step Access RT-PCR kit according to the manufacturer's protocol (Promega, Madison, WI). The primers for *PRDM14* and *GAPDH* genes were used at final concentrations 0.1 µM. One cycle of reverse transcription of isolated RNA at 48ºC (45 min) and 94ºC (2 min) was followed by 35 cycles of PCR at 62ºC (30 sec), 68ºC (1 min) and 68ºC (7 min). Relative levels of gene expression were quantified using the KODAK imager.

Analysis of PRDM14 protein expression in MCF-7 cells using western blot

MCF-7 cells were treated with *PRDM14* gene-specific siRNA and scrambled siRNA preparations (40 nM), encapsulated in phage protein-targeted liposomes or mixed with lipofectamine reagent. After 48 h, cells were lysed with 70 μL of RIPA buffer (Sigma, St. Louis, MO) containing 7 μL of protease inhibitor cocktail (Sigma, St. Louis, MO) and PMSF (2 mM final concentration). The protein concentration in whole cell lysates was measured with a BioRad DC protein assay (Hercules, CA). A portion (15 μg) of the whole cell extract was analysed by electrophoresis in 4-20% polyacrylamide gradient Tris-HCl gels (Bio-Rad, Hercules, CA) and transferred to a PVDF membrane (Millipore, Billerica, Massachusetts). The membrane was blocked in wash buffer (PBS, 5% nonfat dry milk) for 1 h and incubated at 4°C overnight with polyclonal anti-PRDM14 antibody (Abcam, Cambridge, MA) (1:500 dilution). The membrane was washed four times with PBS/0.5% Tween-20 and incubated with peroxidase-conjugated Affinipure Goat Anti-rabbit IgG (1:5000) (Jackson ImmunoResearch, West Grove, PA) at room temperature for 1 h. Membrane was washed four times with PBS/0.5% Tween-20 and visualized using chemiluminescent substrate solution (Pierce, Rockford, Illinois). Membranes were stripped using western blot stripping buffer (Thermo Scientific, Rockford, IL) for 10 min and probed with monoclonal anti-GAPDH antibody (Abcam, Cambridge, MA)(1:2000) for 1 h. The membrane was washed four times with PBS/0.5% Tween-20 and incubated with peroxidase-conjugated Affinipure Goat Anti-mouse IgG (1:5000) (Jackson ImmunoResearch, West Grove, PA) at room temperature for 1 h visualized using chemiluminescent substrate solution.

4. Results

4.1 Selection of breast cancer cell-specific phages

To obtain breast cancer cell-binding phages, the f8/8 landscape display library of phages harboring 8-mer peptides on all 4,000 copies of the major coat protein (Petrenko et al.,

2001) was used for *in vitro* selection on MCF-7 cells. A portion of the library containing 100 billion phage particles was depleted first for phages binding a cell culture flask and then was applied to MCF-7 cells. Unbound phages were removed, whereas bound phages were eluted with mild acid. The eluted phages were amplified, purified and used in subsequent selection rounds. The selection procedure was iterated until an essential enrichment of bound phages was reached at the fourth round of selection. One hundred clones randomly picked from the final selection round were amplified, and their DNA was sequenced and translated to reveal 44 phage clones displaying unique peptides.

4.2 Phage characterization

Selectivity of the phage was determined by measuring their binding to breast cancer cells in comparison with normal breast epithelial MCF-10A cells, hepatocellular carcinoma HepG2 cells and serum. In this assay, equal numbers of phage particles were incubated with serum, the target and control cells in parallel on the same 96-well plate. After incubation, unbound phages were removed by multiple washing and cells were lysed with a mild detergent to recover cell-interacting phages. A relative level of phage binding to different cells and control serum was found by calculating the phage recovery-the ratio of output phage to input phage, determined by phage titering in host *E. coli* cells. At the same input phage concentration (1×10^8 virions/ml) the phage recovery for MCF-7 cells from, 13, 26 and 259 times higher than for control cells HepG2, MCF-10A and serum respectively. Binding of the phage DMPGTVLP to MCF-7 was 83 times higher than binding of a non-relevant control phage isolated from the same library. These data demonstrate high specificity of the selected phages toward target breast cancer cells.

Selected phages were characterized for mode of interaction with the target cells. During interaction with target cancer cells, phage particles can remain attached to surface receptors, or

they can penetrate into the cell through endocytosis or other mechanisms (Poul and Marks, 1999). To determine the mode of phage interaction with MCF-7 cells, the binding of phage to cells was studied under three different conditions: a) in serum free medium at room temperature, b) serum free medium at 37°C, and c) serum-containing medium at 37°C. To determine localization of phages in cells we used different methods of recovery of the cell-associated phage: with acid buffer for elution of surface-bound phage, followed by post-elution washing with neutral buffer (pH shock-released phages) and finally – with CHAPS buffer for recovery of cell-integrated and penetrated phage particles. The distribution of phage particles in various cell fractions (acid eluate, post-elution washes PEW1 and PEW2, and lysate) were determined by titering of the phage in host bacteria (Figure 24).

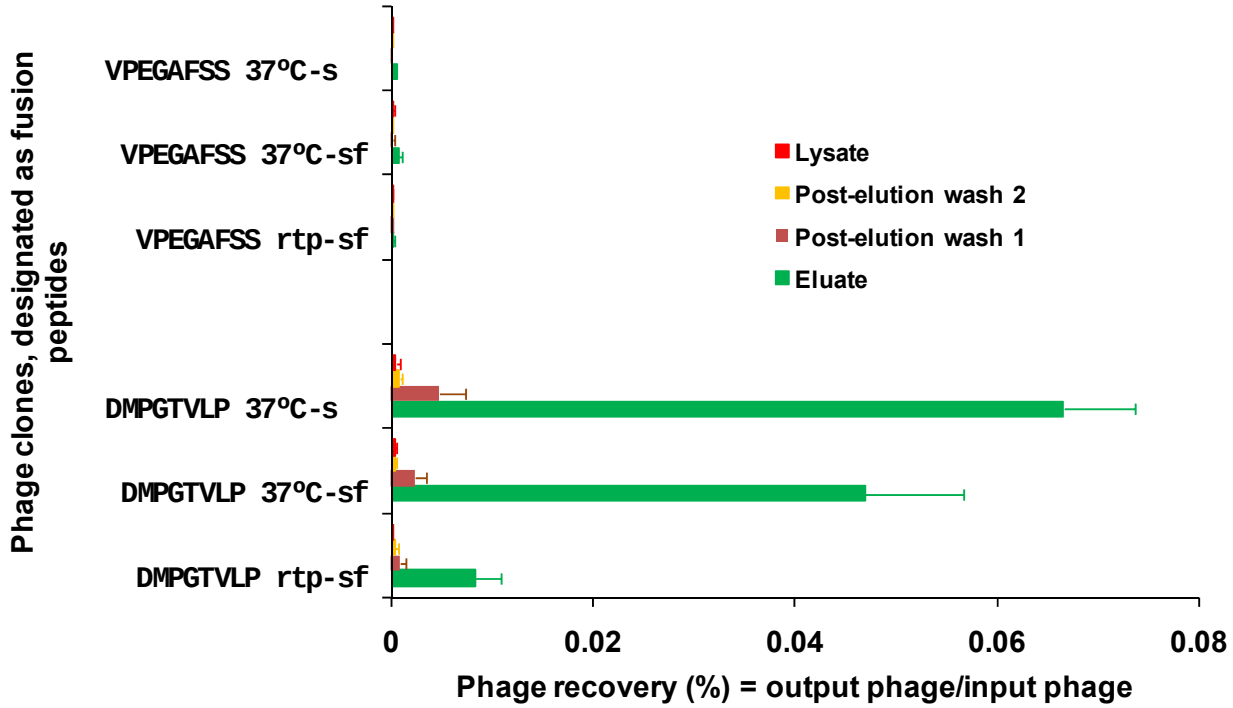

Figure 24. Phage DMPGTVLP mode of interaction with intact MCF-7 cells under three different metabolic conditions. The mode of interaction was based on binding of phages to unique macromolecules on the cell surface and or internalization of phages by mechanisms yet to

be elucidated. Mode of interaction was estimated as percentage phage recovery; output (cell-associated) phage to input phage. *rtp-sf* represents room temperature-serum free, whereas *sf* and *s* depict serum free and serum respectively. The unrelated phage bearing the peptide VPEGAFSS was the control.

The dominant portion of the phage was found in the acid fractions under all conditions, showing that the selected phages remain bound to the cell surface and do not penetrate into the cell during 1 h incubation with cells. The recovery of the phage incubated with cells in serum free medium increased more than six times when temperature was increased from 20^{o}C to 37^{o}C, and then further increased by 40% when the incubation medium was supplemented with serum. The increased binding of the phage to the cell at elevated temperature in the presence of growth factors of the serum can be explained by an active role of cellular metabolism in the binding of the phage. The control phage recovery was negligible in all fractions under the treatment conditions thereby validating the specificity of interaction of selected phage DMPGTVLP with MCF-7 cells.

4.3 siRNA- and phage fusion protein-containing liposomes

Previously, we developed a new approach to preparation of targeted liposomes that relies on the use of the phage fusion coat proteins as targeting ligands. In our approach, a cancer cell-specific phage protein was inserted into the liposome exploring its intrinsic "membranophilic" properties (Jayanna et al., 2009). Fusion proteins carrying tumor-cell binding peptides inherit the major structural features of the "wild-type" major coat protein VIII (Figure 23). They have a positively charged C-terminus (amino acids 45-55), which navigates the protein through the liposome membrane, probably using the mechanisms intrinsic for cationic cell-penetrating peptides (Tseng et al., 2002). The highly hydrophobic "membranophilic" segment (amino acids 27-40) allows the protein to accommodate readily in the membrane (Tseng et al., 2002) while the

amphiphilic N-terminus (amino acids 1-26), which are soluble in water, can interact with PEG residues on the surface of the "stealth" liposomes and display the N-terminal cancer cell-binding octa- or nonamer on the liposome shell (Figure 23).

Since spontaneous insertion of siRNA and fusion phage proteins into drug-loaded liposomes is driven by different mechanisms, we used a three-step assembly of the targeted siRNA-nanomedicines. First, siRNAs were inserted into liposomes formed by a mixture of neutral and positively charged lipids (plus-liposome). This liposome has a positively charged interface that attracts the negatively charged siRNAs and drives their internalization (Gary et al., 2007). Second, the fusion phage protein was inserted into liposomes formed by neutral and negatively charged lipids (minus-liposome). This liposome has a negatively charged interface that attracts the C-termini of the major coat protein, drives their translocation through the lipid bilayer and allows their anchoring at the internal liposomal interface (Soekarjo et al., 1996). Third, the plus-liposomes loaded with siRNAs and minus-liposomes loaded with phage protein were fused together to integrate into the protein-targeted particles containing siRNA.

Liposome formulations were characterized by measuring size and size distribution and the surface charge (ζ). Protein-liposomes showed a mean size and surface charge comparable to their starting plain non-targeted formulation. The size and ζ of the plain formulation used to make siRNA-liposomes was also compared with the final siRNA-protein formulations. Although, protein-free siRNA-liposomes demonstrate a larger size (144 nm) compared with protein-liposomes (87.7 nm, after the overnight incubation, "fused" formulations demonstrated a mean size (105.9 nm) closer to that of the initial protein-liposomes (Figure 25A).

The surface charge of plain undecorated liposomes (-49.34 mV) is comparable to the charge of protein-liposomes (-37.93 mV) suggesting that protein insertion does not affect the

overall zeta potential of the formulation. The surface charge ζ of the fusion liposomes is comparable to the protein-liposomes (-42.8 mV, and -49.3 mV respectively, Figure 25B) and may be due to the high level of shielding of siRNA in the preparations. To check the amount of free siRNA in solution, the fluorescent assay based on the interaction between PicoGreen and siRNA was used. It was shown that the majority of the siRNA (90.5%) is encapsulated in the siRNA-protein–liposomes.

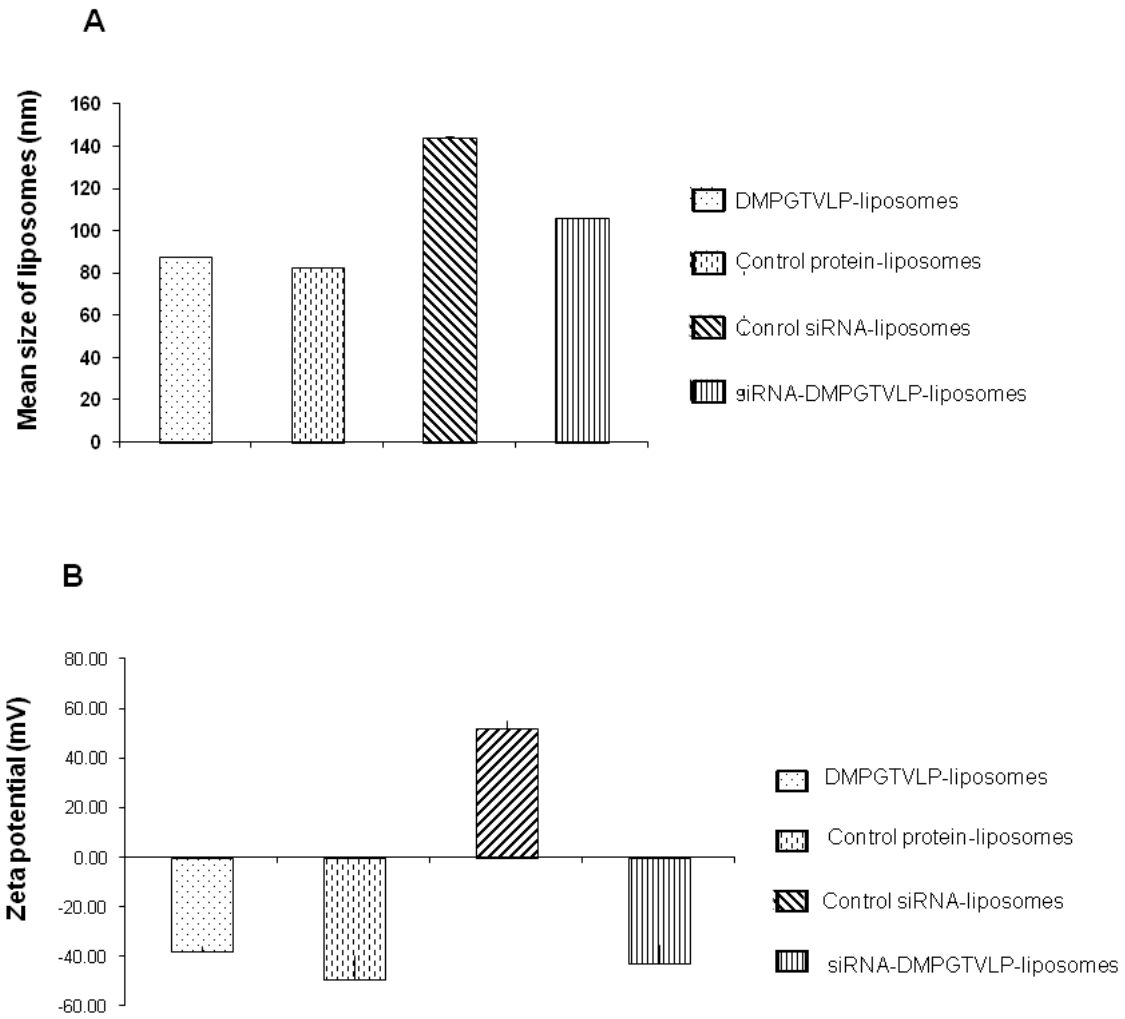

Figure 25. Mean size (A) and Zeta ζ potential (B) of liposome formulations. Liposomes modified with phage proteins (DMPGTVLP-liposomes), liposomes without inserted phage proteins (control protein-liposomes), liposomes without inserted siRNA (control siRNA-liposomes) and siRNA-liposomes targeted with phage protein (siRNA-DMPGTVLP-liposome) are depicted.

The presence and topology of fusion coat protein pVIII in the final siRNA-protein-liposomes was demonstrated by western blot analysis. Proteinase K treatment of the liposomal preparation resulted in dramatic decrease in signal intensity of N-terminus as revealed by anti-fd phage antibodies that bind specifically to N-terminus of the major coat protein. On the other hand, proteinase K treatment did not change the intensity of the C-terminus as probed by antibody specific for the C-terminal region of major coat protein implying the orientation of N_{out}-C_{in} of the inserted peptide into the liposomes (Figure 26**)**

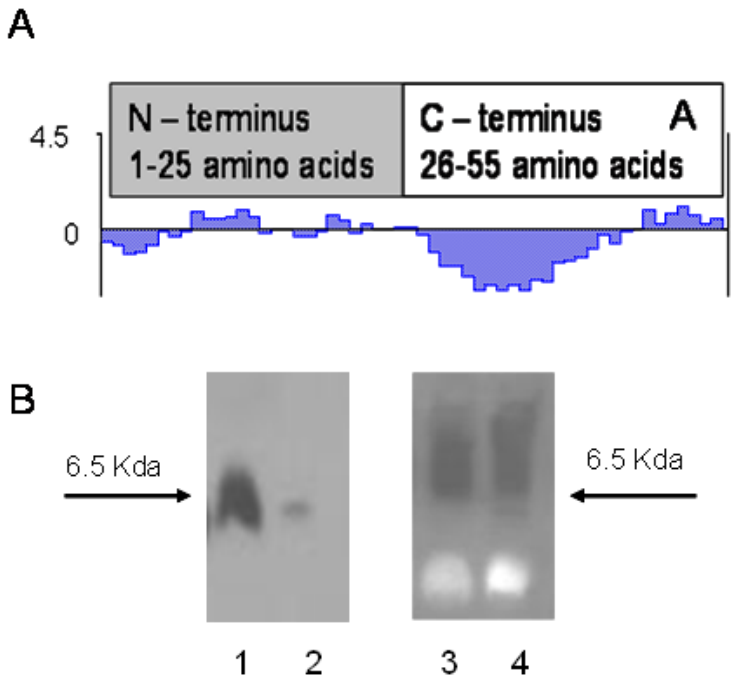

Figure 26. The presence and topology of phage fusion protein in the protein-modified liposomal preparations determined by western blot analysis. (A) Kyte and Dolittle hydrophillicity (hydropathicity) plot of the fusion phage coat protein showing an amphiphilic N-terminus and an intensely hydrophobic segment of the C-terminus. (B) Liposomal preparations were treated with proteinase K and then probed with antibodies specific for either N-terminus (Left) or C-terminus (Right) of the phage coat protein. Liposomal Gene *PRDM14* silencing in MCF-7 breast cancer cells by protein-targeted siRNA-liposomes

siRNA-protein-liposomes were tested for their ability to inhibit expression (silencing) of the target *PRDM14* gene and synthesis of its product—PRDM14 protein in MCF-7 breast cancer

cells. Cells were treated with siRNA–protein liposomes for 72 hrs, in parallel with plane control liposomes, siRNA-liposomes and protein-liposomes. Total RNA was isolated from treated cells and analyzed by RT-PCR with primers specific for the *PRDM14* gene. Relative expression of the gene was normalized against the *GAPDH* gene. It was found that targeted siRNA-protein-liposomes down-regulated *PRDM14* gene by 44% ($p<0.01$) close to the level of down-regulation of the *PRDM14* gene by siRNA-lipofectamine (46%, $p<0.02$), while control liposomes had no effect on *PRDM14* gene expression (Figure 27).

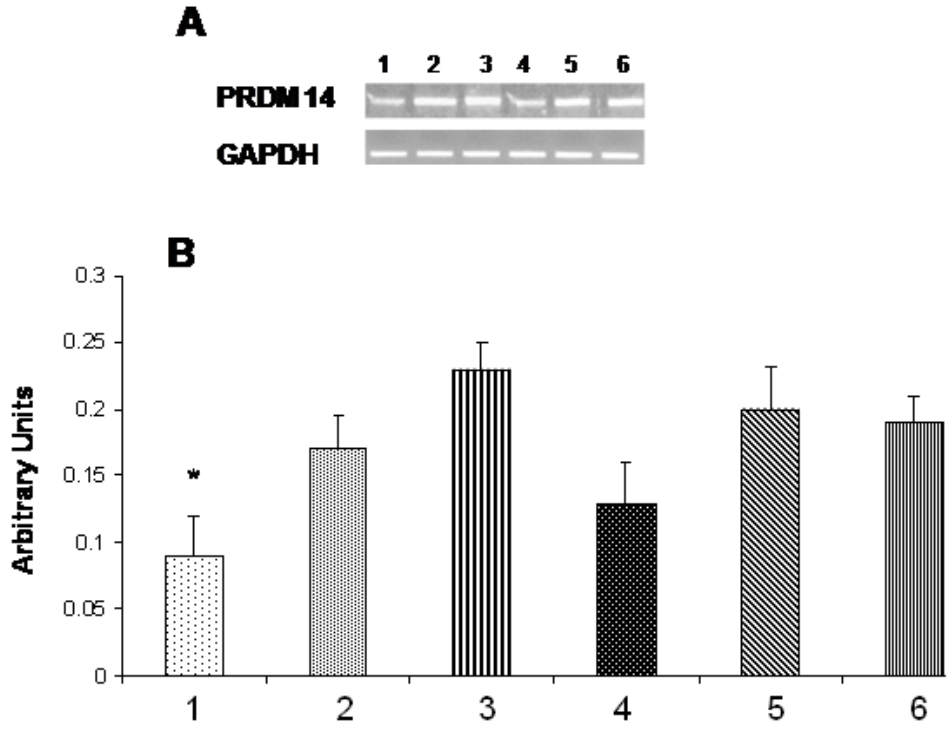

Figure 27. Analysis of *PRDM14* gene transcription by RT-PCR. MCF-7 cells were treated with *PRDM14* gene-specific protein-targeted siRNA–liposomes (40 nM) or protein-targeted scrambled siRNA-liposomes (40 nM) and incubated for 72 h. **A.** Relative transcript level of the target gene in cells treated with: 1. protein-targeted siRNA–liposomes, 2. protein-targeted scrambled siRNA-liposomes, 3. siRNA-liposomes, 4. siRNA-lipofectamine, 5. Scrambled siRNA-lipofectamine, 6. Control non-treated MCF-7 cells. B. The relative semi-quantification was normalized against GAPDH using KODAK ID image analysis software. All data represent the mean ± S.D.

Similarly, western blot analysis revealed that siRNA-protein-liposomes down-regulated *PRDM14* protein expression as compared to controls (Figure 28). These results prove the superiority of the selected phage protein and the targeting delivery of siRNA versus non-targeting.

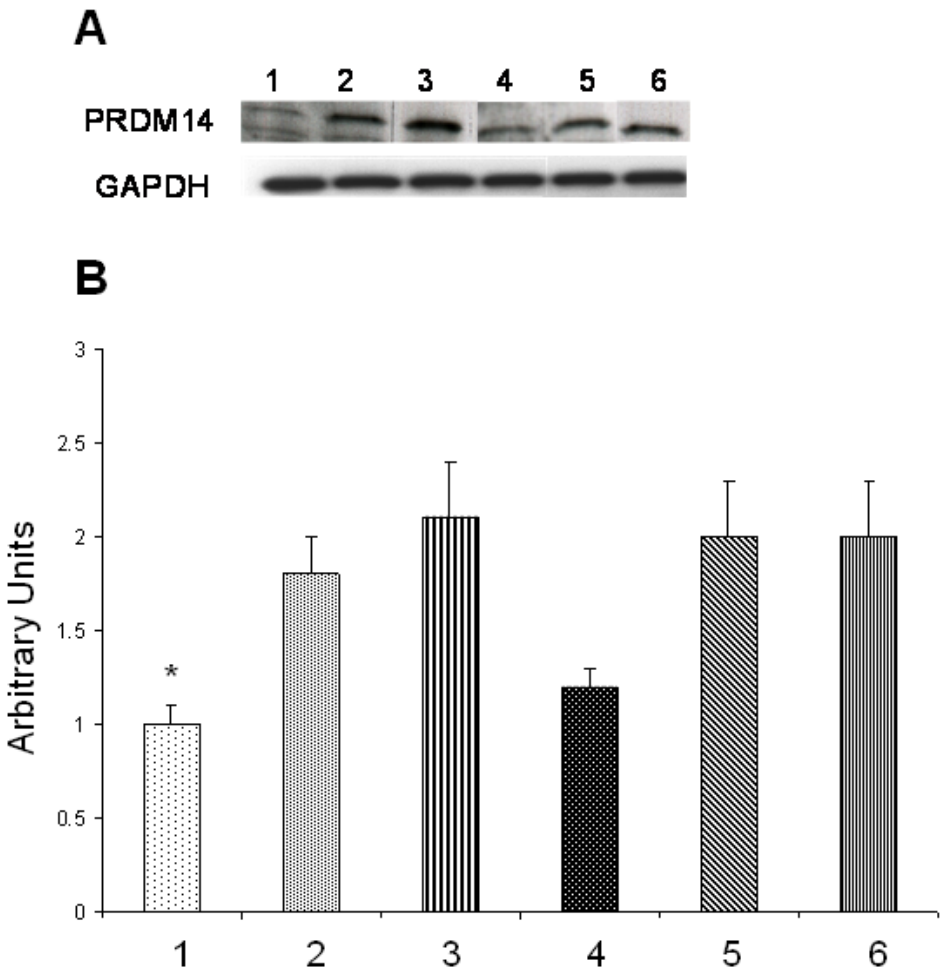

Figure 28. Analysis of PRDM14 protein expression by western blot. MCF-7 cells were treated with *PRDM14* gene-specific protein-targeted siRNA–liposomes (40 nM) or protein-targeted scrambled siRNA-liposomes (40 nM) and incubated for 72 h. A. Relative level of protein synthesis in cells treated with: 1. protein-targeted siRNA–liposomes, 2. protein-targeted scrambled siRNA-liposomes, 3. siRNA-liposomes, 4. siRNA-lipofectamine, 5. Scrambled siRNA-lipofectamine, 6. Control non-treated MCF-cells. B. Western blot band intensities quantified using Image J software (NIH). All data represent the mean ± S.D.

5. Discussion

To enhance potential anticancer efficiency of liposome-encapsulated siRNAs, we specifically targeted them *via* fusion with preselected phage protein specific for MCF-7 breast cancer cells. To simplify the procedure and exclude any chemical conjugation reactions, we used spontaneous insertion of the phage proteins and siRNA into parental liposomes, followed by their fusion under relatively mild conditions. The tumor-specific protein was isolated from the phage that was affinity selected from the multibillion-clone landscape phage library f8/8 by their ability to bind specifically to breast cancer cells. The phage DMPGTVLP (designated by the structure of the encoded guest peptide) demonstrates high selectivity and specificity towards target cells versus non-relevant control cells. The major coat protein of the selected phage was converted into the drug-loaded liposomal vesicles in which the phage spans the lipid bilayer displaying the tumor-binding peptides on the surface of the vesicles. The topology of the fusion protein in modified liposomes was confirmed by protease digestion experiments. Treatment of the siRNA-phage fusion protein-liposomes with proteinase K resulted in complete loss of the N-terminal region while the C-terminus was not destroyed by the enzyme, demonstrating that the C-terminus was translocated inside the liposomal membrane. The protein-liposomes efficiently shielded the *PRDM14* gene-targeted siRNA, as was shown by the PicoGreen fluorescent assay. Additionally, the size and size distribution of protein-targeted siRNA-liposomes did not change in 10% serum demonstrating their high stability.

The novel siRNA-nanopharmaceuticals targeted to the MCF-7 breast cancer cells *via* their association with phage fusion proteins, down-regulated *PRDM14* gene expression and inhibited PRDM14 protein synthesis in MCF-7 cells as effectively as the lipofectamine-siRNA complex that is considered a “gold standard” for delivery of siRNAs into cells *in vitro*. siRNA-

liposomes alone showed no effect on *PRDM14* gene expression implying the specific cell-targeting role of the fusion proteins through their anchoring to the cells and mediating delivery of siRNA-liposomes into the cells.

The new liposome targeting approach based on the use of landscape phage relies on powerful and precise mechanisms of selection, biosynthesis and self-assembly of these nanostructures. A culture of cells secreting filamentous phage is an efficient and convenient protein production system yielding up to 300 mg/liter of pure phage, with the major coat protein constituting 98% of the total protein mass. It can be easily isolated in a pure form using one-step chromatography. Phage itself and its coat proteins are not toxic and have been already tested for safety in preclinical trials in mice (Krag et al., 2006). Furthermore, the technique of polyvalent phage display in the major coat protein pVIII for construction of large ($>10^9$-clones) 8- and 9-mer landscape libraries has been well developed (Petrenko et al., 1996, Kuzmicheva et al., 2009). Hundreds of targeted phage probes against prostate, glial and breast tumor cells have been successfully selected from these libraries using advanced biopanning protocols (Brigati et al., 2008). These and other current advances in siRNA tumor-targeted delivery can offer a new means for their preclinical study as potential anticancer medicines.

CHAPTER 5

IDENTIFICATION OF BREAST CANCER RECEPTORS USING LANDSCAPE PHAGES

1. Abstract

To understand the basis of selectivity of targeted phages toward cancer cells, we have used landscape phages as affinity ligands for identifying their corresponding cell surface receptors. Phages selective for breast cancer were immobilized on monolithic macroporous gels and used to isolate and identify their cognate receptors on breast cancer cells. Three breast cancer selective phages DMPGTVLP, DWRGDSMDS and GSDWMLGQD were found to serve as ligands for nucleolin. Identification of phage receptors on the cancer cell surface may further elucidate the molecular mechanisms upon which phage selectivity is based as targeting ligands for new nanomedicines.

2. Introduction

The mammalian membrane is a dynamic scaffold displaying an array of macromolecules which are required for cell survival, proliferation and differentiation. These macromolecules, including receptors, acquire information from the extracellular milieu and transduce these signals into the intracellular environment through a variety of signal transduction pathways to maintain cellular homeostasis. This process is initiated by binding of monovalent or multivalent ligands to their cognate receptors. This cellular mechanism has been harnessed for active targeted delivery

of nanomedicines. Targeting of anti-tumor drugs with monoclonal antibodies or their fragments toward tumor cell receptors is based on their specific monovalent binding (Carlson et al., 2007). However, this mode of drug delivery can be hindered by non-specific cytotoxicity of monovalent conjugates. Therefore, multivalent ligand-targeted drug delivery is currently being adopted to improve selectivity of targeted drugs toward cancer cells (Wang et al., 2010a; Jayanna et al, 2010). We have previously employed multivalent ligands based on modifications of the landscape phage coat protein to target Doxil to MCF-7 cells. This study demonstrated the ease of insertion of the phage coat protein into Doxil and enhanced cytotoxicity of the modified Doxil toward MCF-7 cells (Wang et al., 2010a and chapter three of this dissertation). To reveal the identity of receptors targeted by these nanomedicines and the basis of their selectivity towards MCF-7 cells, we harnessed the microfibrous nature and multivalent feature of the landscape phage (Brigatti et al., 2008; Petrenko, 2008) in affinity chromatography to isolate phage-binding receptors on the surface of MCF-7 breast cancer cells. This was accomplished in two ways:

(i) fabricating a breast-cancer selective phage cross-linked affinity matrix

(ii) immobilizing breast cancer-selective phage as an affinity ligand on a solid support in affinity chromatography.

In the first procedure, breast cancer selective phages DVYSLAYPD, DMPGTVLP, VEEGGYGIA and VPTDTDYS (Figure 29) were converted into individual affinity matrices by covalent cross-linking through the formation of amide bonds by the reaction of amino groups on the phage surface with multiple amine-reactive *N*-hydroxysuccinimide (NHS) groups linked to the hydrophilic polymer dextran (Smith et al., 1998; Samoylova et al., 2004) as illustrated in Figure 30.

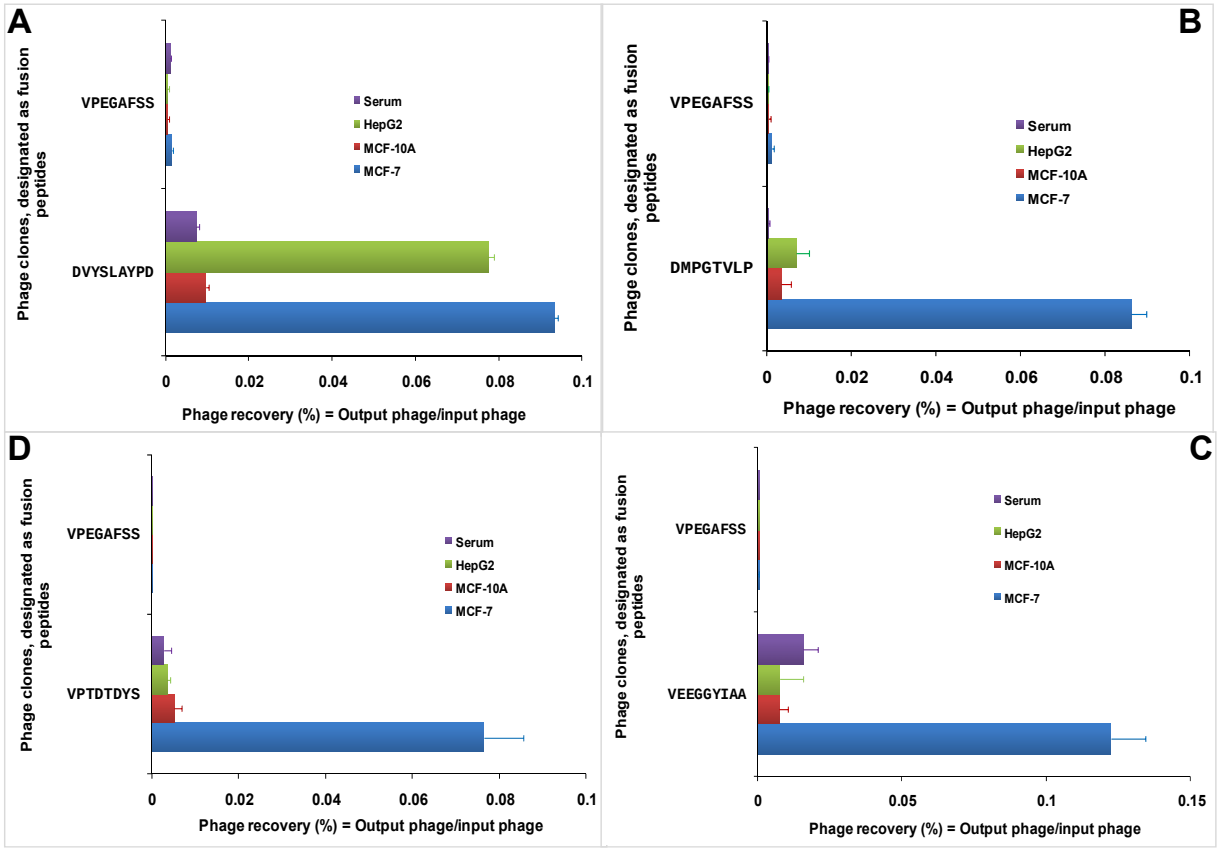

Figure 29. Selectivity of phages, DYSLAYPD, DMPGTVLP, VPTDTDYS, VEEGGYIA and VPEGAFSS toward MCF-7 cells. Selectivity was based on the selective interaction of phages with differentially expressed receptors on the target MCF-7 cells in comparison with the hepatocellular carcinoma cells (HepG2), non-neoplastic cells (MCF-10A) and serum. The unrelated phage clone VPEGAFSS was the control. Phage DVYSLAYPD in panel A is selective for both MCF-7 and HepG2 cells, whereas phages DMPGTVLP, VPTDTDYS and VEEGGYIA in panels B, C and D respectively are selective for MCF-7 cells.

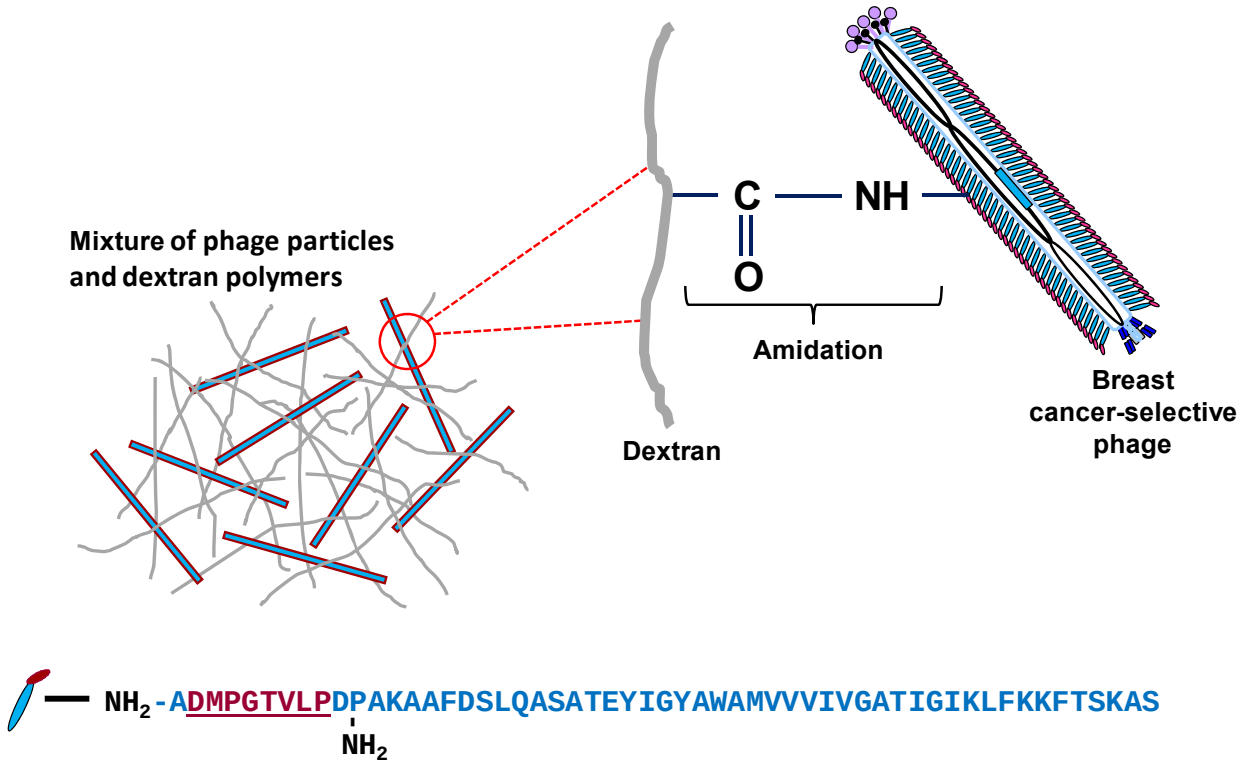

Figure 30. A schematic representation of the phage fabricated affinity matrix.
The 55 amino acids of the major coat protein are shown. The inserted guest peptide responsible for the phage interaction with the MCF-7 receptor is underlined and depicted in red. The major coat protein harbors two amino groups on the N-terminal and on Lys 13 which are exposed on the surface of the phage and can be modified without compromising the virion's structural integrity. The abundance of these groups on the phage surface (two on each of the 4000 copies of the pVIII) favors the cross-linking procedure. As a result, a matrix is formed by multiple amide bonds generated by the covalent reactions of amino groups of the phage and carboxyl groups of NHS-dextran.

Cross-linking of phages was easily achieved using numerous chemically addressable amino groups on the phage surface (Smith et al., 1998). Breast cancer membrane receptors captured in this procedure were eluted with a mild acid and separated by SDS-PAGE. Their structures were identified by nano-liquid chromatography tandem mass spectrometry (Nano-LC MS/MS) as depicted (Figure 31).

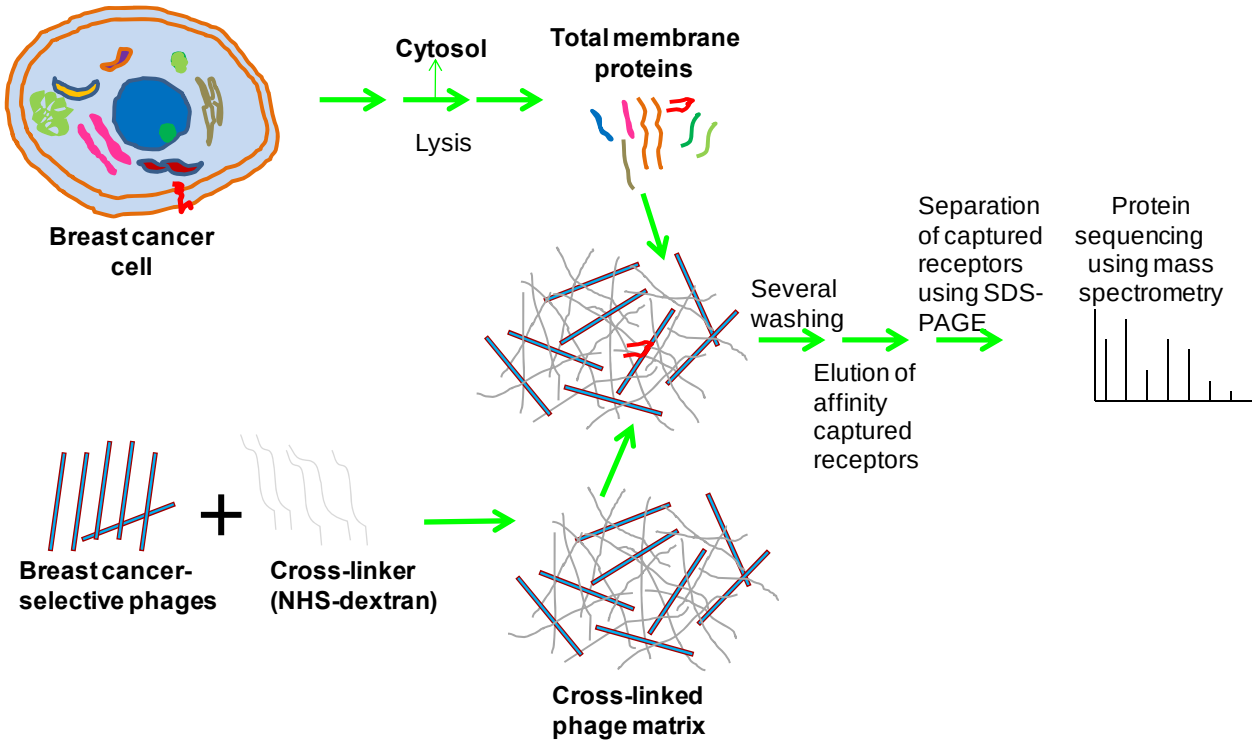

Figure 31. A schematic depiction of breast cancer receptor identification using a cross-linked phage matrix.

The second affinity chromatography procedure entails immobilization of breast cancer-selective phages as affinity ligands on macroporous (dimethylacrylamide) monolithic columns, cryogel® (Protista, Sweden) as described (Noppe et al., 2006). Cryogel® is a hydrophilic, spongy, elastic, methacrylate containing macropores (1-2 µm) and activated epoxy groups (Mallik and Hage, 2006; Peskoller et al., 2009). The activated epoxy group was used for phage immobilization through reaction of epoxy groups on the resin with amine groups on the phage. For effective immobilization of the landscape phage with multiple copies of the pVIII, a long circulation time (16 h) at 4ºC was used. Three breast cancer-selective phages DMPGTVLP, DWRGDSMDS and GSDWMLGQD (Figure 29) were used for this study.

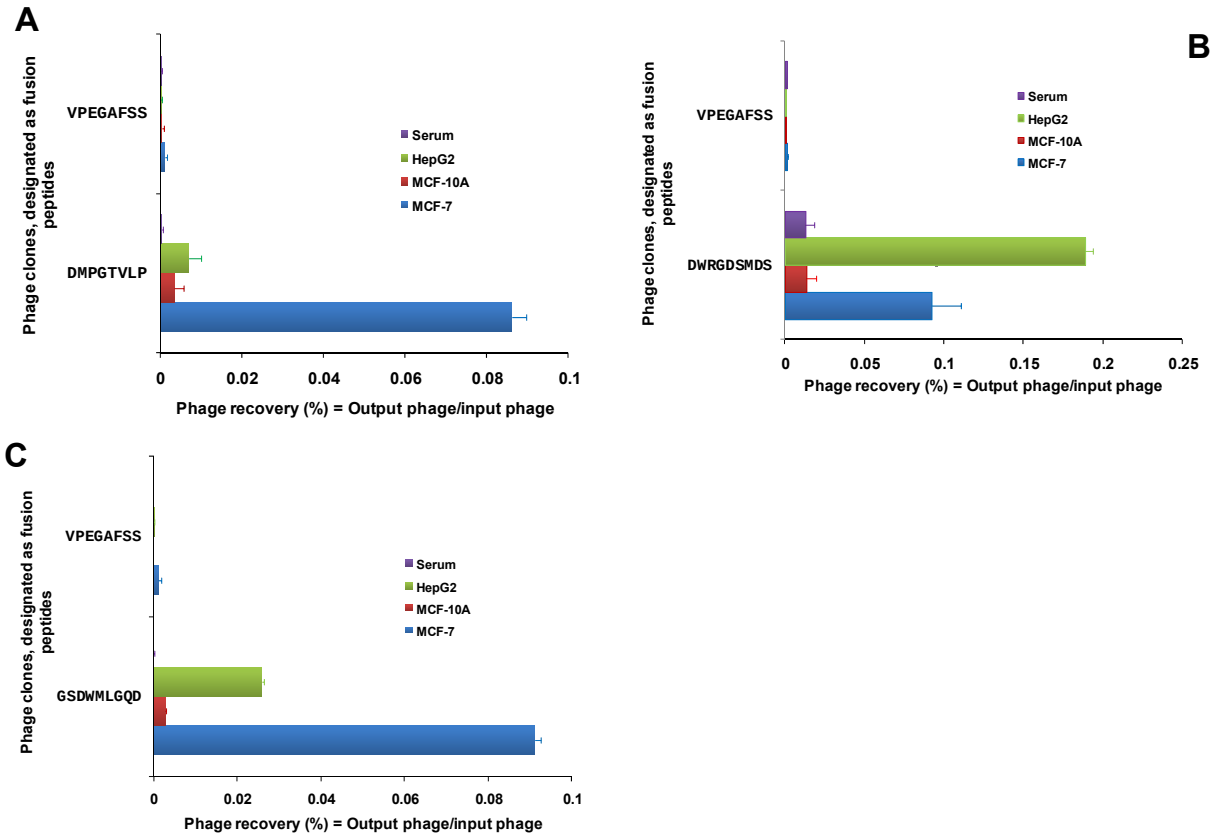

Figure 32. Selectivity of phages, DMPGTVLP, DWRGDSMDS, GSDWMLGQD and VPEGAFSS toward MCF-7 cells. Phage DWRGDSMDS in panel B is selective for both MCF-7 and HepG2 cells, whereas phages DMPGTVLP and GSDWMLGQD in panels A and C, respectively, are selective for MCF-7 cells.

The phages were immobilized on cryogel columns and allowed to react with the MCF-7 cell lysate. After washing the columns with phosphate buffered saline (PBS), bound proteins were eluted using two methods: mechanical force and salt elution. Phage DMPGTVLP-bound receptors were eluted using mechanical force whereas receptors bound to phages DWRGDSMDS and GSDWMLGQD were eluted with 1 M NaCl solution (Figure 29). Eluted proteins were separated on SDS-PAGE and identified by Nano-LC MS/MS. Cytokeratins specific for carcinoma were found as receptors of phages employed with the phage-fabricated

affinity matrices whereas nucleolins were the main proteins identified for the phage ligands immobilized on cryogel®.

Identification of nucleolin as the receptor for the phages and their basis for selectivity toward MCF-7 cells was confirmed in phage competition assays with nucleolin or integrin polyclonal antibodies (Figure 34). In addition, the basis of the molecular interaction between phages and nucleolin was studied using the PepSurf algorithm. The PepSurf algorithm was used to map the breast cancer selective-phage peptide DWRGDSMDS onto the solved three dimensional (3D) structure of endostatin, a ligand of nucleolin, retrieved from the Protein Data Bank (PDB). The algorithm aligns peptides displayed on phages on a graph representing the surface of endostatin. The best match for each peptide is found by aligning it against virtually all possible paths in the graph, combining the most significant matches resulting in prediction of the interaction sites (Mayrose et al., 2007). Furthermore, since the tripeptide RGD is present in the phage peptide DWRGDSMDS and has been shown to bind integrins (Ruoslahti, 1996), we successfully modeled the 3D structure of the phage peptide and docked it into the 3D structure of the $\alpha_v\beta_3$ integrin retrieved from the PDB.

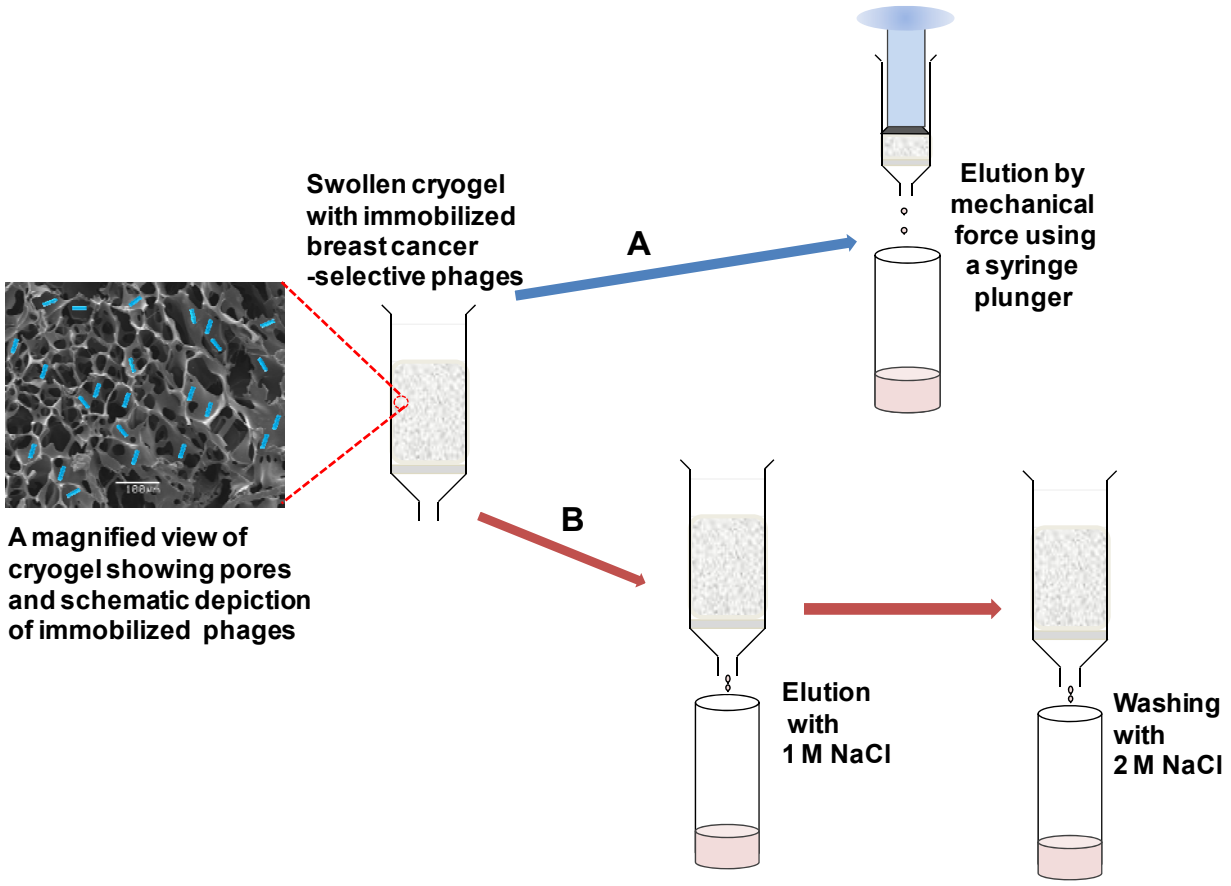

Figure 33. Affinity capture of breast cancer cell receptors using immobilized phages on macroporous monolithic columns. Breast cancer-selective phages were immobilized on macroporous monolithic gels (cryogels). Plasma membrane proteins were passed through the column and recirculated. Unbound proteins were washed off whereas bound proteins were eluted from the column either using either of these two methods: (A) mechanical elution, which involves applying mechanical force to compress the cryogel gel and thereby eluting bound proteins, (B) elution of bound proteins with a salt solution. 1M NaCl was passed through the column to elute bound proteins followed by washing column with 2 M NaCl.

3. Materials and Methods

3.1 Cells, phages and reagents

MCF-7 cells (ATCC HTB 22™) were cultivated in 75 cm^2 cell culture flasks (Corning Inc., Corning, NY) containing L-15 Leibovitz medium with L-glutamine (Sigma-Aldrich, St. Louis, MO) supplemented with 10% fetal calf serum at 37°C in 5% CO_2 until confluence. Phage probes with guest peptides DVYSLAYPD, DMPGTVLP, VEEGGYIAA, VPTDTDYS,

DWRGDSMDS and GSDWMLGQD were obtained by selection against breast cancer MCF-7 cells, as described in chapter 2. Gradient gels (4-20%) for Tris-HCl sodium dodecyl sulfate-polyacrylamide gel electrophoresis (SDS-PAGE), Tris/Glycine/SDS running buffer (25 mM Tris, 192 mM glycine, 0.1% w/v SDS, pH 8.3), 0.8 mm wall Tygon® tubing, peristaltic pump fitting kits with adaptors, Econo gradient pump and Econo UV monitor and model 2110 fraction collector were purchased from Bio-Rad Laboratories (Hercules, CA). 1 mm wall Pharmed® BPT tubing were obtained from Saint-Gobain Performance Plastics (Akron, OH). Dry epoxy-activated monolithic macroporous poly(dimethylacrylamide) columns (50 mm x 8 mm) were obtained from Protista Biotechnology (Lund, Sweden). Polyethylene glycol (PEG) with average molecular weight of 8000 Da was purchased from Fisher Scientific (St Loius, MO). Coupling buffer (1 M $NaHCO_3$, pH 6.9), *N*-hydroxysuccinimide-dextran was custom-synthesized by CarboMer (Westborough, MA) in dimethysulfoxide (DMSO) solvent. Anhydrous calcium sulfate® was obtained from W.A. Hammond Drierite Co. Ltd (Xenia, OH). 1 M Tris-HCl (pH 9.1, neutralizing buffer), 5 M NaCl solution, and C-23 nucleolin rabbit polyclonal IgG were obtained from Santa Cruz Biotechnology (Santa Cruz, CA). Elution buffer was 0.2 M glycine-HCl, pH 2.2. Phosphate-buffered saline (PBS), pH 7.4 was obtained from USB Corporation (Cleveland, OH). Novex® Colloidal Blue Staining Kit was obtained from Invitrogen (Carlsbad, CA).

3.2 Total membrane protein extraction

MCF-7 cells were cultivated in twenty-five 75 cm^2 cell culture flasks until 100% confluent. Membrane proteins were extracted using a BioVision membrane protein extraction kit (Biovision Inc., Mountain View, CA). Extracted membrane proteins were dissolved in 0.5% Triton® X-100 (SigmaUltra by Sigma-Aldrich, St. Louis, MO) in PBS and stored at -80ºC until used.

3.3 Fabrication of phage affinity matrices

Breast cancer-selective phages DVYSLAYPD, DMPGTVLP, VEEGGYIAA, and VPTDTDYS were cross-linked as described elsewhere (Smith et al, 1998; Samoylova et al., 2004). Briefly, 2 x 10^{14} phage particles in coupling buffer were mixed with 15 µl of NHS-dextran in DMSO. The mixture was vortexed immediately. 150 µl of 50% PEG was subsequently added to the mixture and vortexed again. The mixture was rotated overnight at room temperature on a Mix-All™ Laboratory Tube Mixer (Mt. Prospect, IL). Thereafter, the reaction was quenched with 8 ml of 1 M Tris-HCl and 890 µl of 5 M NaCl with rotation for 2 h at room temperature. Then, cross-linked phages were collected by centrifugation at 12,000xg for 15 min. The pellet was washed with PBS five times by centrifugation at 12,000xg for 15 min. The supernatant was discarded and the pellet was resuspended in 500 µl PBS and stored at 4°C.

3.4 Capture of membrane proteins by phage affinity matrices

Cross-linked phage matrix (1 x 10^{14} virions) was incubated with 700 mg of total plasma membrane proteins at 4°C overnight with rotation. The cross-linked phage and the membrane protein complex formed were collected by centrifugation at 20,000xg for 15 min at 4°C. The pellet was washed and resuspended in 1 ml of PBS and centrifuged at 20,000xg for 15 min at 4°C. Plasma membrane proteins, captured by the phage matrix, were eluted with 200 µl elution buffer (0.2 M glycine-HCl, pH 2.2) for 15 min at 4°C. Phage matrix was separated from the eluate by centrifugation at 16,000xg for 10 min. The eluate was transferred to a tube containing 37.5 µl of 1 M Tris-HCl, pH 9.1 and stored at -20°C until fractionation of the component proteins by SDS-PAGE.

3.5 Immobilization of phage probes to monolithic cryogel

Three dry monolithic epoxy cryogels in three 5 ml syringe barrels were swollen in 3 ml sterile water. The phage immobilization on epoxy column procedure was as described (Noppe et al., 2006). Briefly, the upper fitting adaptor was lowered 1 cm close to the surface of the cryogel and made air tight with parafilm "M"® (Laboratory film, Chicago, IL). The cryogel was washed with sterile water and equilibrated with 0.1 M carbonate-bicarbonate buffer, pH 9.5 at a flow rate of 1 ml/min. Thereafter, 2.0 x 10^{11} phage particles DMPGTVLP, DWRGDSMDS and GSDWMLGQD in 10 ml of 0.1 M carbonate-bicarbonate buffer, pH 9.5, were coupled to their respective cryogels by re-circulating them in the buffer for 16 h at a flow rate of 1 ml/min at 4°C using an Econo gradient pump. Subsequently, the column was washed with 0.1 M carbonate-bicarbonate buffer, pH 9.5, until all unbound phages were washed off. The unbound activated epoxy sites on the cryogel were blocked by re-circulation with 25 ml of 0.1 M ethanolamine in 0.1 M carbonate-bicarbonate buffer (pH 9.5) for 3 h at a flow rate of 1 ml/min. Then, the column was washed with 15 ml sterile water and 15 ml PBS until all the ethanolamine had been washed away.

3.6 Capturing of receptors

One ml of MCF-7 cell plasma membrane lysate was added to the monolithic column at a flow rate of 0.5 ml/min. After the protein peak had been loaded and passed out of the column, the column was washed with 30 ml of PBS at a flow rate of 0.5 ml/min. For the phage probe DMPGTVLP, elution was performed by applying pressure onto the column; whereas for DWRGDSMDS and GSDWMLGQD phage columns elution was carried out with 15 ml of 1 M NaCl at a flow rate of 1 ml/min. Fractions of every peak were collected, concentrated using Centricon® with Ultracel YM-10 membrane (Millipore, USA) and purified by SDS-PAGE.

3.7 SDS-PAGE analysis and protein sequencing

Eluates from the affinity matrixes and those from the cryogels were run through Tris-HCl gradient (4-20%) ready gels to fractionate component proteins. Samples were prepared for denaturation electrophoresis in Laemmli sample buffer with 5% β-mecarptoethanol by heating at 95°C for 5 min. Consequently, gels were run at 200 V, ~100 mA for 35 min in 1X Tris-glycine-SDS running buffer, pH 8.3. Protein bands were visualized with a Novex® colloidal blue staining kit (Invitrogen, Carlsbad, CA). Bands of interest were excised and sequenced by Nano-liquid chromatography tandem mass spectrometry (Nano-LC MS/MS) at the University of Alabama at Birmingham Proteomics and Mass Spectrometry Laboratory to identify the protein content.

3.8 Competition assay

The competition of cancer selective-phage DWRGDSMDS with nucleolin antibody and integrin chains α_V and β_3 antibodies and their interaction with MCF-7 cells was studied in 96-well cell culture plates. Confluent MCF-7 cells were incubated with 1:500 dilution of 200 μg/ml nucleolin polyclonal antibody (Santa Cruz ,CA), integrin chains α_V and β_3 antibodies or control serum free medium (no antibody) at room temperature, or 37 ºC for 1 h. Subsequently, cells were incubated with 1 x 10^7 cfu of the corresponding phages for 1 h at room temperature and 37 ºC. Unbound phages were removed and cells were washed eight times with serum free medium. Thereafter, cells were treated with 25 μl lysis buffer (2.5% CHAPS (3-[(3-Cholamidopropyl)dimethylammonio]-1-propanesulfonate), 0.5% BSA) to retrieve cell interacting phages. Recovered phages were titered in host *E. coli* cells. Phage recovery (%) = output (cell-associated) phage/input phage was used to estimate the phage concentration.

3.9 Prediction of interaction between nucleolin, integrin and phage DWRGDSMDS

The PepSurf algorithm was used to map breast cancer selective-phage peptide DWRGDSMDS onto the solved 3D structure of endostatin, a ligand of nucleolin retrieved from the PDB. The algorithm aligned peptides displayed on phages to a graph representing the surface of endostatin. The best match of each peptide was found by aligning it against virtually all possible paths in the graph, combining the most significant matches resulting in prediction of the interaction sites (Figure 39). To predict the binding interaction of the phage protein to integrin, molecular docking simulation was employed. The cancer selective phage with the coat protein structure:

A<u>DWRGDSMDS</u>PAKAAFDSLQASATEYIGYAWAMVVVIVGATIGIKLFKKFTSKAS

(the fusion peptide involved in cancer-selectivity is underlined) was modeled to its 3D counterpart using the iterative threading assembly refinement (I-TASSER) server (Roy et al. 2010; Zhang, 2009; Zhang, 2008). The predicted 3 D coordinates of the protein were docked on the solved structure of $\alpha_v\beta_3$ integrin (1JVE) retrieved from the PDB using the ClusPro protein-protein docking server (Kozakov et al., 2010; Comeau et al., 2004). The vacuum electrostatic prediction of the ligand and receptor were obtained using The PyMOL Molecular Graphics System, Version 1.3, Schrödinger, LLC (San Diego, CA). In addition, all molecules were visualized and manipulated using PyMOL.

4. Results

4.1 SDS-PAGE and sequencing of membrane protein bands.

To identify membrane proteins captured using affinity matrices, the proteins were eluted from the matrices and fractionated using SDS-PAGE. The protein bands were visualized using a colloidal blue staining kit (Figure 34). Protein bands of interest were cut out and sequenced using Nano-LC MS/MS to identify their peptide constituents (Table 3).

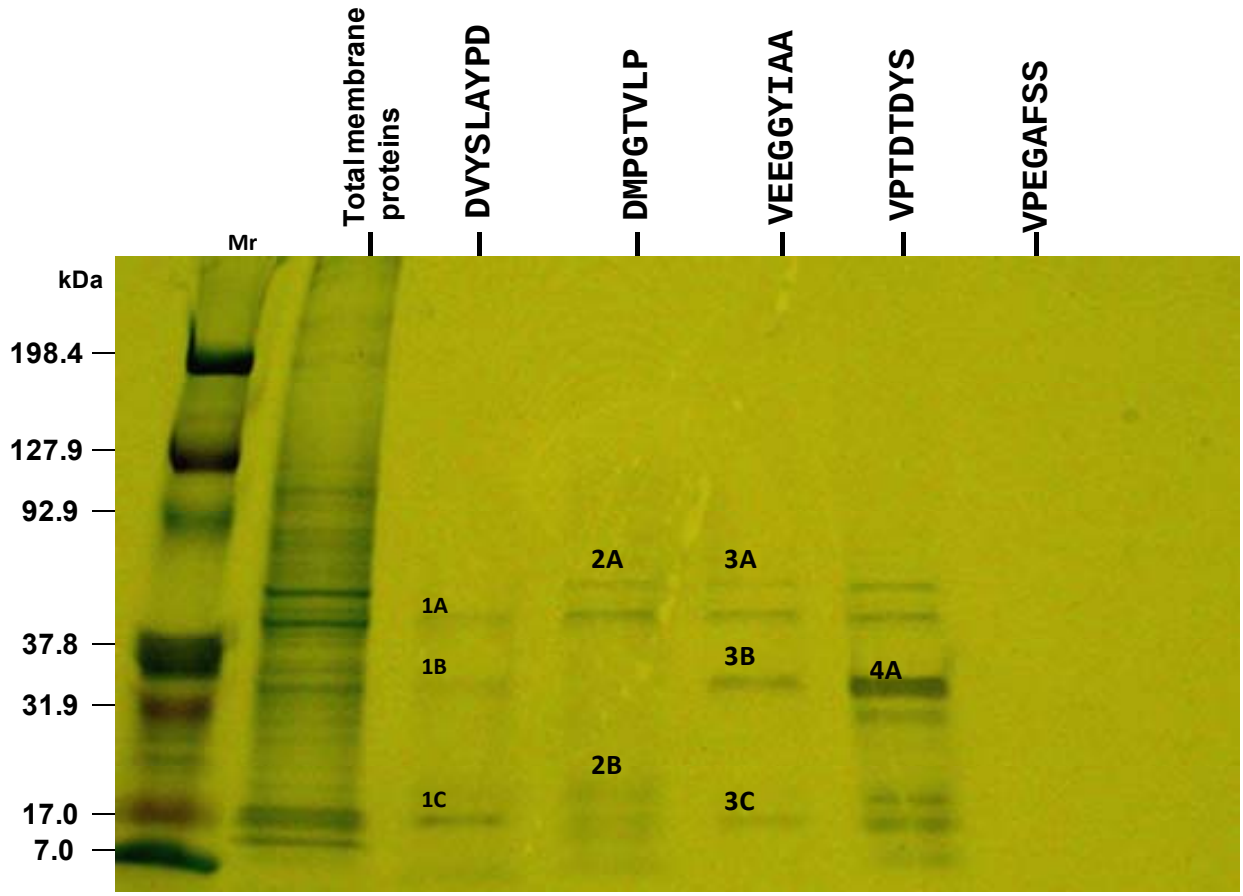

Figure 34. SDS-PAGE of cell lysate fractions and phage eluted membrane proteins. Total membrane protein fractions from MCF-7 cell lysate and phage captured proteins were separated using SDS-PAGE and visualized using a colloidal blue staining kit. Proteins bands 1A-1C, 2A-2B, 3A-3C and 4A captured by phage matrices DVYSLAYPD, DMPGTVLP, VEEGGYIAA and VPTDTDYS, respectively, were excised and identified using Nano-LC MS/MS.

Table 3. Sequencing results for proteins putatively binding phage DVYSLAYPD, DMPGTVLP, VEEGGYIAA and VPTDTDYS. Bands of interest from the SDS-PAGE were excised and sequenced using Nano-LC MS/MS.

1. DVYSLAYPD

Phage captured protein	Protein Identification	P (pro) P (pep)	Score XC
1A	Keratin 8	1.43×10^{-11}	306.26
	Keratin 9	2.88×10^{-11}	30.30
	Pyruvate kinase	2.88×10^{-3}	30.20
	Keratin 18	1.53×10^{-6}	20.25
1B	Keratin 8	1.89×10^{-9}	274.25
	Keratin 18	3.0×10^{-12}	260.29
	Keratin 19	6.10×10^{-11}	150.24
1C	Keratin 1	2.95×10^{-8}	118.23
	Keratin 9	1.42×10^{-8}	80.29

2. DMPGTVLP

Phage captured protein	Protein Identification	P (pro) P (pep)	Score XC
2A	Cytokeratin 18	2.66×10^{-7}	50.22
	Histone H2B	4.18×10^{-8}	50.20
	Keratin 10	1.27×10^{-7}	30.23
	Keratin 9	4.18×10^{-5}	20.18
	Keratin 8	7.14×10^{-4}	20.21
	H2A histone	1.46×10^{-3}	10.11
2B	Keratin 9	4.08×10^{-8}	30.21
	Keratin 1	5.74×10^{-10}	20.23
	Keratin 10	1.19×10^{-6}	20.22

3. VEEGGYIAA

Phage captured protein	Protein Identification	P (pro) P (pep)	Score XC
3A	Cytokeratin 8	4.85×10^{-11}	180.28
	Keratin 9	1.44×10^{-11}	100.31
	Keratin 10	$4.42x\ 10^{-8}$	60.23
	Keratin 1	$1.42x\ 10^{-9}$	58.23
	Keratin 18	3.59×10^{-5}	30.24
3B	Keratin 1	$3.46\ \times 10^{-5}$	48.20
	Keratin 10	4.01×10^{-6}	20.22
	Prohibitin 2	2.49×10^{-5}	20.20
	Keratin 2	3.90×10^{-5}	20.17
3C	Histone H2B	1.16×10^{-6}	38.19
	Histone H2A	$1.1.0 \times 10^{-3}$	10.14

4.2 SDS PAGE and sequencing of captured membrane proteins eluted using mechanical force.

Membrane proteins captured by the breast cancer-selective phage DMPGTVLP were eluted by compressing the cryogel gel using mechanical force. Eluted proteins were separated using SDS-PAGE and visualized using colloidal blue staining kit (Figure 35). The only visible protein band was excised and sequenced using Nano-LC MS/MS (Table 4).

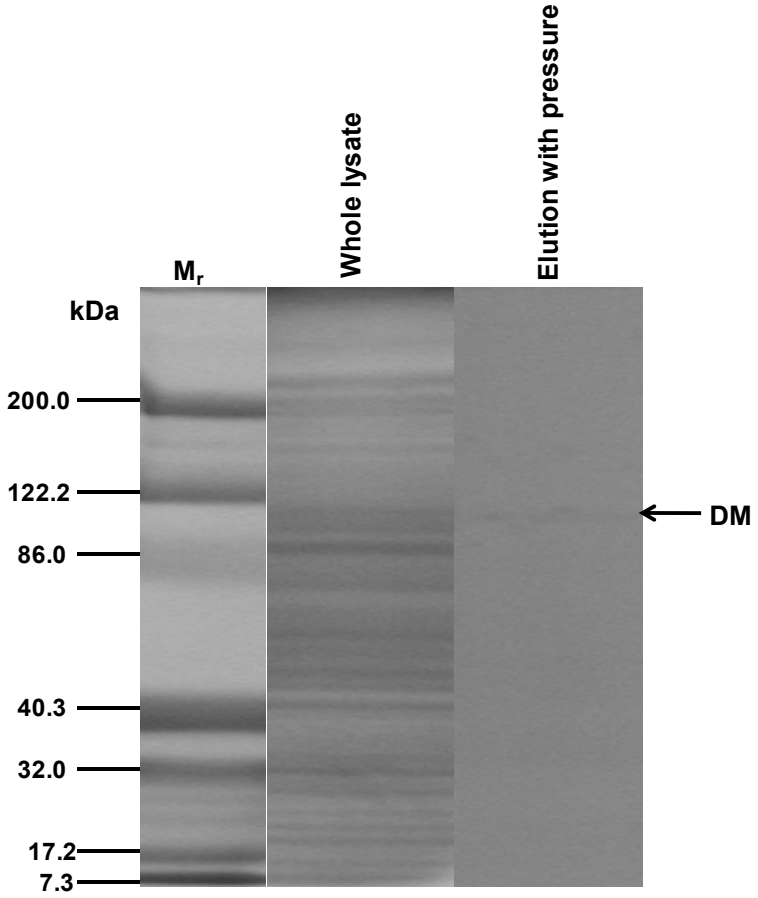

Figure 35 SDS-PAGE phage of the MCF-7 cells total membrane lysate and breast cancer-selective phage DMPGTVLP captured plasma membrane proteins. MCF-7 cell membrane lysate was applied to a cryogel® monolithic column with the phage as the affinity ligand. The phage bound proteins were desorbed by applying pressure on the cryogel. The arrow points to the captured band DM which was found to be nucleolin by Nano-LC-MS/MS sequencing.

Table 4. Sequencing results for the phage – DMPGTVLP

Phage captured protein	Protein identification	Mowse score	Accenssion No
DM	Nucleolin	903	gi|189306
	Cytovillin 2	164	gi|340217
	Alpha actinin 4	142	gi|2804273

4.3 SDS PAGE and sequencing of captured membrane proteins eluted with salt

Membrane proteins captured by the breast cancer-selective phages DWRGDSMDS and GSDWMLGQD were eluted from the cryogel® with 1 M NaCl and washing with 2 M NaCl. Eluted proteins were separated using SDS-PAGE and visualized using a colloidal blue staining kit (Figures 36 and 37). The only visible protein band was excised and sequenced using Nano-LC MS/MS (Tables 5 and 6).

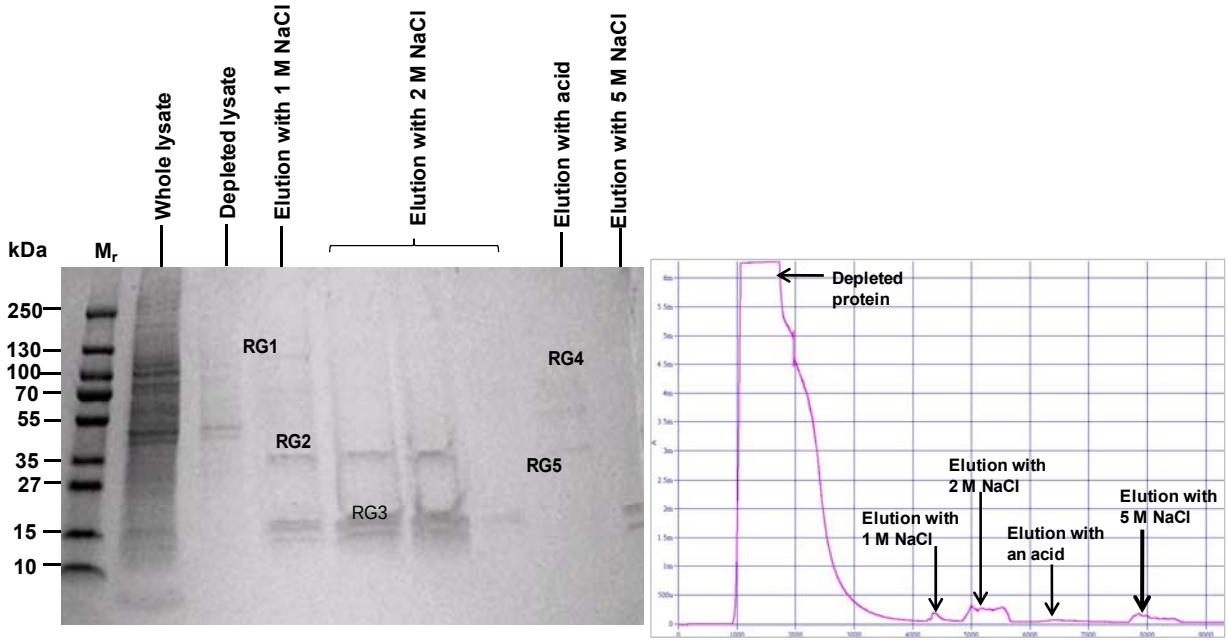

Figure 36. SDS-PAGE and affinity chromatogram of the phage probe DWRGDSMDS against MCF-7 cell plasma membrane lysate. MCF-7 cell membrane lysate was applied to a cryogel monolithic column with phage probe DWRGDSMDS as the affinity ligand. The phage bound proteins were eluted with 1 M sodium chloride, washed with 2 M sodium chloride and thereafter with a mild acid and finally with 5 M NaCl. The chromatographic profile was visualized with a Bio-Rad Econo UV Monitor. The arrows point to eluted proteins. The eluted protein bands' structures were determined by Nano-LC-MS/MS sequencing.

Table 5. Sequencing results for the phage probe – DWRGDSMDS

Phage captured protein	Protein identification	Mowse score	Accession No
RG1	Nucleolin	534	gi|189306
	Topoisomerase I	422	gi|339806
	Alpha-adaptin A related protein	97	gi|15963476
RG2	Histone cluster 1, H1b	761	gi|4885381
RG3	HIST1H2BM protein	644	gi|45768638
	Histone cluster 1, H2ac	166	gi|4504245
RG4	Lamin A/C isoform 2	463	gi|5031875
	ATP-binding cassette, sub-family F (GCN20), member 2, isoform CRA_c	63	gi|119574400
RG5	Histone H1b	422	gi|356168

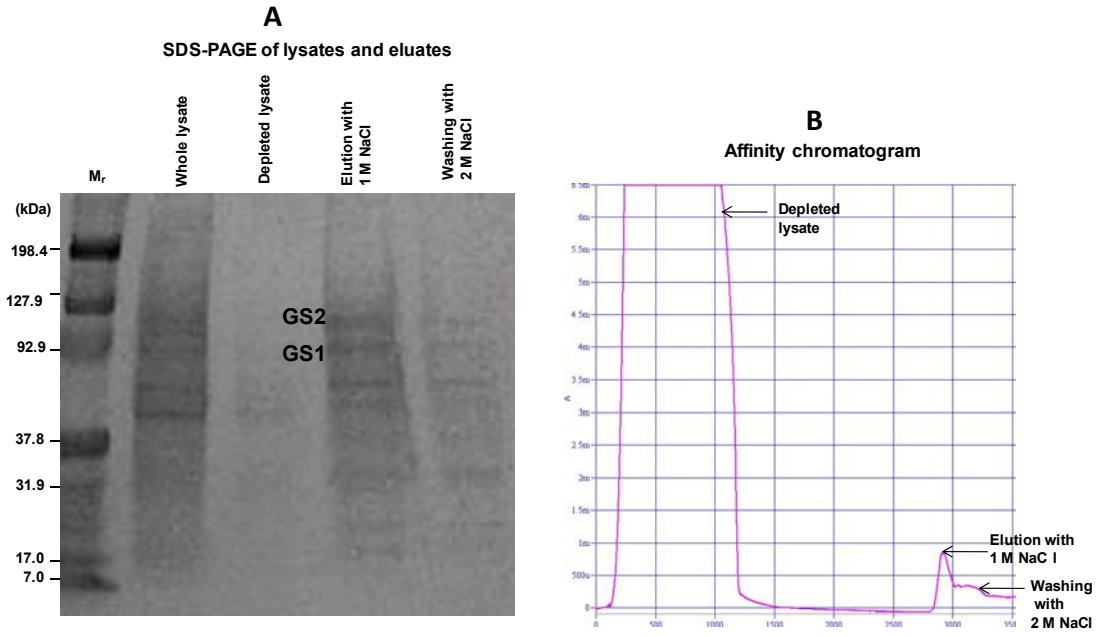

Figure 37. SDS-PAGE and affinity chromatogram of the phage probe GSDWMLGQD against MCF-7 cell plasma membrane lysate. MCF-7 membrane lysate was applied to cryogel monolithic column with phage probe GSDWMLGQD as affinity ligands. The phage bound proteins were eluted with 1 M sodium chloride and, thereafter, washed with 2 M sodium chloride. The chromatographic profile was visualized with a Bio-Rad Econo UV Monitor (Panel B). Peptides were separated by running on 4-20% gradient Tris-HCl PAGE gel. Peptide bands were visualized by colloidal blue staining (Panel A). The arrows point to eluted proteins. The eluted protein bands' structures were determined by Nano-LC-MS/MS sequencing.

Table 6. Sequencing results for the phage probe – GSDWMLGQD

Phage captured protein	Protein identification	Mowse score	Accession No
GS1	Protein disulfide isomerase A4 precursor	2091	gi|4758304
	Ezrin	1468	gi|21614499
	Radixin	1430	gi|28436809
	Heat shock 70kDa protein 8 isoform 1	542	gi|5729877
	ATP-dependent DNA helicase II	517	gi|10863945
	HSP90AA1 protein	492	gi|83318444
	Nucleolin	449	gi|189306
	Lamin A/C isoform 2	206	gi|5031875
GS2	Nucleolin	708	gi|189306
	Heat shock protein HSP 90-alpha 2	221	gi|61656603

4.4 Competition assay

To confirm the interaction of the cancer selective phage DWRGDSMDS with nucleolin and integrin, a competition assay was employed. Anti-nucleolin C23 polyclonal antibodies, anti-integrin α_v and anti-β_3 antibodies ability to compete with the phage for binding to their receptors on MCF-7 cells at room temperature were tested (Figure 38). Increase in phage interaction was observed at 37ºC which is consistent with our results in chapter two, mode of phage interaction with MCF-7 cells. Anti-nucleolin antibody was found to inhibit phage interaction with MCF-7 at both room temperature and 37ºC compared to the two integrin subunit antibodies.

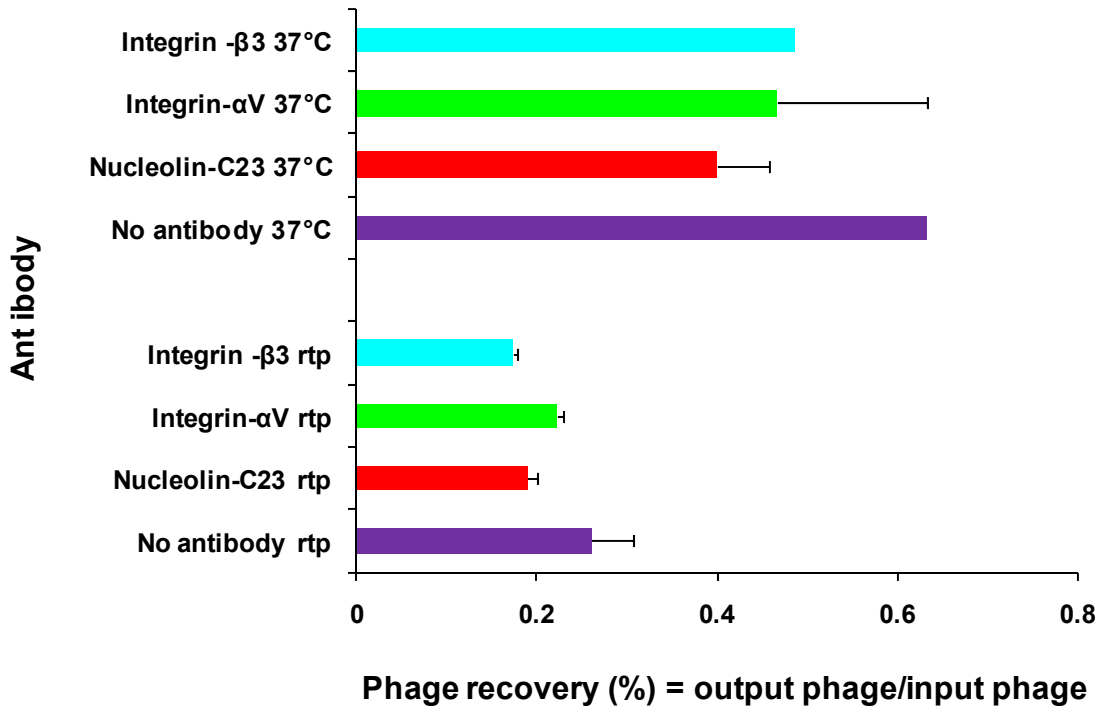

Figure 38. Competition assay of phage, nucleolin antibody, integrin subunits α_V and β_3 interactions with MCF-7 cells. Antibodies to nucleolin, integrin subunits α_V and β_3 were tested for their ability to competitively inhibit the interaction of the cancer-selective phage DWRGDSMDS with MCF-7 cells at room temperature (rtp) and 37°C. The data shown are expressed as the phage recovery which is the ratio of output phage to input phage in percentage. The "no antibody" was the control.

4.5 Prediction of molecular interactions between phage DWRGDSMDS and nucleolin

To predict the binding of the phage DWRGDSMDS to nucleolin, the PepSurf algorithm was used to align the primary structure of the phage fusion peptide to the solved 3D structure of endostatin, a nucleolin ligand. The arginine clusters, determined by alanine scanning mutagenesis, to be important for binding nucleolin are indicated in blue regions (Fu et al., 2009). Interestingly, the Arg residue in the phage protein DWRGDSMDS aligned to one of these clusters. The alignment of the two proteins with a p-value of 6.0072×10^{-5} is shown in panel B. PyMOL was used to generate the electrostatic potential of the protein based on PyMOL vacuum electrostatics. The basic Arg residue of the phage protein DWRGDSMDS aligned to a blue

region of the molecule surface, whereas, the three acidic aspartate residus aligned to the red regions as shown (panel C).

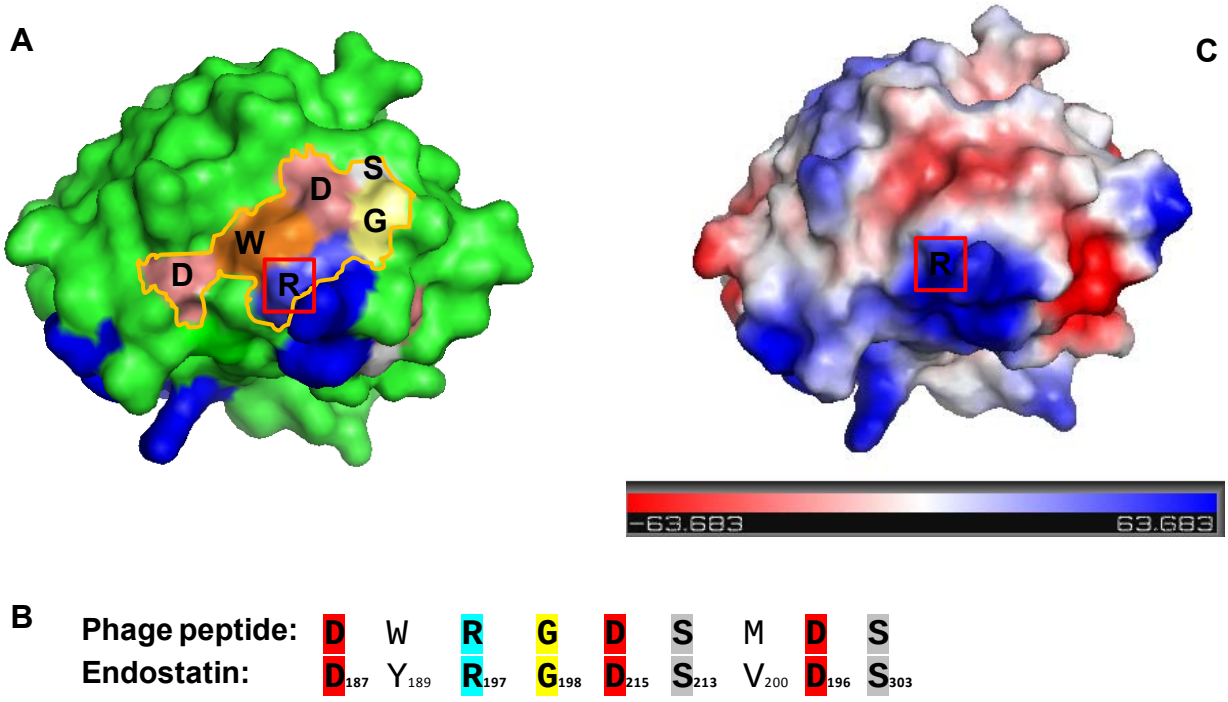

Figure 39. Prediction nucleolin binding sites on endostatin and phage protein DWRGDSMDS. (A) A surface representation of endostatin (PDB,1koe). The blue (basic) regions represent Arg clusters in heparin binding motifs of endostatin. These clusters have been demonstrated by alanine scanning mutagenesis to contribute significantly to endostatin interactions with nucleolin (Fu et al., 2009). Interestingly, the PepSurf algorithm revealed that the Arg residue (red square) on phage DWRGDSMDS is identical with one of the Arg clusters. Panel B shows the alignment of the phage peptide with the 3D structure of endostatin. The p-value of the alignment is 6.0072 x 10^{-5}. Panel C depicts the electrostatic model of endostatin. The van der Waals surface is colored according to the default electrostatic potential implemented in PyMOL. Endostatin was colored by calculated charge ranging from red -63 to blue 63 kT/e. The binding sites of nucleolin are in blue. Vacuum electrostatics, manipulation and visualization were generated using PyMOL.

4.6 Molecular modeling of the 3D structure of the phage coat protein

The 3D structure of the phage major protein with guest peptide DWRGDSMDS was modeled using the I-TASSER server. The 3D model was generated based on multiple-threading alignment. First, the algorithm retrieved templates of proteins with similar folding from the PDB, excised continuous fragments from the PDB template and finally reassembled the fragments into

full length models. The regions on the model corresponding to the fusion protein DWRGDSMDS were colored and labeled (Figure 40A). PyMOL vacuum electrostatics were applied to generate the surface potential of the modeled protein ranging from red (-52 kT/e) to blue (52 kT/e). The red dotted oval depicts the Arg residue of DWRGDSMDS predicted to be involved in binding to integrin (Figure 40B).

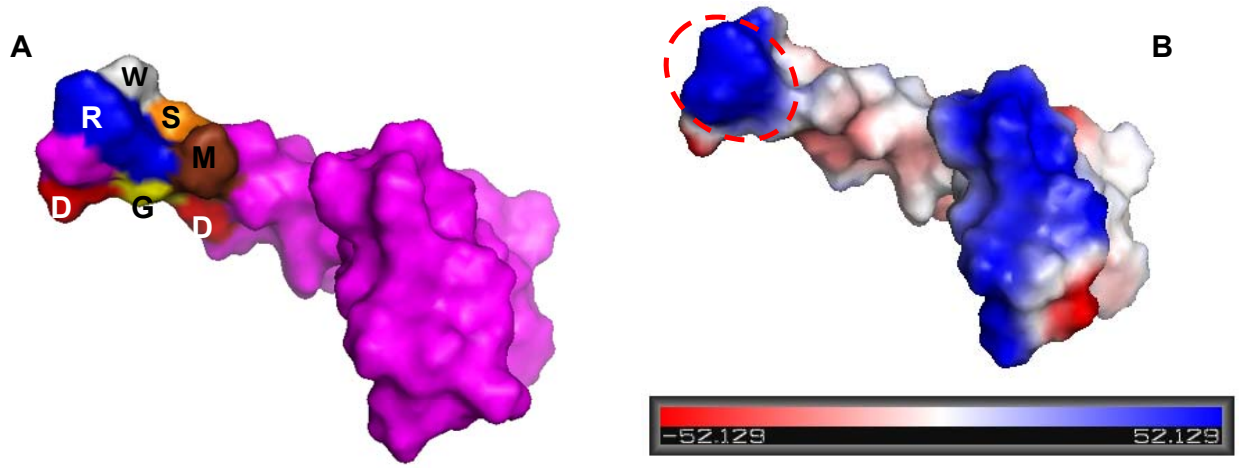

Figure 40. Molecular modeling of the phage major coat protein with the fusion peptide DWRGDSMDS. (A) shows the surface representation of the phage coat protein displaying fusion peptides. The amino acids residues of the peptide are labeled and colored; Arg (R) residue is labeled blue. (B) The van der Waals surface of the modeled phage coat protein with electrostatic potential ranging from (blue) -52 kT/e to red 52 kT/e. The red dotted oval indicates the position of the Arg residue (blue) predicted to be involved in binding integrin.

4.7 Molecular docking of the modeled phage coat protein DWRGDSMDS against the extracellular domain of integrin.

Molecular docking of the modeled phage coat protein displaying DWRGDSMDS against $\alpha_v\beta_3$ integrin was carried out using the CluPro server. CluPro first ran a rigid body docking program based on fast Fourier transform correlation approach. Secondly, the 1000 best energy conformations were clustered and the largest 30 clusters were used for refinement (Kozakov et al., 2010). The phage protein docked into the ligand-binding site with the orange boundary generated by PyMOL vacuum electrostatics (Figure 41A). This site has also been confirmed

experimentally (Xiong et al., 2002). Figure 41 B (inset) shows the Arg and Asp residues of DWRGDSMDS predicted to be involved in binding the propeller domain of α_v and βA domain of β_3 integrin subunits, respectively. The surface electrostatic potential of $\alpha_v\beta_3$ integrin was generated using PyMOL vacuum electrostatics (Figure 41C). The surface potential ranged from red (-74 kT/e) to blue (74 kT/e). The red region with the orange boundary (Figure 41C) correlated with the docking sites of the phage protein (Figures 41A and B).

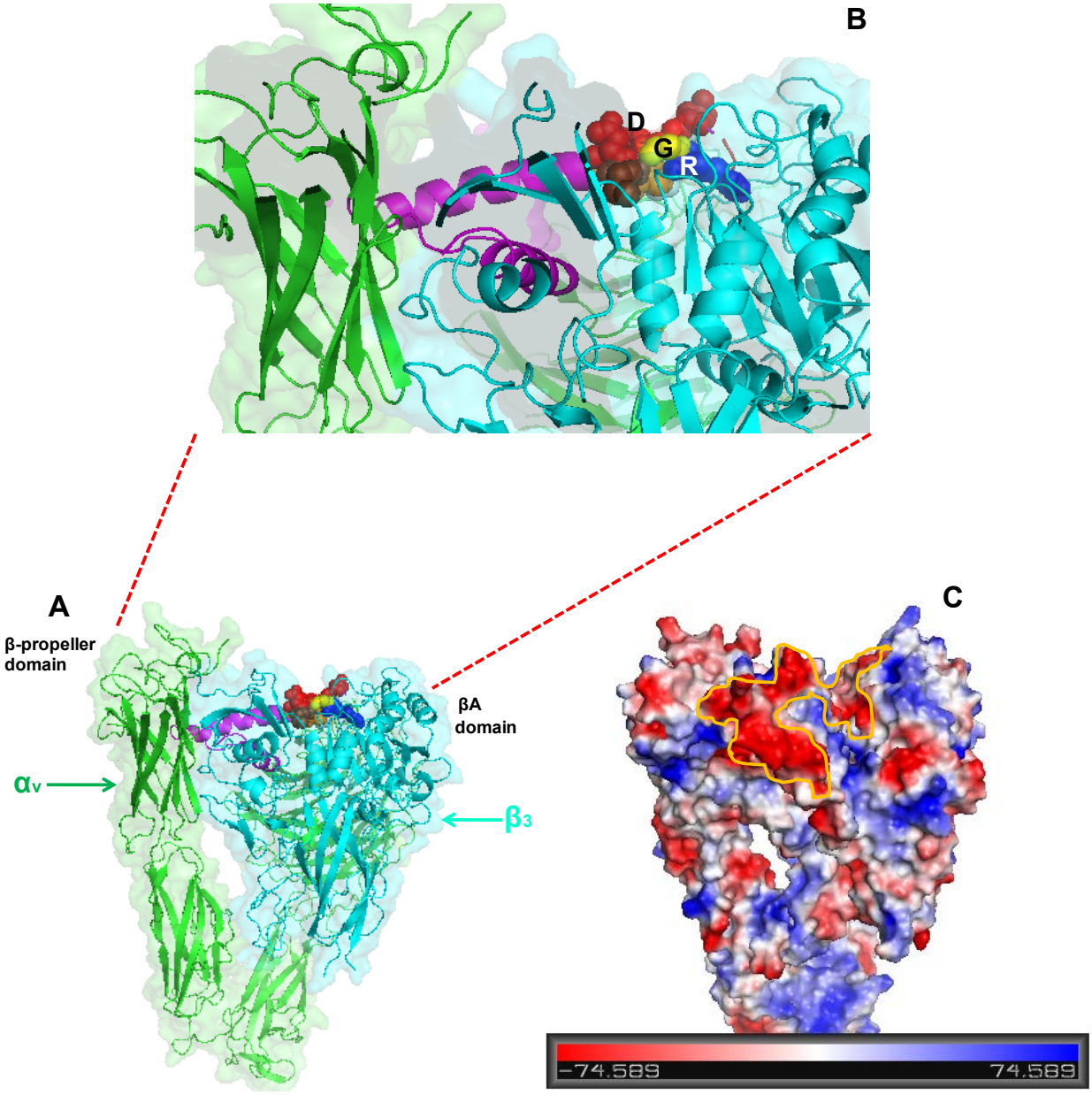

Figure 41. Molecular docking of phage coat protein with the fusion peptide DWRGDSMDS against integrin. (A) Molecular docking of the phage coat protein into the cartoon and transparent surface representation of the extracellular portion of the $\alpha_v\beta_3$ integrin (PDB, 1JV2). The phage fusion protein DWRGDSMDS residues are colored and shown as spheres. (B) Depiction of phage peptide residues Arg and Asp in contact with integrin. (C) A surface rendering of the extracellular portion of $\alpha_v\beta_3$ integrin with electrostatic potentials generated by the PyMOL vacuum electrostatics method. The red region with the orange boundary depicts the docking of the phage coat protein with electrostatic potential ranging from red (-74 kT/e) to blue (74 kT/e). Molecular visualization and manipulations were obtained using PyMOL software.

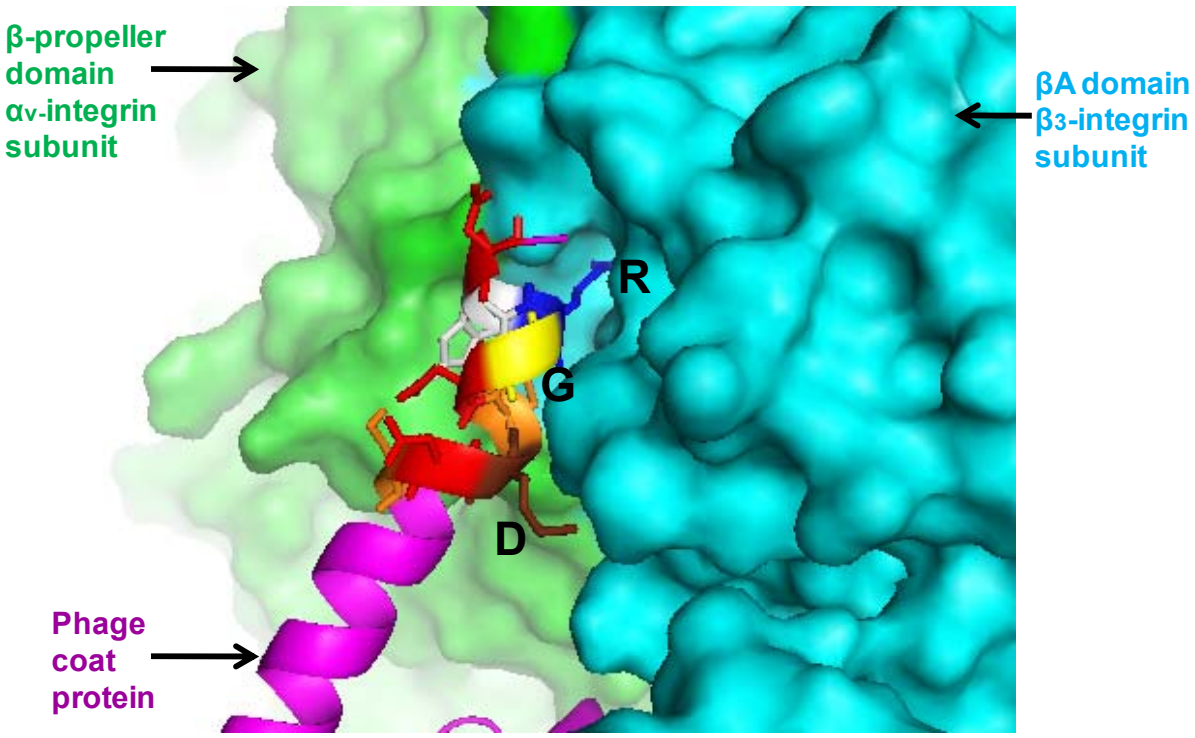

Figure 42. Molecular modeling of the interaction of phage protein DWRGDSMDS and the extracelluar domain of $\alpha_v\beta_3$ integrin. Arg (blue) is predicted to be involved in binding the α_v-subunit whereas the Asp (red) contacts the β_3 subunit. The Gly (yellow) residue is at the interface between the two subunits.

5. Discussion

The ability of breast cancer-selective phages to capture receptors on breast cancer cell surfaces is not only useful for determining the molecular basis of phage selectivity toward cancer cells but would also be applicable for precise targeting of nanomedicine in personalized medicine. In the current study, we exploited the multivalent display of breast cancer-selective peptides on landscape phages to isolate and identify receptors on the breast cancer cell surface thereby elucidating the molecular mechanisms of their selectivity. Breast cancer-selective phages, obtained from chapter two of this dissertation, were employed to identify the receptors overexpressed on MCF-7 cell surface based on two methods.

First, the breast cancer-selective phages DVYSLAYPD, DMPGTVLP, VEEGGYGIA and VPTDTDYS were developed into affinity matrices to capture their counterpart proteins on the MCF-7 cell surface. The proteins identified using this method were mainly carcinoma specific cytokeratins (CK) such as CK8, CK18 and CK19, which have been identified as carcinoma biomarkers (Olofsson et al., 2007; Hembrough et al., 1996; Dive et al., 2010). This finding is relevant to tumor-targeted nanomedicine delivery since carcinomas; the most common human tumors can release an abundance of cytokeratins which appear largely confined to tumor tissues because of their low solubility. As such; they may be useful for actively targeting delivery of nanomedicines. Furthermore, the anti-CK8 antibody TS1 has been demonstrated to be effective in tumor targeting (Holm et al., 2007). It is important to note that frequent isolation of cytokeratins using this method may be the result of a relative inability of mild acid to elute other signaling proteins from the phage matrix aside cytokeratins.

Secondly, breast cancer-selective phages DMPGTVLP, DWRGDSMDS and GSDWMLGQD were used as affinity ligands in affinity chromatography to capture their counterpart proteins on MCF-7 cells. The predominant proteins isolated using this method were nucleolin as well as other proteins such as heat shock protein-70, heat shock protein-90 and histones. This is not surprising since these proteins play anti-apoptotic roles in cancer pathogenesis. Nucleolin in particular, has been demonstrated to inhibit apoptosis by stabilizing Bcl-2 and GADD54 mRNAs and destabilizing p53 mRNA through its RNA binding domains (Ishimaru et al. 2010). Nucleolin is a multifaceted and ubiquitous non-histone nucleolar phosphoprotein, which shuttles between the nucleus and the cytoplasm (Mongelard and Bouvet, 2007). Interestingly, the protein has been shown to be overexpressed on the surface of cancer cells and has been exploited as a biomarker for cancer diagnosis and development of targeted

nanomedicines (Semenkovich et al., 1990; Soundararajan et al., 2008). Furthermore, nucleolin functions as a molecular chaperon to histone and has been demonstrated to mediate the anti-apoptotic effect of heat shock protein-70 (Storck et al., 2007; Jiang et al. 2010). However, we were unable to isolate integrin, the receptor for the RGD tripeptide, even with the phage DWRGDSMDS containing RGD. In a similar study, Samoylova et al., 2004, using a phage affinity matrix developed by cross-linking glioma-selective phage ELRGDSLP containing the RGD tripeptide, isolated CD44 using a mild acid for elution. These results indicate the inadequacy of using a mild acid or salt solution to elute some ligands, such as integrin, from affinity matrices. Therefore, integrin elution may require the use of more stringent elution buffers.

To confirm the interaction of phage DWRGDSMDS with nucleolin and integrin, phage interaction with MCF-7 cells in the presence of anti-nucleolin , anti- α_v integrin or anti-β_3 integrin antibodies at room temperature and 37ºC was tested. Phage interaction with MCF-7 cells in the absence or presence of these antibodies at 37ºC was higher at room temperature. This is consistent with our investigation of the mode of phage interaction with MCF-7 cells in chapter two of this dissertation. At both temperatures, all antibodies were found to reduce the interaction of phages with MCF-7 cells with the anti-nucleolin antibody effect being higher than the effects of the integrin subunit antibodies. The interaction of breast cancer selective peptides with nucleolin and integrin may be due to the presence of a common binding site for the peptide on the two receptors or the presence of a common binding motif like RGD on the phage peptide that is able to interact with the receptors.

To further confirm the molecular basis of the interaction of the breast cancer-selective phage DWRGDSMDS with nucleolin and integrins, computational structural biology was used.

Since the nucleolin 3D structure was not available in the PDB, the primary structure of the phage fusion peptide was aligned to the solved structure of endostatin (PBD, 1koe) using the Pepsurf algorithm. Endostatin is one the ligands of nucleolin and also an endogenous inhibitor of angiogenesis and tumor growth. It also possesses, in its sequence, the RGD tripeptide (O'Reilly et al., 1997). PepSurf alignment revealed the presence of the RGD motif in endostatin and the Arg residue in RGD of the phage peptide aligned with one of the 11 clusters of Arg residues in the heparin binding motifs of endostatin essential for interaction with nucleolin as determined by alanine scanning mutagenesis (Sasaki et al., 1999; Fu et al., 2009). Also, prediction of surface electrostatics of endostatin using PyMOL showed the same Arg residue was likely to be important for endostatin interaction with its cognate receptors (Figure 39). Furthermore, we modeled the 3D structure of the phage coat protein and docked it onto the 3D structure of $\alpha_v\beta_3$ integrin (PDB, 1JV2) to predict the molecular interaction between them. The phage RGD motif docked between the β-propeller domain of the α_v-integrin subunit and βA domain of the β_3-integrin subunits (Figure 41). The Arg residue of the phage is predicted to interact with the α_v-subunit, whereas, the Asp contacted the β_3-subunit. The Gly residue was located at the interface between the two subunits (Figure 42). This result is in concordance with the study of cyclic RGD molecular interactions with $\alpha_v\beta_3$ integrin (Xiong et al., 2002). In addition, (Faye et al., 2009), using experimental data and molecular modeling support, demonstrated the binding of endostatin at the interface between the β-propeller domain of the α_v-integrin subunit and the βA domain of the β_3-integrin subunits. Taken together, we can surmise that the RGD tripeptide motif is likely to be an energy hot spot on the phage protein DWRGDSMDS for interaction with nucleolin in the same manner as integrin-ligand interactions. The assumption of the availability of other hot spots on the phage peptide for interaction with nucleolin should not be excluded since protein-

protein interaction sites frequently consist of several unconnected hot spots (Keskin et al., 2007). The presence of the Arg residue in the phage peptide may account for its binding ability since Arg residues are able to form up to five hydrogen bond interactions and its positive charge is important for electrostatic interactions and salt bridge formations. The negatively charged aspartic acid residues are also important for electrostatic interactions. The neighboring tryptophan, based on its bulky side chain, possesses a large hydrophobic surface and can protect fragile hydrogen bonds from water.

In conclusion, the molecular dissection of phage peptide selectivity towards breast cancers may pave the way for precise targeted delivery of nanomedicines to breast tumors and a variety of other malignancies.

CHAPTER 6

CONCLUSIONS

Effective management of cancer is prevented by non-specific cytotoxicity of medicines to normal tissues and organs. An explosion of knowledge regarding the molecular pathogenesis of disease and the emergence of new methods of nanotechnology has resulted in the development of the concept of active targeted drug delivery. Applications of this new concept have the potential to improve cancer drug efficacy and to reduce their side effects. Arrays of nanomaterials are currently being tested for use in cancer diagnosis and treatment. Among these, the landscape phage is an attractive nanotechnology platform for application in biomedical research because of robustness of the phage protein membranophilic properties. The screening of multibillion landscape phage libraries against cancer cells offers an innovative approach to the generation of a repertoire of ligands for active cancer drug targeted delivery.

We hypothesized that targeting of nanomedicines using breast cancer-selective phage proteins would enhance nanomedicine efficacy. This concept has been proved by previous studies by our group employing the breast cancer-selective phage probe DMPGTVLP (Wang et al., 2010a). To corroborate these results, we employed two new breast cancer- selective phage proteins, DWRGDSMDS and GSDWMLGQD, to target Doxil™ to MCF-7 cells. These targeted nanomedicines showed specific interaction towards MCF-7 cells as revealed by flow cytometric analysis and epifluorescence microscopy. Interestingly, DWRGDSMDS targeted Doxil encapsulating 72 μM doxorubicin, demonstrated a significant higher cytotoxicity toward MCF-7

in comparison with the control untargeted Doxil encapsulating the same doxorubicin concentration. As a further step in validating the application of this concept, phage DMPGTVLP-targeted liposomes encapsulating *PRDM14* gene siRNAs were applied to MCF-7 cells. The targeted formulation demonstrated significant down-regulation of *PRDM14* gene expression and protein levels in MCF-7 cells in comparison with non-targeted siRNA. Additionally, to elucidate the molecular mechanisms of phage selectivity for breast cancer cells, we used them as affinity matrixes in affinity chromatography to identify their cognate receptors. Nucleolin was identified as the receptor of phages DWRGDSMDS, GSDWMLGQD and DMPGTVLP. Consequently, the results of these studies should pave the way for precise delivery of nanomedicines to a variety of malignancies particularly in those cancers expressing surface nucleolin.

REFERENCES

Aina, O. H., Liu, R., Sutcliffe, J. L., Marik, J., Pan, C. X., and Lam, K. S. (2007). From combinatorial chemistry to cancer-targeting peptides. Mol Pharm *4*, 631-651.

Allen, T. M. (2002). Ligand-targeted therapeutics in anticancer therapy. Nat Rev Cancer *2*, 750-763.

Arap, W., Pasqualini, R., and Ruoslahti, E. (1998). Cancer treatment by targeted drug delivery to tumor vasculature in a mouse model. Science *279*, 377-380.

Balestrieri, M. L., and Napoli, C. (2007). Novel challenges in exploring peptide ligands and corresponding tissue-specific endothelial receptors. Eur J Cancer *43*, 1242-1250.

Brigati, J. R., Samoylova, T. I., Jayanna, P. K., and Petrenko, V. A. (2008). Phage display for generating peptide reagents. Curr Protoc Protein Sci *Chapter 18*, Unit 18 19.

Calcabrini, A., Meschini, S., Stringaro, A., Cianfriglia, M., Arancia, G., and Molinari, A. (2000). Detection of P-glycoprotein in the nuclear envelope of multidrug resistant cells. Histochem J *32*, 599-606.

Carlson, C. B., Mowery, P., Owen, R. M., Dykhuizen, E. C., and Kiessling, L. L. (2007). Selective tumor cell targeting using low-affinity, multivalent interactions. ACS Chem Biol *2*, 119-127.

Chang, D. K., Lin, C. T., Wu, C. H., and Wu, H. C. (2009). A novel peptide enhances therapeutic efficacy of liposomal anti-cancer drugs in mice models of human lung cancer. PLoS One *4*, e4171.

Cho, K., Wang, X., Nie, S., Chen, Z. G., and Shin, D. M. (2008). Therapeutic nanoparticles for drug delivery in cancer. Clin Cancer Res *14*, 1310-1316.

Comeau, S. R., Gatchell, D. W., Vajda, S., and Camacho, C. J. (2004). ClusPro: an automated docking and discrimination method for the prediction of protein complexes. Bioinformatics *20*, 45-50.

Dharap, S. S., Wang, Y., Chandna, P., Khandare, J. J., Qiu, B., Gunaseelan, S., Sinko, P. J., Stein, S., Farmanfarmaian, A., and Minko, T. (2005). Tumor-specific targeting of an anticancer drug delivery system by LHRH peptide. Proc Natl Acad Sci U S A *102*, 12962-12967.

Dive, C., Smith, R. A., Garner, E., Ward, T., George-Smith, S. S., Campbell, F., Greenhalf, W., Ghaneh, P., and Neoptolemos, J. P. (2010). Considerations for the use of plasma cytokeratin 18 as a biomarker in pancreatic cancer. Br J Cancer *102*, 577-582.

Elbayoumi, T. A., Pabba, S., Roby, A., and Torchilin, V. P. (2007). Antinucleosome antibody-modified liposomes and lipid-core micelles for tumor-targeted delivery of therapeutic and diagnostic agents. J Liposome Res *17*, 1-14.

Faye, C., Moreau, C., Chautard, E., Jetne, R., Fukai, N., Ruggiero, F., Humphries, M. J., Olsen, B. R., and Ricard-Blum, S. (2009). Molecular interplay between endostatin, integrins, and heparan sulfate. J Biol Chem *284*, 22029-22040.

Frisch, B., Hassane, F. S., and Schuber, F. (2010). Conjugation of ligands to the surface of preformed liposomes by click chemistry. Methods Mol Biol *605*, 267-277.

Fu, Y., Chen, Y., Luo, X., Liang, Y., Shi, H., Gao, L., Zhan, S., Zhou, D., and Luo, Y. (2009). The heparin binding motif of endostatin mediates its interaction with receptor nucleolin. Biochemistry *48*, 11655-11663.

Gary, D. J., Puri, N., and Won, Y. Y. (2007). Polymer-based siRNA delivery: perspectives on the fundamental and phenomenological distinctions from polymer-based DNA delivery. J Control Release *121*, 64-73.

Gullotti, E., and Yeo, Y. (2009). Extracellularly activated nanocarriers: a new paradigm of tumor targeted drug delivery. Mol Pharm *6*, 1041-1051.

Haley, B., and Frenkel, E. (2008). Nanoparticles for drug delivery in cancer treatment. Urol Oncol *26*, 57-64.

Hembrough, T. A., Kralovich, K. R., Li, L., and Gonias, S. L. (1996). Cytokeratin 8 released by breast carcinoma cells in vitro binds plasminogen and tissue-type plasminogen activator and promotes plasminogen activation. Biochem J *317 (Pt 3)*, 763-769.

Holm, P., Jafari, R., and Sundstrom, B. E. (2007). Functional mapping and single chain construction of the anti-cytokeratin 8 monoclonal antibody TS1. Mol Immunol *44*, 1075-1084.

Ilyichev, A. A., Minenkova, O. O., Kishchenko, G. P., Tat'kov, S. I., Karpishev, N. N., Eroshkin, A. M., Ofitzerov, V. I., Akimenko, Z. A., Petrenko, V. A., and Sandakhchiev, L. S. (1992). Inserting foreign peptides into the major coat protein of bacteriophage M13. FEBS Lett *301*, 322-324.

Iorns, E., Lord, C. J., Turner, N., and Ashworth, A. (2007). Utilizing RNA interference to enhance cancer drug discovery. Nat Rev Drug Discov *6*, 556-568.

Ishimaru, D., Zuraw, L., Ramalingam, S., Sengupta, T. K., Bandyopadhyay, S., Reuben, A., Fernandes, D. J., and Spicer, E. K. (2010). Mechanism of regulation of bcl-2 mRNA by nucleolin and A+U-rich element-binding factor 1 (AUF1). J Biol Chem *285*, 27182-27191.

Ivanenkov, V. V., Felici, F., and Menon, A. G. (1999). Targeted delivery of multivalent phage display vectors into mammalian cells. Biochim Biophys Acta *1448*, 463-472.

Jain, R. K. (2001). Normalizing tumor vasculature with anti-angiogenic therapy: a new paradigm for combination therapy. Nat Med *7*, 987-989.

Jayanna, P. K., Bedi, D., Deinnocentes, P., Bird, R. C., and Petrenko, V. A. (2009). Landscape phage ligands for PC3 prostate carcinoma cells. Protein Eng Des Sel *23*, 423-430.

Jayanna, P. K., Bedi, D., Gillespie, J. W., DeInnocentes, P., Wang, T., Torchilin, V. P., Bird, R. C., and Petrenko, V. A. (2010). Landscape phage fusion protein-mediated targeting of nanomedicines enhances their prostate tumor cell association and cytotoxic efficiency. Nanomedicine *6*, 538-546.

Jelinek, R., Terry, T. D., Gesell, J. J., Malik, P., Perham, R. N., and Opella, S. J. (1997). NMR structure of the principal neutralizing determinant of HIV-1 displayed in filamentous bacteriophage coat protein. J Mol Biol *266*, 649-655.

Jemal, A., Siegel, R., Xu, J., and Ward, E. (2010). Cancer statistics, 2010. CA Cancer J Clin *60*, 277-300.

Jiang, B., Zhang, B., Liang, P., Song, J., Deng, H., Tu, Z., Deng, G., and Xiao, X. (2010). Nucleolin/C23 mediates the antiapoptotic effect of heat shock protein 70 during oxidative stress. Febs J *277*, 642-652.

Keskin, O., Gursoy, A., Ma, B., and Nussinov, R. (2007). Towards drugs targeting multiple proteins in a systems biology approach. Curr Top Med Chem *7*, 943-951.

Kim, S. S., Garg, H., Joshi, A., and Manjunath, N. (2009). Strategies for targeted nonviral delivery of siRNAs in vivo. Trends Mol Med *15*, 491-500.

Koivunen, E., Arap, W., Valtanen, H., Rainisalo, A., Medina, O. P., Heikkila, P., Kantor, C., Gahmberg, C. G., Salo, T., Konttinen, Y. T., *et al.* (1999). Tumor targeting with a selective gelatinase inhibitor. Nat Biotechnol *17*, 768-774.

Kolonin, M. G., Bover, L., Sun, J., Zurita, A. J., Do, K. A., Lahdenranta, J., Cardo-Vila, M., Giordano, R. J., Jaalouk, D. E., Ozawa, M. G., *et al.* (2006). Ligand-directed surface profiling of human cancer cells with combinatorial peptide libraries. Cancer Res *66*, 34-40.

Kozakov, D., Hall, D. R., Beglov, D., Brenke, R., Comeau, S. R., Shen, Y., Li, K., Zheng, J., Vakili, P., Paschalidis, I., and Vajda, S. (2010). Achieving reliability and high accuracy in automated protein docking: ClusPro, PIPER, SDU, and stability analysis in CAPRI rounds 13-19. Proteins *78*, 3124-3130.

Krag, D. N., Shukla, G. S., Shen, G. P., Pero, S., Ashikaga, T., Fuller, S., Weaver, D. L., Burdette-Radoux, S., and Thomas, C. (2006). Selection of tumor-binding ligands in cancer patients with phage display libraries. Cancer Res *66*, 7724-7733.

Krumpe, L. R., and Mori, T. (2006). The Use of Phage-Displayed Peptide Libraries to Develop Tumor-Targeting Drugs. Int J Pept Res Ther *12*, 79-91.

Kuzmicheva, G. A., Jayanna, P. K., Sorokulova, I. B., and Petrenko, V. A. (2009). Diversity and censoring of landscape phage libraries. Protein Eng Des Sel *22*, 9-18.

Lammers, T., Hennink, W. E., and Storm, G. (2008). Tumour-targeted nanomedicines: principles and practice. Br J Cancer *99*, 392-397.

Law, B., Weissleder, R., and Tung, C. H. (2006). Peptide-based biomaterials for protease-enhanced drug delivery. Biomacromolecules *7*, 1261-1265.

Lee, T. Y., Wu, H. C., Tseng, Y. L., and Lin, C. T. (2004). A novel peptide specifically binding to nasopharyngeal carcinoma for targeted drug delivery. Cancer Res *64*, 8002-8008.

Li, S. D., Chono, S., and Huang, L. (2008). Efficient oncogene silencing and metastasis inhibition via systemic delivery of siRNA. Mol Ther *16*, 942-946.

Lyden, D., Hattori, K., Dias, S., Costa, C., Blaikie, P., Butros, L., Chadburn, A., Heissig, B.,

Marks, W., Witte, L.*, et al.* (2001). Impaired recruitment of bone-marrow-derived endothelial and hematopoietic precursor cells blocks tumor angiogenesis and growth. Nat Med *7*, 1194-1201.

Mallik, R., and Hage, D. S. (2006). Affinity monolith chromatography. J Sep Sci *29*, 1686-1704.

Markman, M. (2006). Pegylated liposomal doxorubicin in the treatment of cancers of the breast and ovary. Expert Opin Pharmacother *7*, 1469-1474.

Mayrose, I., Penn, O., Erez, E., Rubinstein, N. D., Shlomi, T., Freund, N. T., Bublil, E. M., Ruppin, E., Sharan, R., Gershoni, J. M.*, et al.* (2007). Pepitope: epitope mapping from affinity-selected peptides. Bioinformatics *23*, 3244-3246.

Medina, O. P., Soderlund, T., Laakkonen, L. J., Tuominen, E. K., Koivunen, E., and Kinnunen, P. K. (2001). Binding of novel peptide inhibitors of type IV collagenases to phospholipid membranes and use in liposome targeting to tumor cells in vitro. Cancer Res *61*, 3978-3985.

Moghimi, S. M., and Szebeni, J. (2003). Stealth liposomes and long circulating nanoparticles: critical issues in pharmacokinetics, opsonization and protein-binding properties. Prog Lipid Res *42*, 463-478.

Monette, M., Opella, S. J., Greenwood, J., Willis, A. E., and Perham, R. N. (2001). Structure of a malaria parasite antigenic determinant displayed on filamentous bacteriophage determined by NMR spectroscopy: implications for the structure of continuous peptide epitopes of proteins. Protein Sci *10*, 1150-1159.

Mongelard, F., and Bouvet, P. (2007). Nucleolin: a multiFACeTed protein. Trends Cell Biol *17*, 80-86.

Mount, J. D., Samoylova, T. I., Morrison, N. E., Cox, N. R., Baker, H. J., and Petrenko, V. A. (2004). Cell targeted phagemid rescued by preselected landscape phage. Gene *341*, 59-65.

Munn, L. L. (2003). Aberrant vascular architecture in tumors and its importance in drug-based therapies. Drug Discov Today *8*, 396-403.

Nishikawa, N., Toyota, M., Suzuki, H., Honma, T., Fujikane, T., Ohmura, T., Nishidate, T., Ohe-Toyota, M., Maruyama, R., Sonoda, T.*, et al.* (2007). Gene amplification and overexpression of PRDM14 in breast cancers. Cancer Res *67*, 9649-9657.

Noppe, W., Plieva, F. M., Galaev, I. Y., Vanhoorelbeke, K., Mattiasson, B., and Deckmyn, H. (2006). Immobilised peptide displaying phages as affinity ligands. Purification of lactoferrin from defatted milk. J Chromatogr A *1101*, 79-85.

O'Reilly, M. S., Boehm, T., Shing, Y., Fukai, N., Vasios, G., Lane, W. S., Flynn, E., Birkhead, J. R., Olsen, B. R., and Folkman, J. (1997). Endostatin: an endogenous inhibitor of angiogenesis and tumor growth. Cell *88*, 277-285.

Olofsson, M. H., Ueno, T., Pan, Y., Xu, R., Cai, F., van der Kuip, H., Muerdter, T. E., Sonnenberg, M., Aulitzky, W. E., Schwarz, S.*, et al.* (2007). Cytokeratin-18 is a useful serum biomarker for early determination of response of breast carcinomas to chemotherapy. Clin Cancer Res *13*, 3198-3206.

Pappalardo, J. S., Quattrocchi, V., Langellotti, C., Di Giacomo, S., Gnazzo, V., Olivera, V., Calamante, G., Zamorano, P. I., Levchenko, T. S., and Torchilin, V. P. (2009). Improved transfection of spleen-derived antigen-presenting cells in culture using TATp-liposomes. J Control Release *134*, 41-46.

Park, J. W., Kirpotin, D. B., Hong, K., Shalaby, R., Shao, Y., Nielsen, U. B., Marks, J. D.,

Papahadjopoulos, D., and Benz, C. C. (2001). Tumor targeting using anti-her2 immunoliposomes. J Control Release *74*, 95-113.

Pasqualini, R., Koivunen, E., and Ruoslahti, E. (1997). Alpha v integrins as receptors for tumor targeting by circulating ligands. Nat Biotechnol *15*, 542-546.

Pastorino, F., Brignole, C., Di Paolo, D., Nico, B., Pezzolo, A., Marimpietri, D., Pagnan, G.,

Piccardi, F., Cilli, M., Longhi, R.*, et al.* (2006). Targeting liposomal chemotherapy via both tumor cell-specific and tumor vasculature-specific ligands potentiates therapeutic efficacy. Cancer Res *66*, 10073-10082.

Peer, D., Karp, J. M., Hong, S., Farokhzad, O. C., Margalit, R., and Langer, R. (2007). Nanocarriers as an emerging platform for cancer therapy. Nat Nanotechnol *2*, 751-760.

Peskoller, C., Niessner, R., and Seidel, M. (2009). Development of an epoxy-based monolith used for the affinity capturing of Escherichia coli bacteria. J Chromatogr A *1216*, 3794-3801.

Petrenko, V. (2008). Evolution of phage display: from bioactive peptides to bioselective nanomaterials. Expert Opin Drug Deliv *5*, 825-836.

Petrenko V.A. and G.P. Smith. (2005). Vectors and Modes of Display. In: Phage Display in Biotechnology and Drug Discovery (Editor S. Sidhu). CRC Press, Taylor & Francis Group, Boca Raton, FL, U.S.A., 714pp

Petrenko, V. A., Smith, G. P., Gong, X., and Quinn, T. (1996). A library of organic landscapes on filamentous phage. Protein Eng *9*, 797-801.

Pirollo, K. F., and Chang, E. H. (2008). Targeted delivery of small interfering RNA: approaching effective cancer therapies. Cancer Res *68*, 1247-1250.

Poul, M. A., and Marks, J. D. (1999). Targeted gene delivery to mammalian cells by filamentous bacteriophage. J Mol Biol *288*, 203-211.

Prokop, A., and Davidson, J. M. (2008). Nanovehicular intracellular delivery systems. J Pharm Sci *97*, 3518-3590.

Rajotte, D., Arap, W., Hagedorn, M., Koivunen, E., Pasqualini, R., and Ruoslahti, E. (1998). Molecular heterogeneity of the vascular endothelium revealed by in vivo phage display. J Clin Invest *102*, 430-437.

Rasmussen, U. B., Schreiber, V., Schultz, H., Mischler, F., and Schughart, K. (2002). Tumor cell-targeting by phage-displayed peptides. Cancer Gene Ther *9*, 606-612.

Romanov, V. I., Durand, D. B., and Petrenko, V. A. (2001). Phage display selection of peptides that affect prostate carcinoma cells attachment and invasion. Prostate *47*, 239-251.

Roy, A., Kucukural, A., and Zhang, Y. I-TASSER: a unified platform for automated protein structure and function prediction. Nat Protoc *5*, 725-738.

Ruoslahti, E. (1996). RGD and other recognition sequences for integrins. Annu Rev Cell Dev Biol *12*, 697-715.

Samoylova, T. I., Cox, N. R., Morrison, N. E., Globa, L. P., Romanov, V., Baker, H. J., and Petrenko, V. A. (2004). Phage matrix for isolation of glioma cell membrane proteins. Biotechniques *37*, 254-260.

Samoylova, T. I., Petrenko, V. A., Morrison, N. E., Globa, L. P., Baker, H. J., and Cox, N. R. (2003). Phage probes for malignant glial cells. Mol Cancer Ther *2*, 1129-1137.

Sasaki, T., Larsson, H., Kreuger, J., Salmivirta, M., Claesson-Welsh, L., Lindahl, U., Hohenester, E., and Timpl, R. (1999). Structural basis and potential role of heparin/heparan sulfate binding to the angiogenesis inhibitor endostatin. Embo J *18*, 6240-6248.

Sawant, R. M., Cohen, M. B., Torchilin, V. P., and Rokhlin, O. W. (2008). Prostate cancer-specific monoclonal antibody 5D4 significantly enhances the cytotoxicity of doxorubicin-loaded liposomes against target cells in vitro. J Drug Target *16*, 601-604.

Schrama, D., Reisfeld, R. A., and Becker, J. C. (2006). Antibody targeted drugs as cancer therapeutics. Nat Rev Drug Discov *5*, 147-159.

Sergeeva A,Kolonin MG,Molldrem JJ,Pasqualini R,Arap W. (2006). Display technologies: application for the discovery of drug and gene delivery agents. Adv Drug Deliv Rev; 58: 1622-1654

Semenkovich, C. F., Ostlund, R. E., Jr., Olson, M. O., and Yang, J. W. (1990). A protein partially expressed on the surface of HepG2 cells that binds lipoproteins specifically is nucleolin. Biochemistry *29*, 9708-9713.

Seymour, L. W. (1992). Passive tumor targeting of soluble macromolecules and drug conjugates. Crit Rev Ther Drug Carrier Syst *9*, 135-187.

Sharma, R. I., Pereira, M., Schwarzbauer, J. E., and Moghe, P. V. (2006). Albumin-derived nanocarriers: substrates for enhanced cell adhesive ligand display and cell motility. Biomaterials *27*, 3589-3598.

Smith, G. P. (1985). Filamentous fusion phage: novel expression vectors that display cloned antigens on the virion surface. Science *228*, 1315-1317.

Smith, G. P., Petrenko, V. A., and Matthews, L. J. (1998). Cross-linked filamentous phage as an affinity matrix. J Immunol Methods *215*, 151-161.

Soekarjo, M., Eisenhawer, M., Kuhn, A., and Vogel, H. (1996). Thermodynamics of the membrane insertion process of the M13 procoat protein, a lipid bilayer traversing protein containing a leader sequence. Biochemistry *35*, 1232-1241.

Soundararajan, S., Chen, W., Spicer, E. K., Courtenay-Luck, N., and Fernandes, D. J. (2008). The nucleolin targeting aptamer AS1411 destabilizes Bcl-2 messenger RNA in human breast cancer cells. Cancer Res *68*, 2358-2365.

Storck, S., Shukla, M., Dimitrov, S., and Bouvet, P. (2007). Functions of the histone chaperone nucleolin in diseases. Subcell Biochem *41*, 125-144.

Tseng, Y. L., Liu, J. J., and Hong, R. L. (2002). Translocation of liposomes into cancer cells by cell-penetrating peptides penetratin and tat: a kinetic and efficacy study. Mol Pharmacol *62*, 864-872.

Vasir, J. K., and Labhasetwar, V. (2005). Targeted drug delivery in cancer therapy. Technol Cancer Res Treat *4*, 363-374.

Veiseh, O., Gunn, J. W., and Zhang, M. (2010). Design and fabrication of magnetic nanoparticles for targeted drug delivery and imaging. Adv Drug Deliv Rev *62*, 284-304.

Wang, T., D'Souza, G. G., Bedi, D., Fagbohun, O. A., Potturi, L. P., Papahadjopoulos-Sternberg, B., Petrenko, V. A., and Torchilin, V. P. (2010a). Enhanced binding and killing of target tumor cells by drug-loaded liposomes modified with tumor-specific phage fusion coat protein. Nanomedicine (Lond) *5*, 563-574.

Wang, T., Yang, S., Petrenko, V. A., and Torchilin, V. P. (2010b). Cytoplasmic delivery of liposomes into MCF-7 breast cancer cells mediated by cell-specific phage fusion coat protein. Mol Pharm *7*, 1149-1158.

Wang, W., Tang, N., Zhang, C. L., Liu, X. J., Hu, H., Zhang, Z. X., and Liang, W. (2006). [Cell penetrating peptides enhance intracellular translocation and function of siRNA encapsulated in Pegylated liposomes]. Yao Xue Xue Bao *41*, 142-148.

Whitehead, K. A., Langer, R., and Anderson, D. G. (2009). Knocking down barriers: advances in siRNA delivery. Nat Rev Drug Discov *8*, 129-138.

Xiong, J. P., Stehle, T., Zhang, R., Joachimiak, A., Frech, M., Goodman, S. L., and Arnaout, M. A. (2002). Crystal structure of the extracellular segment of integrin alpha Vbeta3 in complex with an Arg-Gly-Asp ligand. Science *296*, 151-155.

Yu, J., and Smith, G. P. (1996). Affinity maturation of phage-displayed peptide ligands. Methods Enzymol *267*, 3-27.

Zhang, Y. (2008). I-TASSER server for protein 3D structure prediction. BMC Bioinformatics *9*, 40.

Zhang, Y. (2009). I-TASSER: fully automated protein structure prediction in CASP8. Proteins *77 Suppl 9*, 100-113.

Zheng, X., Vladau, C., Zhang, X., Suzuki, M., Ichim, T. E., Zhang, Z. X., Li, M., Carrier, E., Garcia, B., Jevnikar, A. M., and Min, W. P. (2009). A novel in vivo siRNA delivery system specifically targeting dendritic cells and silencing CD40 genes for immunomodulation. Blood *113*, 2646-2654.

Zitzmann, S., Ehemann, V., and Schwab, M. (2002). Arginine-glycine-aspartic acid (RGD)-peptide binds to both tumor and tumor-endothelial cells in vivo. Cancer Res *62*, 5139-5143.

http://www.merckmanuals.com/home/sec22/ch251/ch251f.html